A Modelling Study of the Garden City, Kansas, Storm during VORTEX-95

by

David Anselmo

Department of Atmospheric and Oceanic Sciences

McGill University

Montreal, Quebec

A thesis submitted to the Faculty of Graduate Studies and Research

in partial fulfillment of the requirements of the degree of

Master of Science

0-612-55035-4

Abstract

Despite advances in mesometeorology and computer technology, high-resolution numerical simulations of small-scale severe weather events remain extremely challenging. This is primarily due to insufficient initial conditions and inadequate convective parameterization schemes (CPSs). This thesis serves to illustrate how these difficulties may be overcome in a real-data simulation of the Garden City, Kansas, tornadic thunderstorm, which occurred during the VORTEX (Verification of the Origins of Rotation in Tornadoes Experiment) field experiment of 1995.

Using a sophisticated mesoscale model at 18 km horizontal resolution, a successful reproduction of the environment over southwestern Kansas is obtained. However, modifications to the CPS are required to trigger the Garden City storm at the correct time and location. Utilizing severe weather parameters, it is found that the simulated atmosphere is susceptible to tornadic supercells. The results of a sensitivity study also indicate that a neighbouring storm may have influenced tornadogenesis in the Garden City supercell.

Résumé

Malgré les progrès en mésométéorologie et en informatique, les simulations numériques à haute résolution de phénomènes atmosphériques violents de petite échelle demeurent difficiles à réaliser. Ceci est en partie dû à de conditions initiales insuffisantes et à des schémas de paramétrisation de la convection (SPC) inadéquats. Cette thèse illustre comment ces difficultés peuvent être surmontées lors d'une simulation avec données réelles d'un orage qui a généré une tornade près de Garden City au Kansas. Ce violent orage s'est produit durant le programme VORTEX (Verification of the Origins of Rotation in Tornadoes Experiment – expérience de vérification des origines de la rotation dans les tornades) en 1995.

En utilisant un modèle numérique sophistiqué avec une résolution horizontale de 18 km, nous obtenons avec succès une représentation des conditions atmosphériques dans le sud-ouest du Kansas. Cependant, des modifications au SPC sont nécessaires afin de générer l'orage de Garden City au bon endroit et au bon moment. À l'aide de paramètres de temps violent, nous constatons que l'atmosphère simulée constitue un environnement propice au développement des supercellules et des tornades. Les résultats d'une étude de sensibilité indiquent qu'un orage avoisinant a possiblement influencé la formation d'une tornade dans la supercellule de Garden City.

Table of Contents

List of Figures

Figure Page No.

List of Tables

Acknowledgments

Most of all, I wish to thank my thesis supervisor, Dr. Peter Yau, whose guidance and encouragement have enabled me to search out and follow my own direction, without straying from the proper course. There has not been a moment in the past two years when he has not been available to patiently listen to my ideas or answer my questions. I have benefited greatly from his teaching over this time, both as a student and as a person.

I would also like to thank all of the members of our mesoscale research group for their assistance in completing this thesis, especially, Dr. Vasubandhu Misra for his suggestions and advice on all topics, Badrinath Nagarajan for the countless hours he spent helping with the technical aspects of this work, Dr. Yubao Liu for his valued insight into the many challenges of numerical modelling, and Stephen Déry and Pascal Guillemette for their translation of the abstract.

There are also many good friends, which include all of those listed above and others too numerous to mention, whom I would like to thank for making my two years in Montréal an incredible experience that I will never forget.

I also wish to thank my entire family for their unwavering love and support throughout my two years away from home. This gratitude I also extend to my longtime friends, who have constantly reminded me of their care while I have been away. Lastly, I would like to thank my best friend, Catherine, whose patience, understanding, and support have greatly eased the burden of my work during the past few hectic months, and whose close companionship I would not trade for anything in the world.

Chapter 1

Introduction

1.1 Difficulties in the Modelling of MCSs

A mesoscale convective system (MCS) is defined as any precipitation system on spatial scales from 20 km to 500 km that includes deep convection during some period of its lifetime (Zipser 1982). The numerical modelling of the convective events within this class, which include thunderstorms, squall lines, and Mesoscale Convective Complexes (MCCs) (Maddox et al. 1986), remains one of the most challenging areas of research in atmospheric science. In particular, despite a tremendous increase in our understanding of mesometeorology over the past 20 years, atmospheric scientists still do not possess the ability to consistently perform accurate simulations and forecasts of the severe weather that occurs on length scales less than 50 km.

A major obstacle for an accurate simulation or forecast concerns their extreme sensitivity to initial conditions, which at the present time is accentuated by the poor quality of high-resolution observations (Stensrud and Fritsch 1994a,b; Zhang and Fritsch 1986). Spatially, conventional observational networks are too sparse to retrieve the critical data required to properly initialize a mesoscale model. This is especially true for the vertical sampling of atmospheric fields by upper air stations, which are spaced an average distance of 200 km apart and which survey the atmosphere only twice a day.

Moreover, just as models employ discretized versions of the equations of motion, initial conditions are also only a discretized representation of an atmospheric state that is naturally continuous. Thus, prior to any calculations, non-trivial errors are inherently introduced through the operation of an assimilation and interpolation scheme to fit scattered points of measurement to a uniform grid. Unfortunately, the full potential offered by the assimilation of high-resolution radar and satellite data has not yet been realized (Benoit et al. 1997). Thus, the task of providing mesoscale models with initial conditions that are satisfactory for the simulation of fine-scale events remains arduous.

The inescapable property of all numerical models to diverge from truth as an integration in time proceeds due to approximations in the governing equations, round-off error, and non-linear processes serves to amplify the inaccuracies of initial conditions. Therefore, it is imperative that a numerical model be initialized with data that is as close to reality as possible. In the modelling of synoptic-scale weather patterns, such as cyclones or blocking systems, analyzed data sets provide adequate initial conditions for a reasonably accurate forecast of a few days. Note, though, that this is also a by-product of the ease with which current operational models simulate large-scale dynamical and physical processes, which are well-resolved and well-understood, and therefore, are properly accounted for mathematically. Nevertheless, the differences between a forecast and reality inevitably grow after initialization, such that predictability in these cases is still limited, currently to a period of approximately five days.

In the modelling of meso-β systems, which evolve on much smaller length (20 km - 200 km) and time scales, this period of confidence is greatly reduced, perhaps only to several hours. As suggested by the deficiencies described above, a major contributor to this is insufficient initial conditions. Additionally, although modern computer technology enables mesoscale models to operate with a grid-spacing and time step that are small enough to capture meso-β events, such as supercell thunderstorms, the mathematical relationships necessary to reproduce them properly at this scale and using this type of model have not yet been developed (Rogers and Fritsch 1996). An increase in resolution also means an increase in variability such that smaller grid-lengths cannot be applied indiscriminately, but rather, a good comprehension of the important processes that occur at fine-scales, together with the proper mathematical translation must be attained.

Thus, another element of modelling that severely compromises the success of mesoscale simulations is that of inaccurate parameterization schemes (Ziegler and Rasmussen 1998). Many atmospheric processes are unresolved by mesoscale models. However these processes play a very important role in the large-scale environment through the transfer of heat, moisture, mass, and momentum. Hence, implicit parameterization schemes have been formulated to account for these subgrid-scale processes by representing them in terms of variables that are resolved by the model. Examples of parameterized processes include gravity wave drag, radiative exchanges, and the development of cumulus clouds. Unfortunately, these schemes are based on many assumptions and approximations, which introduce another source of error to the system. Also, as already mentioned, our limited knowledge of many of the extremely fine-scale processes has led to poor representations by these schemes, which of course, further impairs numerical simulations. In particular, Molinari and Dudek (1992), Stensrud and Fritsch (1994b), Hong and Pan (1998), Rogers and Fritsch (1996), and Kain and Fritsch (1998) have highlighted many deficiencies of existing penetrative cumulus parameterizations. These include overly sensitive trigger mechanisms which lead to the improper initiation of convection, unsuitable convective trigger functions for the scales at which the model is applied, and the absence of representation of microphysical processes, vertically sloping cumuli, and non-linear interactions within clouds. Since this study is focused on the modelling of a severe convective event, a large amount of time will be spent investigating a particular convective parameterization scheme (CPS).

1.2 Motivation

Given the great difficulties in the numerical modelling of small-scale convection and MCSs, it is not surprising that researches have seldom simulated supercell thunderstorms from real data. Thus far, most computer simulations of these events have been executed using three-dimensional numerical cloud-models (Grasso and Cotton 1995; Wicker and Wilhelmson 1995; Kulie and Lin 1998; Brooks et al. 1994; Gilmore and Wicker 1998), which are initialized with horizontally homogeneous initial conditions that are generated from a single sounding. Storm development is then usually triggered by the release of a warm "bubble" within the domain. This idealistic methodology avoids many of the problems previously described, while still providing an extremely powerful learning tool. Unfortunately, it also severely limits the realism of the study (e.g. by employing an unnatural mechanism for storm initiation (Kulie and Lin 1998)) and its application to many cases of severe convective outbreaks. Specifically, the interaction of multiple storms may be studied much more thoroughly using a real-data simulation, due to the inclusion of horizontally inhomogeneous fields. The tremendous potential of advancing our knowledge of severe storm morphology and evolution through such work has been alluded to by several researchers (Markowski et al. 1998a; Wakimoto et al. 1998; Kulie and Lin 1998).

The difficulties in simulating MCSs with a mesoscale model using real data have been clearly illustrated in past numerical studies (Zhang and Fritsch 1986; Kain and Fritsch 1998; Stensrud and Fritsch 1994a,b; Stensrud et al. 1997). In the study by Stensrud et al. (1997), a horizontal resolution of 25 km was applied to simulate several different singular convective events. According to the authors, the simulation is considered good if the model can place convection in a location within 100 km of that given by the observations. Despite this philosophy, their primary aim remained to properly reproduce the *mesoscale environment*, while striving to obtain the correct mode of convection in the correct location.

This project might then be considered a response to the challenge to properly reproduce the evolution of a significant, isolated meso-β event using real data with a mesoscale model. Admittedly, the prospects of fully realizing this objective are extremely difficult given the present shortcomings in initial conditions and parameterization schemes. It is, nonetheless, our ultimate goal to demonstrate the process by which an accurate simulation of a supercell thunderstorm can be achieved when real data is used to initialize a sophisticated mesoscale model. It should be stressed at the onset that the subject of this study, the Garden City storm during VORTEX (Verification of the Origins of Rotation in Tornadoes Experiment), embodies perhaps the most difficult scenario in MCS modelling: that of weak, large-scale environmental forcing over a broad area of high CAPE (Hong and Pan 1998; Stensrud and Fritsch 1994b). Non-trivial complications arise due to the acute sensitivity of this type of simulation to initial conditions and convective trigger functions.

Over the central plains of the United States, which is the most fertile breeding ground for tornadoes on Earth, the intense research effort VORTEX has operated with the expressed intent of improving the predictability of tornadic thunderstorms (Rasmussen et al. 1994). During the summer months of 1994 and 1995, VORTEX observational crews set out across the southern region of the Great Plains to gather unprecedented high-resolution data covering the genesis, mature, and dissipating stages of severe storms. Late in the afternoon on 16 May 1995, VORTEX researchers tracked a tornadic supercell as it formed over the far southwestern corner of Kansas and propagated in a northeastward direction while rapidly gaining strength (Wakimoto et al. 1998). Approximately 90 minutes after initiation, the thunderstorm spawned the first of four tornadoes as it proceeded past Garden City, Kansas, and eventually dissipated after a lifetime of four and a half hours.

The availability of a tremendous amount of data from VORTEX during the most critical stages of storm development provides further motivation for this study as it assists in achieving a proper simulation and allows for a comprehensive validation of model output. Speculation has also surfaced that tornadogenesis within the Garden City storm may have been influenced by a previous convective system (Markowski et al. 1998a,b; Wakimoto et al. 1998). Thus, this well-documented case study presents an opportunity to apply a mesoscale model to determine whether horizontal variations of key environmental parameters, which were produced by an interaction between storms, may have played a part in the development of a tornadic thunderstorm.

The remainder of this thesis is structured as follows. In Chapter 2, the objectives and methods of VORTEX are discussed in greater detail, and published articles that pertain to this case study are identified. As well, an analysis of the conditioning of the environment over the Great Plains leading up to severe convective activity is presented, followed by a thorough description of the evolution of the Garden City supercell and a neighbouring storm. In Chapter 3, the mesoscale model and its most important features are introduced, while modifications to the model, which were specified according to numerous sensitivity studies, are outlined in Chapter 4. In Chapter 5, an extensive examination of model results with a focus on the simulated Garden City storm and the surrounding environment is given. A sensitivity study also accompanies this analysis. Finally, in Chapter 6, the significant points of this work are reviewed, followed by a discussion of the possibilities for future work.

Chapter 2

Garden City Storm Case Study

2.1 VORTEX

Despite the advance of remote sensing technology, there is still a lack of high-resolution data for supercell thunderstorms. Even in the U.S., high-resolution surveillance of the genesis, mature, and dissipating stages of a supercell is rarely possible due to an immobile Doppler radar network with limited areal coverage and the nomadic nature of the storms (Brandes 1993; Wakimoto et al. 1998; Wakimoto and Liu 1998). Unfortunately, the advancement of theoretical and modelling research of thunderstorms is greatly hampered by the absence of quality observations. This is especially true for the study of the inner dynamics of supercells, or more specifically, mesocyclogenesis and tornadogenesis. To address this shortcoming, the multi-agency research effort, VORTEX, was launched in the middle of this decade, and it remains active today with continued analysis of archived data and the recent inception of the VORTEX-99 field experiment.

The essence of VORTEX's mandate is to study the interaction between a potentially tornadic thunderstorm and its environment so as to improve our understanding of tornadogenesis, and ultimately, to acquire a better ability to forecast and issue warnings of tornadic thunderstorms (Rasmussen et al. 1994). The operation of this enormous project requires the cooperation of several public organizations including the National Center for Atmospheric Research (NCAR), the National Oceanic and Atmospheric Administration (NOAA), the National Severe Storms Laboratory (NSSL), the National Weather Service (NWS), the Atmospheric Environment Service (AES) of Canada, and numerous universities.

The most intensive observational phase to date was carried out between April 1 and June 15, 1995 over an area of the central plains that encompassed major portions of southern Kansas, Oklahoma, and northern Texas. Climatologically, this period represents the most active time of the year for the formation of tornadoes within a territory referred to as the Tornado Alley. For this field study, the VORTEX operating domain was blanketed by 235 surface and upper air stations, which produced a very high temporal and spatial resolution data set (Figure 2.1). In addition, approximately twelve ground-based vehicles capable of rapid measurements of temperature, humidity, wind speed, wind direction, and air pressure, and the spontaneous deployment of weather balloons were utilized (Wakimoto et al. 1998). Detailed observations of storms from an extremely close-range throughout their entire life-cycle were achieved by two vehicles equipped with portable Doppler radars and two aircrafts (NOAA P-3 and NCAR Electra), which carried both conventional and Doppler radar systems. Naturally, this intense coverage was complemented by standard radar and satellite surveillance.

Over the past few years, the analysis and research phase of the VORTEX-95 field experiment has produced many articles that have appeared in various journals. In particular, there have been several publications on the Garden City storm of 16 May 1995, including a very detailed account of the evolution of this supercell by Wakimoto et al. (1998) and Wakimoto and Liu (1998). Papers with a focus on specific characteristics of the storm have since followed, including a discussion of the variability of storm-relative environmental helicity (SREH) leading up to and during the event (Markowski et al. 1998b), and the hypothesized influence of a low-level outflow boundary in the formation of tornadoes within the Garden City storm (Markowski et al. 1998a). In another paper by Brown (1998), the retrieved radar data was utilized to develop a technique to aid in the interpretation of Tornadic Vortex Signatures (TVSs), the

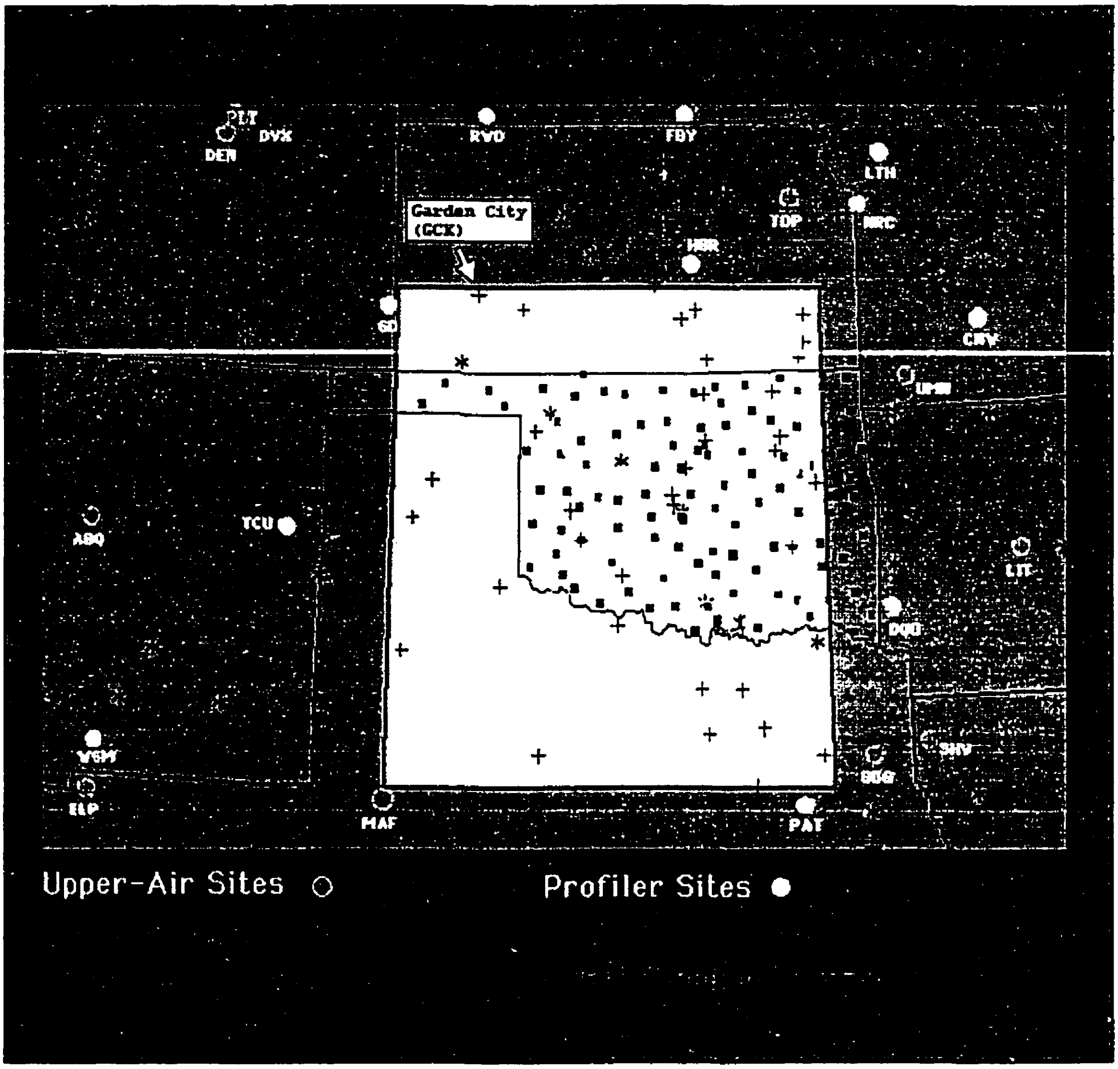

Figure 2.1. VORTEX operating domain for the 1995 field experiment (boxed, lightest shading). The location of the surface observations from Garden City is indicated. The station identifier DDC denotes Dodge City, which is a site of upper-air observations and a Doppler radar, and is situated approximately 75 km to the east-southeast of Garden City.

appearance of which in radar imagery indicates the presence of tornadogenesis (Burgess et al. 1993). Some of these articles will be referred to in upcoming sections as part of our analysis of observations and modelled output.

2.2 Environmental Setting of 16 May 1995

The afternoon of 16 May 1995 was subject to a widespread scatter of convective activity across the mid-central and mid-eastern United States that included the emergence of the Garden City thunderstorm at approximately 2200 UTC (5:00 PM local standard time (LST); hereafter all times in UTC, LST = UTC - 5 hours). Throughout the preceding twelve hours, prevailing winds conditioned the environment on the lee-side of the Rocky Mountains to a state highly susceptible to deep convection. The Canadian Meteorological Centre's (CMC) 500-hPa analysis for 1200 UTC 16 May 1995 shows a cut-off low situated southwest of California that forced a steady transport of hot, dry air from the Mexican Plateau down the eastern slope of the Rockies and over the central states (Figure 2.2). At 850-hPa, relatively cool, moist air originating over the Gulf of Mexico was advected northward along the eastern side of the Rocky Mountains and underneath the warm, dry air mass aloft (Figure 2.3). A low-level jet over Kansas and northern Oklahoma indicates that the moisture transport into the VORTEX-95 domain was particularly large and implies strong baroclinicity in the lower atmosphere. This combination of mid- and low-level flows is common prior to the formation of severe thunderstorms over the central plains during the warm season, since an environment in which a hot, dry air mass overlies a cool, moist air mass possesses a high level of convective instability.

The 0000 UTC sounding launched at Dodge City, Kansas, which is located approximately 75 km to the east-southeast of Garden City (see Figure 2.1), illustrates this profile clearly (Figure 2.4). Above 750-hPa, a deep and extremely dry layer suggests that extensive compressional warming due to persistent large-scale subsidence has occurred. This is substantiated by a nearly dry-adiabatic lapse rate throughout the lower portion of

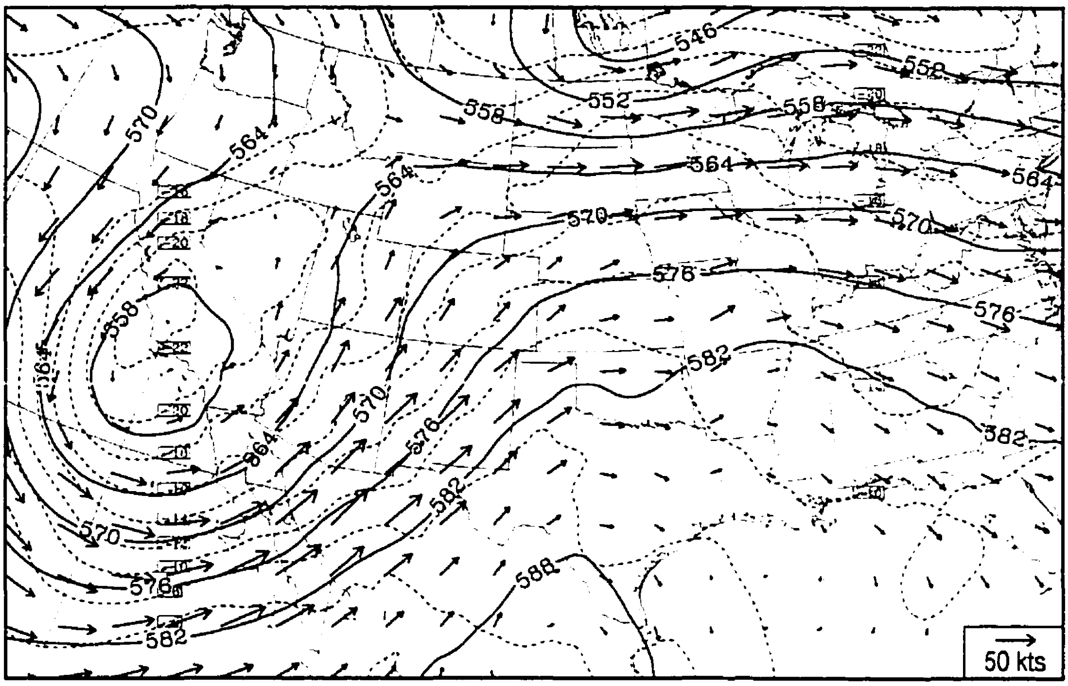

Figure 2.2. Analysed 500-hPa geopotential height (dam) (solid lines), temperature (°C) (dashed lines), and wind vector for 1200 UTC 16 May 1995. Contour interval for geopotential height is 6 dam and for temperature is 2 °C.

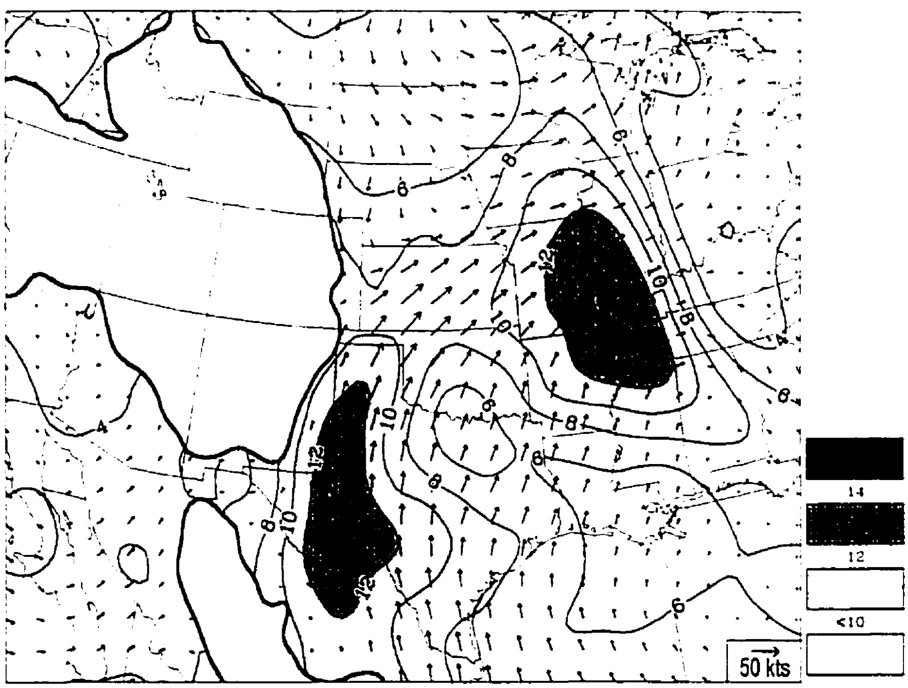

Figure 2.3. Analysed 850-hPa specific humidity (g kg^{-1}) (thin solid lines) and wind vector for 1200 UTC 16 May 1995. Contour interval for specific humidity is 2 g kg^{-1}, and values greater than 10 g kg^{-1} are shaded. Heavy solid line denotes the area below surface.

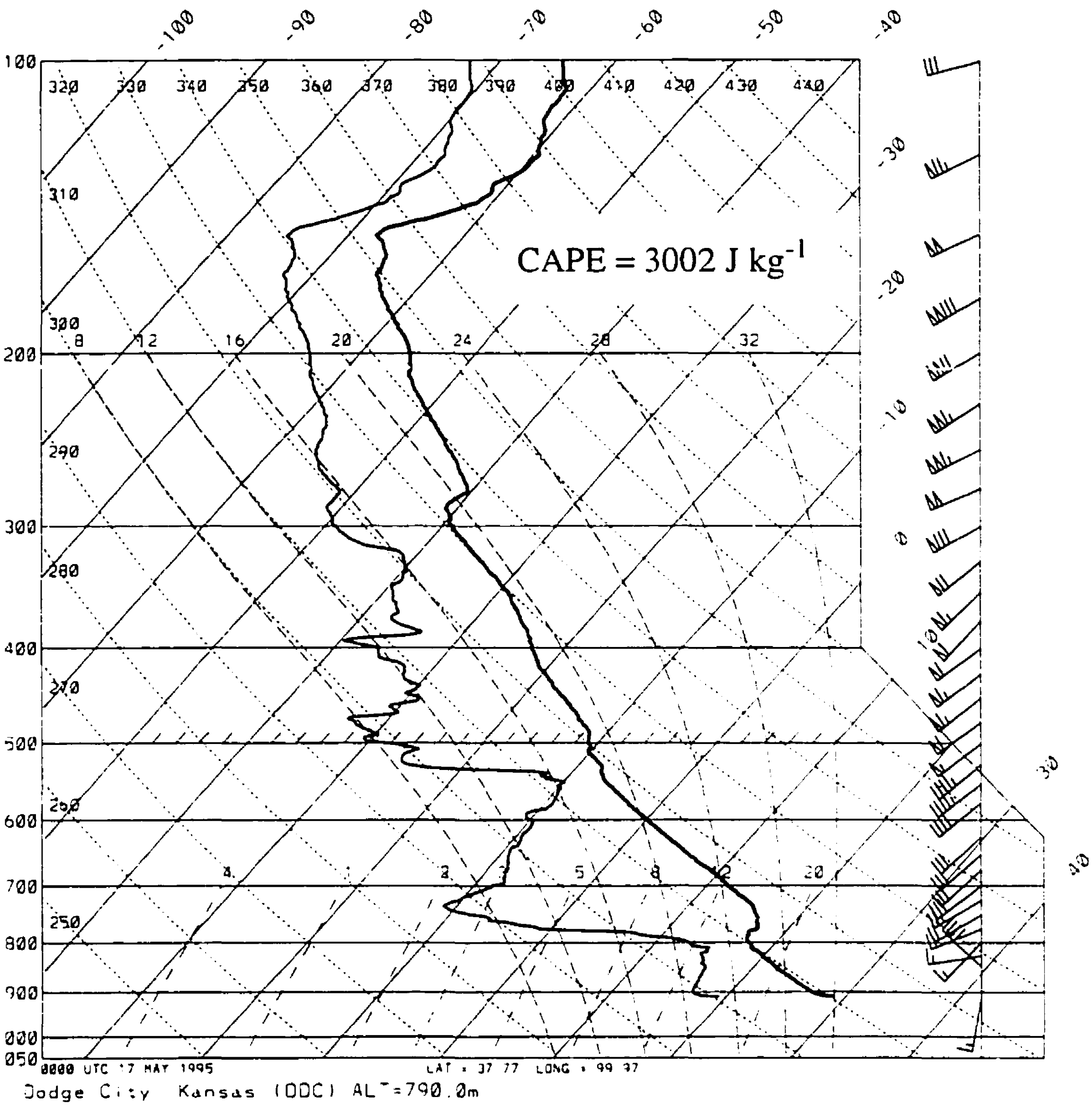

Figure 2.4. Upper-air sounding for 0000 UTC 17 May 1995 at Dodge City (DDC). Vertical profile of the wind is shown with the half-barb, full barb, and flag denoting 5, 10, and 50 knots, respectively. Location of the launch site relative to Garden City is shown in Figure 2.1, and to the Garden City storm in Figure 2.9.

the column. Between 800-hPa and 750-hPa lies the residual of a strong low-level inversion that was generated by nocturnal radiational cooling, and subsequently weakened by intense solar heating of the Earth's surface. Below this feature, vigorous vertical mixing has produced an easily identifiable atmospheric boundary layer (ABL). Also note that the air within this 100-hPa isentropic layer is considerably more moist than the air aloft, which testifies to the source of the low-level air mass.

All of the characteristics of the environmental sounding just described epitomize a unique atmospheric state that has been classified as Miller Type I (Fawbush and Miller 1954; Bluestein 1993, section 3.4.5). The steep lapse-rate of the dry air aloft yields a deep layer of conditional instability, while the shallow inversion maintains this instability by restraining buoyant parcels of air, and allows for a significant accumulation of CAPE. That is, the thin, stable layer acts as a convective lid, suppressing low-level vertical motions so that an air parcel cannot easily reach its level of free convection (LFC). However, since the lowest atmospheric layer is close to saturation, an instance of positive vertical velocity may provide the necessary expansional cooling for condensation to occur. At this point, defined as the lifted condensation level (LCL), the release of latent heat associated with a phase change will aid further vertical motion so that a parcel may overcome its convective inhibition (CIN), the magnitude of which reflects the strength of the capping lid. This scenario is often referred to as a loaded-gun sounding since only a minor decay in the strength of the inversion or a slight pulse of upward motion may be necessary for an air parcel to freely convect, thus, releasing all of the stored CAPE.

The vulnerability of this environment to deep cumulus development may be exploited by a forcing for ascent, or trigger, which is either organized on the large-scale, for example through the advection of warm air or positive vorticity, or on the mesoscale by a dryline or outflow boundary, as is often the case in the outbreak of isolated thunderstorms. That is, boundary layer instabilities generated by surface fluxes of heat and moisture, low-level moisture convergence, and upper-level divergence often serve to initiate penetrative convection (e.g. Smith and Yau 1993).

On 16 May 1995, the synoptic flow was instrumental in preparing the environment over the central plains for deep convective activity. However, in this region there was a notable absence of large-scale forcing for ascent (see Figure 2.2). Thus, the lifting required to trigger the Garden City supercell was provided by mesoscale features. A surface analysis performed by Wakimoto et al. (1998) for 2100 UTC depicts a surface trough that transected Kansas from the northeast to the southwest and lied ahead of a cold front, which stretched northeastward to a surface low positioned near the Great Lakes region (Figure 2.5). Concurrently, a dryline extended northward from Texas to intersect the trough west of Garden City. A dryline is a low-level boundary which separates a cool, moist air mass flowing northward from the Gulf of Mexico from a hot, dry air mass flowing eastward from the southwestern states and Mexico. This feature is approximately located by the 9 g kg^{-1} isohume (Schaefer 1986), and is often observed in spring on days with severe convective activity over the southern plains (Rhea 1966; Bluestein and Parker 1993). Referring to Figure 2.5, the two air masses are easily distinguished by exceptionally large differences in dewpoint depression across the boundary.

A plot of the isopleths of surface specific humidity at 2200 UTC (not shown) reveals an eastward bulge in the dryline immediately south of the intersection of the dryline and the surface trough. The northwest to southeast oriented section (i.e. northern portion) of the dryline bulge is characterized by enhanced low-level moisture convergence, which favours the formation of severe thunderstorms (Schaefer 1986). Additionally, an analysis of the 250-hPa flow at 0000 UTC 17 May 1995 shows the territory west of Garden City to lie beneath the left-exit region of an upper-level jet streak (Figure 2.6). Thus, this feature provided forcing for ascent through the mechanism of upper-level divergence (Beebe and Bates 1995) over an area that was experiencing convergence at low levels. It was in this region of strong mesoscale forcing that the Garden City supercell erupted just prior to 2200 UTC 16 May 1995. Model simulations, however, revealed that the presence of a localized boundary layer instability also played an integral part in the initiation of this severe convective event. The discovery of this additional factor will be discussed in more detail in Chapter 4.

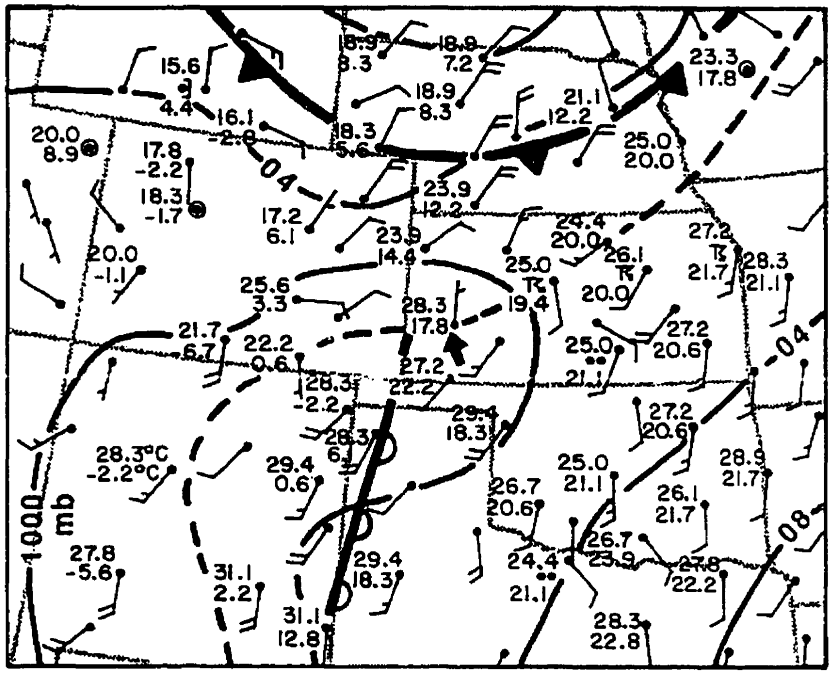

Figure 2.5. Surface analysis at 2100 UTC 16 May 1995. Temperature (°C), dewpoint temperature (°C), and wind speed and direction from selected stations are plotted (see Figure 2.4 for wind speed notation). Isobars (solid lines), trough (dashed line), dryline (scalloped line), and cold front are also indicated. Isobars have a contour interval of 4 mb. Black arrow denotes the position of surface observations from Garden City. (from Wakimoto et al. 1998)

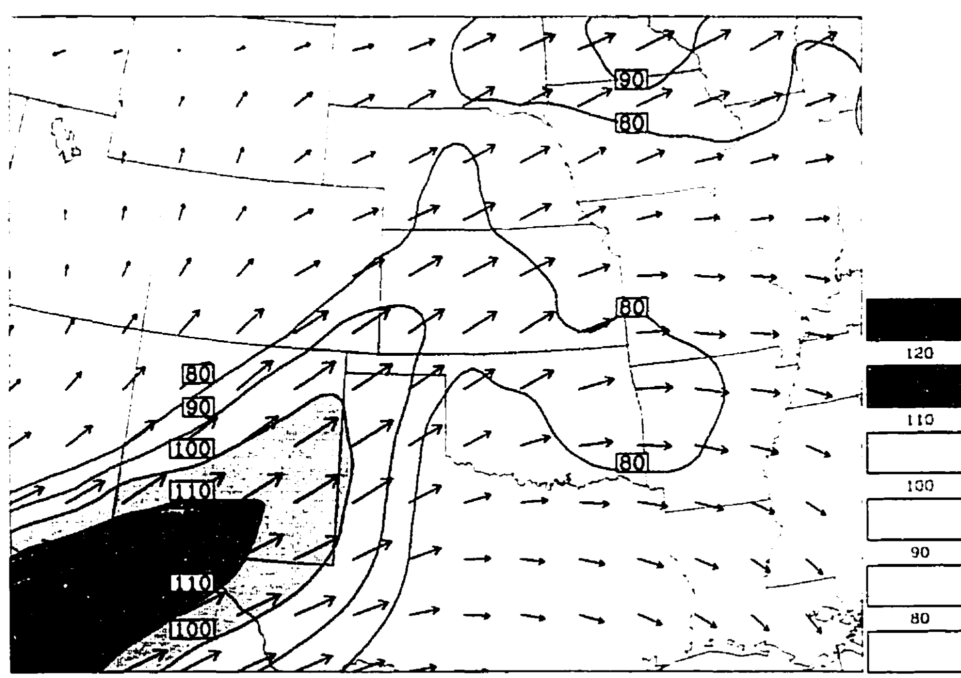

Figure 2.6. Analysed 250-hPa wind vector and wind speed (shaded contours) for 0000 UTC 17 May 1995. Only wind speeds greater than 80 knots are indicated, and with a contour interval of 20 knots.

2.3 Convective Activity over the VORTEX-95 Domain

2.3.1 Convection previous to the Garden City storm and the pre-existing outflow boundary

At approximately 1730 UTC, a small precipitating patch appeared in radar imagery roughly 110 km to the south of Dodge City. Over the following three and a half hours, this convective activity organized into a multicell storm as it traveled in a northeastward direction along a path situated just over 40 km to the southeast of Dodge City. Starting at 2034 UTC, a series of low-level radar scans originating from this site depicted the westward propagation of a fine-line echo from this system as it proceeded out of radar range to the northeast. A radar fine-line or clear-air echo appears in radar imagery as a long, narrow strip of moderate reflectivity that may be generated by a low-level disturbance, such as the outflow boundary or gust front of a severe storm (Wilson et al. 1994). A gust front is a surge of evaporatively cooled air that is produced when a strong downdraft is deflected by the Earth's surface into the horizontal (Bluestein 1993, section 3.4.6). As the outflow moves away from the source storm, it lifts small particles of dirt and insects into an area that is sufficiently concentrated to scatter radar energy. Since a gust front is confined to the boundary layer, the signal is most readily observed when the disturbance is close to the radar site. In this case study, the low-level boundary produced a more prominent echo in the 0.5° elevation angle reflectivity imagery as it approached Dodge City from the east. A surface mesoscale analysis by Markowski et al. (1998b) shows the position of the outflow boundary relative to the Garden City storm at 2300 UTC (Figure 2.7).

Markowski et al. (1998a,b) have hypothesized that this boundary may have influenced tornadogenesis within the Garden City supercell several hours after emanating from the previous convective system. Their argument follows from the establishment of a shallow, localized baroclinic zone by cold evaporative downdrafts which diverge away from a

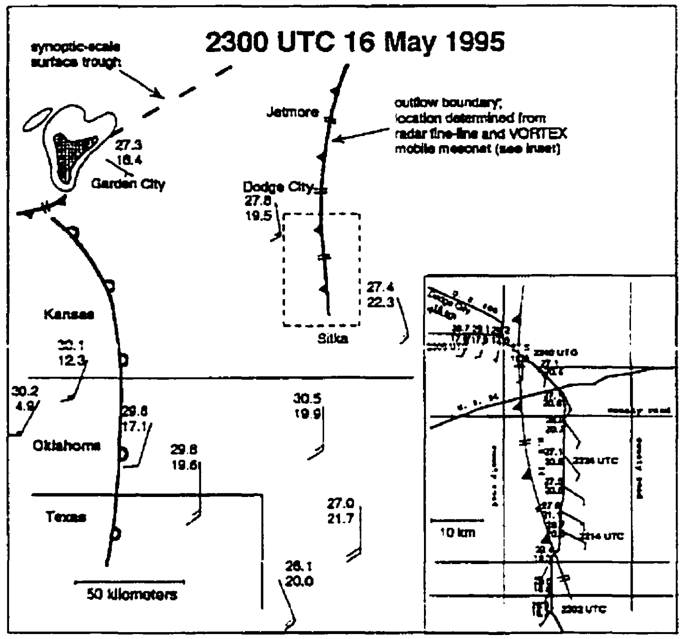

Figure 2.7. Surface mesoscale analysis for 2300 UTC 16 May 1995. Radar reflectivity contours of 30 dBZ and 50 dBZ (dBZ >50 shaded) denote the position of the Garden City storm. Outflow boundaries (lines with solid triangles and hashes), dryline (scalloped line), and surface trough (dashed line) are also indicated. Temperature (^{o}C), dewpoint temperature (^{o}C), and wind speed and direction are plotted at selected sites (wind speed notation same as in Figure 2.4). Observations from VORTEX mobile mesonet are shown in inset. (from Markowski et al. 1998b)

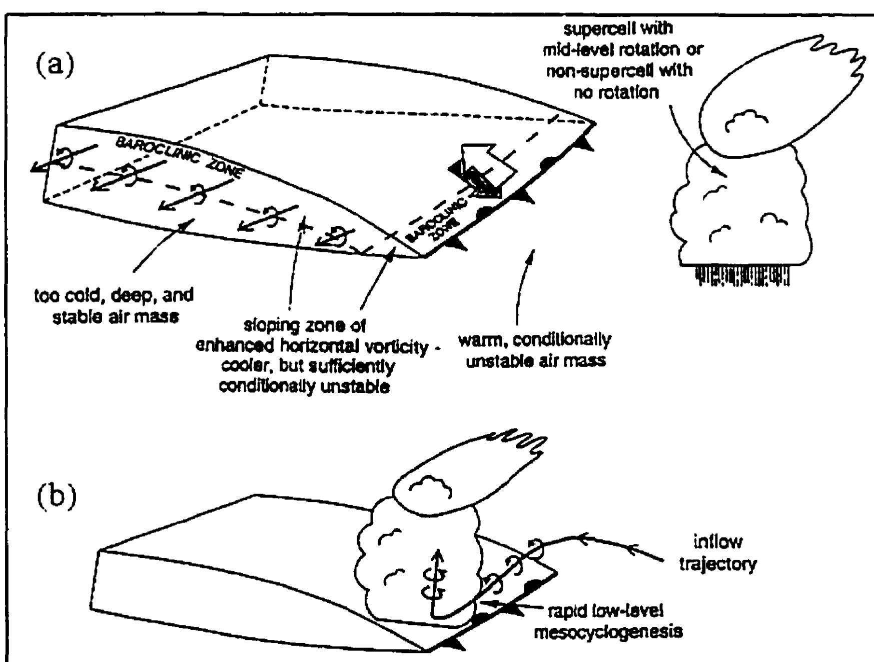

Figure 2.8. Conceptual model of an updraft-boundary interaction with resulting mesocyclogenesis. (from Markowski et al. 1998a)

storm at the surface and underrun warmer air aloft. The newly formed buoyancy gradient generates additional low-level horizontal vorticity, over and above that of the undisturbed environment, through solenoidal effects. Subsequently, the updraft of an approaching thunderstorm may utilize this vorticity enriched air mass in the creation of tornadoes via tilting and stretching, hours after the source storm has dissipated (Figure 2.8).

The idea that an updraft-boundary interaction may have implications in the forecasting of tornadoes has been alluded to in previous studies (Rasmussen and Blanchard 1998; Weaver and Nelson 1982; Maddox et al. 1980). In operational nowcasting of severe weather and in the issuance of public warnings, the occurrence of a mesocyclone is regarded as a precursor to supercell tornadogenesis. A mesocyclone is defined as a vertically oriented rotating column of air, approximately 10 km to 15 km in diameter, that possesses a vertical vorticity of greater than 0.01 s^{-1} (Bluestein 1993, section 3.4.8; Brooks et al. 1994). Unlike tornadoes, which are extremely difficult to identify in Doppler radar imagery (Burgess et al. 1993), mesocyclones are easily detected by a sharp gradient in radial winds. However, over-reliance on the signature of the mesocyclone and the absence of a one-to-one relation between mesocyclogenesis and tornadogenesis could lead to a high number of false-alarms (Brooks et al. 1994). Similarly, the overuse of the parameter SREH (storm-relative environmental helicity), which is a measure of the rotational character of the environment, may also lead to high false-alarm rates because of its erratic behavior in both space and time (Davies-Jones 1993). Observations have shown that only 30% - 50% of the supercells with a mesocyclone develop tornadoes (Burgess et al. 1993). Recent data suggests a lower percentage of 20% (Wakimoto et al. 1998). It is possible that the updraft-boundary interaction theory may provide the missing link between mesocyclogenesis and tornadogenesis. However, a vigorous test of this hypothesis is only possible through the application of a mesoscale model, which allows the presence of horizontal inhomogeneities in the initial conditions. Thus, in this real-data numerical study, we aim to determine the impact of the low-level outflow boundary of the previous convective system on tornadogenesis in the Garden City supercell.

2.3.2 *Garden City storm*

Shortly before 2200 UTC, low-level vertical motions punctured a degraded convective lid in an isolated area over southwestern Kansas. The subsequent release of nearly 3000 J kg^{-1} of CAPE led to the explosive intensification of a tornadic supercell. The sequence of satellite images in Figure 2.9 depicts the rapid growth of this storm as it propagated to the northeast along a surface trough. The dramatic wind shift and temperature drop at the Garden City surface station between 2300 UTC and 2330 UTC recorded the passage of the storm's gust front. Close to the time of the last image, the first tornado touched down about 10 km to the east-southeast of Garden City. Members of the VORTEX mobile ground crew and the NCAR P-3 aircraft observed the storm during this period, at which time they witnessed the formation of two mesocyclones and the successive spin-up of the F1 (Fujita 1981) scale tornado. Although VORTEX coverage terminated with the dissipation of this tornado, *Storm Data* reports indicate the formation of 3 additional twisters, with strengths ranging from F0 to F3, as the storm continued past Garden City (NCDC 1995). Radar imagery shows that by 0230 UTC 17 May, the structure of the Garden City storm had begun to deteriorate considerably.

The unparalleled observational data obtained by the VORTEX teams, who tracked the storm through its most critical stages of development, provides an incredibly detailed account of the complicated dynamical processes that occur within a tornadic supercell (Wakimoto et al. 1998; Wakimoto and Liu 1998). The following description of the textbook evolution of the Garden City storm follows from the radar imagery acquired at Dodge City.

At approximately 2230 UTC, the fast maturing thunderstorm split into left and right moving cells, with the left mover dissipating and the right mover intensifying in time. The 0.5° elevation angle reflectivity image at 2320 UTC displays two distinct entities, as well as other extremely interesting features (Figure 2.10). For instance, the right mover is characterized by a sharply defined hook echo at its most southern corner. This signature indicates the presence of dislocated updraft and downdraft columns, which are necessary for the development of a long-lived, violent supercell. The shape of the echo is the product of an intense updraft which allows little time for either precipitation to form or to

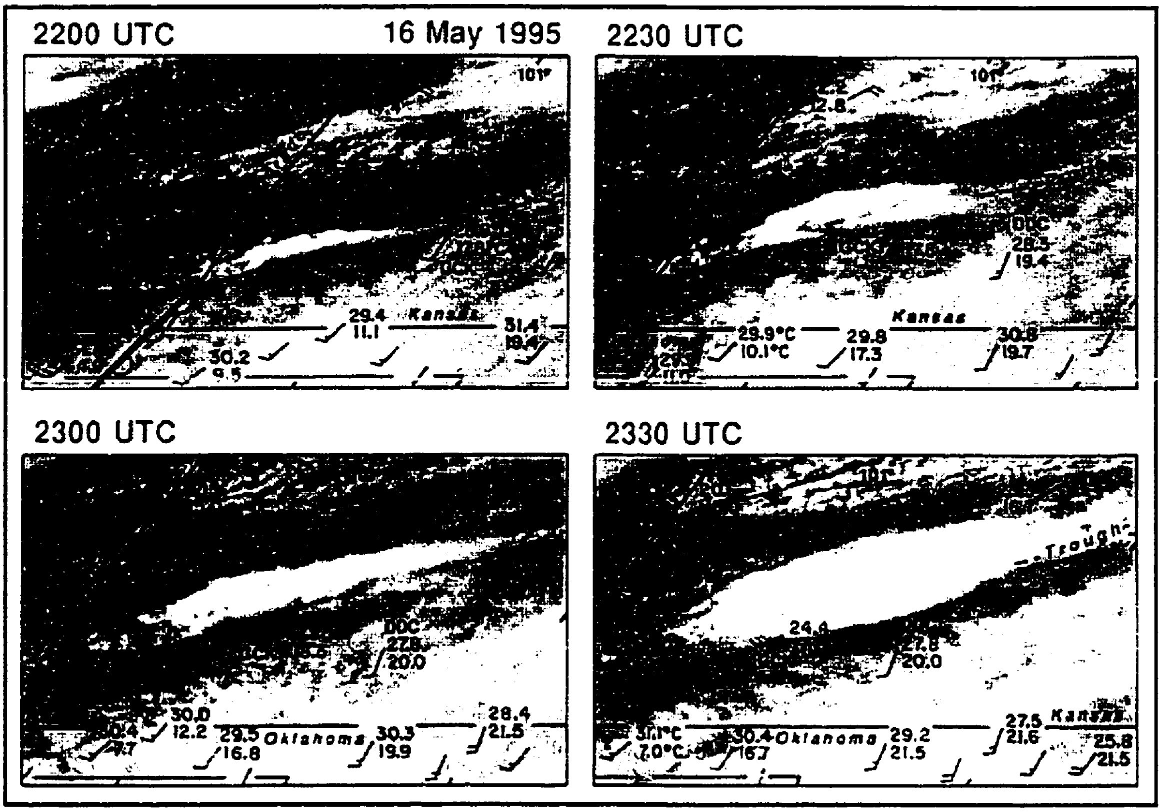

Figure 2.9. High-resolution visible satellite imagery with surface data superimposed at 2200 UTC, 2230 UTC, 2300 UTC, and 2330 UTC 16 May 1995. Temperature (°C), dewpoint temperature (°C), wind speed and direction for selected sites are shown (see Figure 2.4 for wind speed notation). Trough (dashed line), dryline (scalloped line), and state boundaries (solid lines) are also indicated. The identifiers GCK and DDC denote Garden City and Dodge City surface stations, respectively. Dodge City is also the location of a Doppler radar. (from Wakimoto et al. 1998)

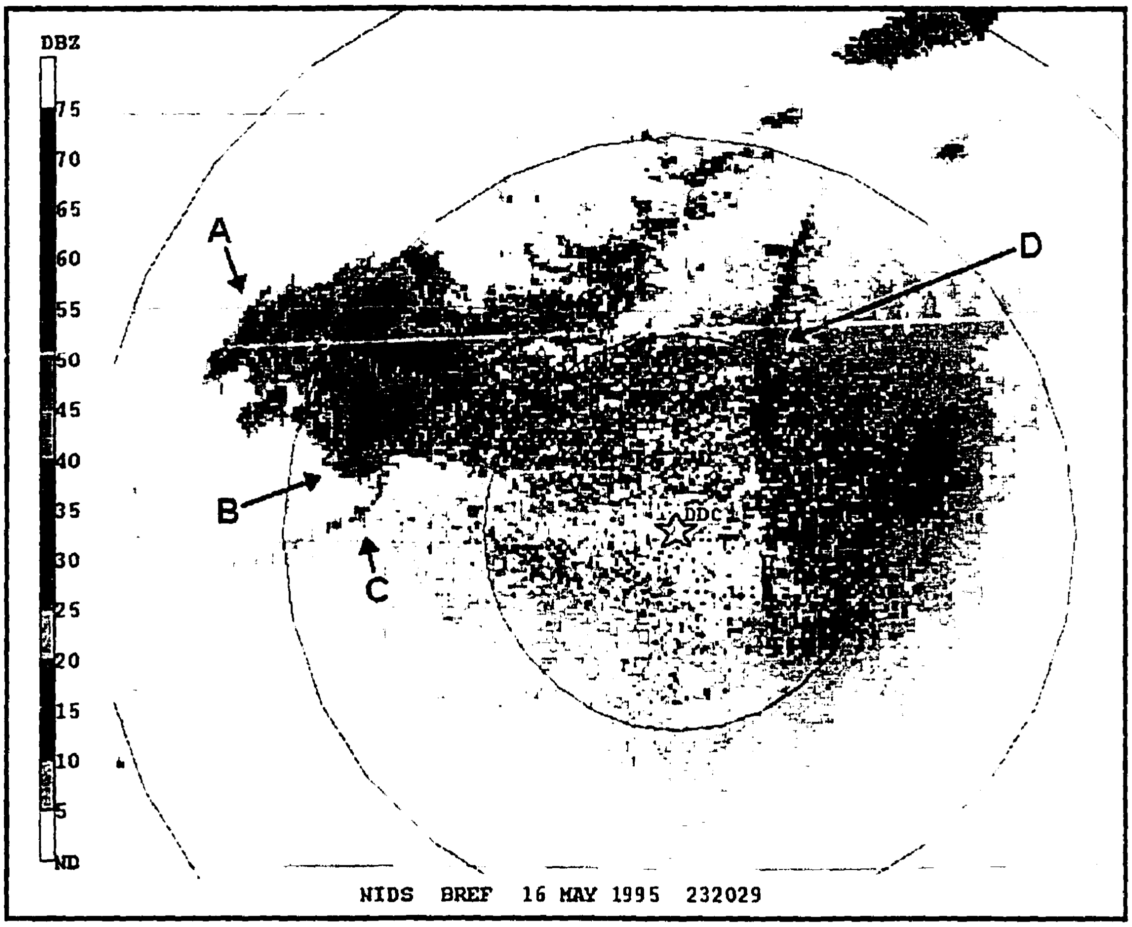

Figure 2.10. 0.5° elevation angle plan position indicator (PPI) scan of radar reflectivity from the Doppler radar located at Dodge City (DDC) at 2320:29 UTC 16 May 1995. The arrows extending from the positions A, B, C, and D indicate the left-moving cell, hook echo region, Garden City storm outflow boundary, and radar fine-line from previous convective system, respectively. The star denotes the location of the radar site, and the range rings are every 50 km.

fall into the column, hence, resulting in a minimal scattering of incident radar energy. Instead, the hydrometeors are carried into the downdraft column, thereby generating a much stronger return. Due to the high level of rotation within the storm, the two up and down columns essentially wrap around one another to give a hook shape to the echo.

Immediately south of the hook echo region, a fine-line associated with the storm's gust front is observed to propagate southeastward away from the updraft-downdraft core. Also at this time, the fine-line generated by the outflow boundary of the previous convective system is clearly identified 25 km to the east (and northeast) of Dodge City. However, this boundary is not yet within the proper theoretical range for it to influence the rotational character of the approaching supercell (Markowski et al. 1998a). Subsequent images show a rapid decrease in the distance between the Garden City storm and the pre-existing outflow boundary. Yet, the two features are only sufficiently close to interact with each other after the first two tornadoes had dissipated. Therefore, the supercell must have generated these twisters without any influence of the previous storm.

From this reflectivity image, the Garden City storm appears to have an areal extent of at least 60 km x 60 km in its most mature form. A Doppler image at the same time depicts the presence of a mesocyclone at precisely the same location as the hook echo region, with a speed difference in radial winds of 84 knots between neighbouring pixels (not shown). The placement of this mesocyclone agrees well with the theory that a common location for tornadogenesis is within the steepest horizontal gradient of vertical motion, that is, between the updraft and downdraft columns (Grasso and Cotton 1995; Brandes 1993).

For a more detailed description of the development of the mesocyclone and first tornado, the readers are referred to Wakimoto et al. (1998) and Wakimoto and Liu (1998). The following chapter introduces the mesoscale model that was employed to simulate the Garden City storm.

Chapter 3

Model Description

The simulations in this study were performed using version 3.2 of the Mesoscale Compressible Community (MC2) model, which was developed at Recherche en Prévision Numérique (RPN), a research division of the CMC. The description of the model given below follows Benoit et al. (1997).

3.1 Non-hydrostatic Dynamics

The MC2 limited-area atmospheric model is a three-dimensional fully compressible non-hydrostatic model which utilizes semi-implicit semi-Lagrangian time-stepping algorithms. To accommodate high-resolution simulations, MC2 solves the Navier-Stokes equations, which are sometimes referred to as the anelastic or fully compressible Euler equations, normally on a polar stereographic projection true at 60°N. The application of a semi-implicit type algorithm enables an efficient representation of fast propagating waves, such as acoustic waves, which are treated implicitly, while slow propagating waves are treated explicitly. The efficiency of the model is further enhanced by a semi-Lagrangian scheme, which permits the use of larger time steps by preserving numerical stability in the event that the Courant number exceeds unity. Spatial derivatives are discretized by finite differences on a three-dimensional staggered grid, which is arranged in the horizontal and the vertical according to an Arakawa C-grid and a Tokioka B-grid, respectively.

Orography is represented in the model by the use of Gal-Chen levels, which are terrain-following at the surface, but flatten in the horizontal with increasing height. An adjustment to the vertical coordinate allows arbitrary spacing of the vertical levels such that higher resolution may be applied to the lower atmosphere to better resolve the evolution of the planetary boundary layer (PBL). The top boundary of the model is characterized by a zero vertical velocity, and a sponge layer may be implemented over a distance below to dampen vertically propagating waves, thereby minimizing reflections off the rigid lid.

3.2 Model Physics

The MC2 is interfaced with the extremely versatile, community developed RPN physics package, which is shared by all of CMC's operational and research models. This set of parameterization schemes offers tremendous flexibility to the user through the availability of numerous selective options. Listed below are the primary components of the package.

The force-restore method is used to predict the land surface temperature from a heat budget, while the sea surface temperature is held constant throughout the integration. Surface evaporation over land is calculated using a soil moisture availability factor, which is specified in the initial conditions. Mixing within the PBL is parameterized by a prognostic equation for turbulent kinetic energy, and vertical transfers induced by turbulent motion are represented by vertical diffusion over the entire depth of the atmosphere.

Both the infrared and solar radiation parameterization schemes are fully interactive with clouds. That is, the effects of water vapour, carbon dioxide, ozone, and clouds are represented in the infrared radiation scheme, while the solar radiation scheme accounts for the same atmospheric elements, as well as Rayleigh scattering and multiple scattering.

The parameterization of gravity wave drag, which utilizes the variation in subgrid-scale orography to generate gravity waves, follows that of McFarlane (1987).

Grid-resolvable precipitation is simulated using Kong and Yau's (1997) explicit cold microphysics scheme. This parameterization includes both warm rain and ice-phase processes by solving explicitly prognostic equations for water vapour, cloud water, rain water, and ice particles. As for the treatment of subgrid-scale precipitation, several schemes are offered to the user including a modified version of the Kuo scheme (Mailhot 1994) and the Kain-Fritsch scheme (Fritsch and Chappell 1980; Kain and Fritsch 1993). As well, an optional routine is available to represent the process of shallow convection. This scheme accounts for thin, nonprecipitating cumuli, which are thought to play an important role in the atmospheric water cycle through the vertical flux of water vapour out of the boundary layer.

The algorithms that were employed to parameterize the processes of deep and shallow convection in our simulations of the Garden City storm case study will be described much more thoroughly in Chapter 4.

3.3 Nesting and Initialization

Since MC2 is a limited-area model, lateral and upper boundary conditions must be prescribed at every time step. To achieve this, nesting data sets are provided at regular time intervals, covering the entire integration, with a linear interpolation performed between consecutive sets of data to determine the appropriate nesting values at each individual time step. This data is usually obtained from a low-resolution global or hemispheric model, although it may originate from an objective analysis of observations.

An especially attractive feature of MC2 is its self-nesting capability, which enables the model to utilize output from a previous run as nesting data for a subsequent application at a higher resolution. This process of cascading is useful when the objective is to run the model at a high resolution, however, the initialization data is only available at a coarse resolution. The first simulation by MC2 (i.e. with the coarsest grid) is usually configured to have the same grid-spacing as that of the source used for initialization such that a smooth transition into the MC2 system is made.

At the end of every time step, horizontal and vertical nesting of the given data is performed over a sponge zone to damp spurious wave reflections off the boundaries (Thomas et al. 1998). Within this layer, model values are adjusted to more closely match the newly specified boundary values, with a greater weight applied to those grid points that are nearest to the boundary.

The description above primarily pertains to the operation of MC2 in simulation mode, which is the most common method of application. In this mode, the model is somewhat forced towards a particular solution during the integration by a constant supply of known or previously forecast boundary values. In contrast, the model may also be operated in forecast mode, whereby data is only provided at the time of initialization. Therefore, the model does not benefit from continual updates by regularly supplied boundary conditions.

For this case study, MC2 was run in simulation mode with all of the necessary initial and boundary conditions extracted from archived CMC analysis data sets. This data was produced by the CMC's regional data assimilation system (Chouinard et al. 1994), and is available every six hours on a 35 km horizontal resolution grid. The initial and boundary conditions required to operate MC2 consist of the meteorological fields of geopotential height, temperature, specific humidity (or dewpoint depression), and horizontal winds, which are available on the following isobaric levels: 1000, 925, 850, 700, 500, 400, 300, 250, 200, 150, 100, 70, 50, 30, 20, and 10-hPa. Also for initialization, it is necessary to specify surface characteristics that are defined by orography, land-sea mask, surface roughness, and launching height (a measure of subgrid-scale orography), which are not time-dependent, and land temperature, sea surface temperature, deep ground temperature, soil moisture availability, snow cover, ice cover, and surface albedo, which are obtained from a monthly climatology or current analysis. Finally, the model was run on the NEC SX-4 supercomputer located at CMC.

Many experimental simulations were conducted to determine the optimal configuration of MC2 for the Garden City storm case study. Modifications to the model based on these sensitivity studies are discussed in the following chapter. However, a description of such details as the initialization time, the size, placement, and resolution of the domain, and the time step for all simulations is reserved until Chapter 5. It is also in this chapter that the control run results are presented and analysed, and a more traditional sensitivity study is performed.

Chapter 4

Modifications to the Model from Sensitivity Studies

4.1 Choice of Convective Parameterization Scheme

The process of deep convection plays a critical role in the evolution of the large-scale environment through the vertical transport of heat, moisture, and momentum. However, it is also a subgrid-scale process in most numerical models. Hence, over the past twenty-five years, a wide variety of algorithms have been formulated to simulate the development of penetrative cumulus clouds in both research and operational forecast models. From a broad perspective, these convective parameterization schemes (CPSs) differ mainly in their closure assumptions and scale considerations. More specifically, considerable differences exist in the mechanisms employed to initiate convective precipitation and in the subsequent vertical redistribution of heat, moisture, and mass. Examples of CPSs include the Arakawa-Schubert scheme (Arakawa and Cheng 1993), the Kuo scheme (Kuo 1974; Raymond and Emanuel 1993), the Betts-Miller scheme

(Betts and Miller 1993), and the Kain-Fritsch scheme (Kain and Fritsch 1993), which is a more sophisticated version of the Fritsch-Chappell scheme (Fritsch and Chappell 1980).

The challenge confronted by these schemes is that the development of unstable clouds is perhaps the most perplexing of all subgrid-scale processes (Emanuel and Raymond 1993; Rogers and Fritsch 1996; Molinari and Dudek 1992). Unfortunately, the proper parameterization of convective precipitation is essential to a successful simulation or forecast. In particular, the CPS possesses a tremendous amount of control over the accuracy of the model solution due to the simulation's extreme sensitivity to the convective trigger function (Stensrud and Fritsch 1994b; Kain and Fritsch 1992). The convective trigger function is defined as the complete set of criteria used to determine the location and timing of deep convection in numerical models (Kain and Fritsch 1992).

The suitability of a CPS for a particular numerical simulation is primarily dependent upon the character of the convection that is to be reproduced. This, in turn, is a function of scale, latitude (or climate), and the mechanism responsible for initiation, all of which are mutually dependent. Although more artificial, another very important factor is the horizontal resolution of the simulation. Until recently, the most widely used CPS was the Kuo scheme, mainly because the principles that this approach was founded on to generate implicit rainfall are most applicable at low resolutions (i.e. 50 km or greater). As the average mesh size has decreased with increasing computer power, newer schemes have become more popular.

In the Kuo scheme, convective clouds form in regions that are subject to large-scale, low-level moisture convergence in the presence of deep conditional instability. Converging winds in the lower atmosphere provide the lifting necessary to generate precipitation, however, they are usually associated with synoptic weather systems, such as cyclones. That is, this CPS relies on large-scale environmental forcing to initiate convection. Therefore, this approach is not well-suited for the simulation of small-scale convective systems, such as supercell thunderstorms, since they often appear in areas that are characterized by an absence of well-defined large-scale forcing. Also, in the initiation of these singular systems, it is essential that only a limited number of grid points satisfy the convective trigger function, which is not likely in the Kuo scheme.

These claims were verified by an attempt to simulate the numerous mesoscale convective outbreaks on 16 May 1995 with the Kuo scheme and a mesh size of 35 km. After several hours of integration, moderate amounts of convective precipitation had been generated, but over wide regions of the central plains, rather than in select localities as observed. In particular, a broad area of the VORTEX-95 operating domain was subject to implicit rainfall, without any indication of individually evolving convective systems. Thus, there was no possibility of analysing a numerical reproduction of the Garden City storm with the Kuo scheme.

As an alternative representation of unstable clouds offered in MC2, the Kain-Fritsch scheme is founded on the plume cloud-model concept (Kain and Fritsch 1990), which is far more appropriate for the simulation of small-scale, cellular convective systems. Whereas the Kuo CPS relies on large-scale dynamics to initiate deep convection, the Kain-Fritsch scheme employs a trigger function that is sensitive to positively buoyant low-level air parcels at individual grid points. According to Fritsch and Kain (1993), this scheme is designed for model mesh sizes that are fine enough to resolve the environment of individual cumuli (i.e. 10 km - 30 km).

The success of the Kain-Fritsch scheme in the simulation of real-data cases is well-documented (Molinari and Dudek 1992; Wang and Seaman 1997; Kuo et al. 1996), and it may be attributed to the scheme's closure assumption, which states that the convective process is assumed to remove the CAPE of a grid element within an advective time period. Thus, the intensity of parameterized convection is proportional to the degree of convective instability; a property which holds for deep convective processes in the real atmosphere. The convective trigger function for the Kain-Fritsch CPS follows from the original scheme developed by Fritsch and Chappell (1980). At each grid point a mixed-layer parcel of air, whose temperature and moisture content reflect the lowest 60-mb, is lifted to its LCL where it is checked for buoyancy. A temperature perturbation, ΔT, related to the model resolvable-scale vertical velocity at the LCL, w_{LCL} (cm s^{-1}), by the formula

$$\Delta T = C_1 w_{LCL}^{1/3}, \tag{4.1}$$

where C_1 (^{o}C s$^{1/3}$ cm$^{-1/3}$) is a unit number, is added to the temperature of the saturated updraft (i.e. the parcel temperature at the LCL), T_{LCL}^{u}. If this sum is greater than the grid element temperature at the LCL, T_{LCL}, then the air parcel is positively buoyant. Otherwise, the air parcel is stable, and another mixed-layer parcel representing the 60-mb layer 50 mb higher than the previous layer is lifted and checked for buoyancy. This process continues until a level 300 mb above the ground where if the parcel is still stable, no convection occurs and the algorithm considers the next grid point.

Algebraically, the determining criteria of the Kain-Fritsch trigger function appears as

$$\begin{aligned} T_{LCL}^{u} + \Delta T &> T_{LCL}, \qquad \textit{buoyant} \\ T_{LCL}^{u} + \Delta T &\le T_{LCL}, \qquad \textit{stable.} \end{aligned} \tag{4.2}$$

In the event that a buoyant air parcel is found, calculations commence to determine whether the parcel's layer-averaged upward motion is sufficient to overcome the negative buoyancy of the grid-point sounding to reach its LFC. Should this occur, the Kain-Fritsch scheme adjusts the atmosphere so that 90% of the CAPE is removed within a specified convective timescale. Essentially, updrafts and downdrafts eliminate the instability by exchanging high equivalent potential temperature values of the lower atmosphere with lesser values from the atmosphere above cloud base (Kain and Fritsch 1998).

Beyond the convective trigger function, the suitability of this CPS for the simulation of cellular convective systems is also demonstrated by its realistic representation of many of the processes that occur within a developing cumulonimbus. These include moist downdrafts, simultaneous updrafts and downdrafts, compensating environmental vertical motions outside the convecting column, entrainment and detrainment at cloud edge, and evaporation of convectively produced condensate.

As expected, simulations of the Garden City storm case study conducted with the Kain-Fritsch scheme at both 35 km and 18 km horizontal resolution produced more accurate results than those obtained using the Kuo scheme. In the preliminary 18 km runs, most organized patterns of precipitation were simulated reasonably well across the entire model domain. Although neither the Garden City supercell, nor its neighbouring storm were captured by this version of the model, the promise offered by the Kain-Fritsch scheme in reproducing these two isolated systems prompted a careful investigation of model output and VORTEX data. Consequently, several factors responsible for their absence were identified. The modifications that were necessary to trigger the Garden City storm are discussed in the next section, and for the neighbouring storm in Chapter 5. These adjustments were developed using a mesh size of 18 km.

4.2 Modifications to the Kain-Fritsch Scheme

4.2.1 Implementing an additional convective trigger function

In addition to providing mesoscale models with an excellent method with which the extremely important, yet extremely complex, subgrid-scale process of deep convection may be accurately parameterized, the Kain-Fritsch scheme also offers tremendous flexibility. In particular, additional trigger functions may be easily incorporated into the algorithm to work alongside the conventional trigger devised by Fritsch and Chappell, while taking advantage of a sophisticated treatment of cumulus development.

In the numerical modelling of some convective events, the conventional trigger is not sufficiently sensitive to all of the factors that force deep convection in the real atmosphere (while being overly sensitive to many others). For example, when applied to the 16 May 1995 case study, the Fritsch-Chappell trigger was unable to generate the Garden City supercell. Although the simulated atmosphere overlying the VORTEX-95 operating domain was properly conditioned for the outbreak of severe convective activity, an absence of strong large-scale forcing precluded the vertical velocities necessary to satisfy the buoyancy-based criteria of the Kain-Fritsch scheme. It has been recognised that a deep, convectively unstable atmosphere, in which the dominant lifting mechanisms are organized on the mesoscale, is especially difficult to simulate (Stensrud and Fritsch 1993; Stensrud and Fritsch 1994a,b; Kain and Fritsch 1992; Rogers and Fritsch 1996; Hong and Pan 1998). This may be primarily attributed to inadequate convective trigger functions. Stensrud and Fritsch (1994b), Rogers and Fritsch (1996), and Kain and Fritsch (1992) have stated that the correct initiation of the convective process is as important as the realism of the CPS.

Thus, a major goal of mesoscale modelling research has been to formulate more accurate mathematical trigger functions. In a modelling study of an environmental state much like that of the Garden City storm case study, Stensrud and Fritsch (1994a,b) noted that deep convection was initiated only in regions where lifting associated with mesoscale features, such as an outflow boundary or dryline, was able to remove the capping inversion so that parcels could reach their LFC. In severe weather forecasting, it is extremely difficult to correctly predict the timing and location of a sufficiently degraded convective lid that would allow explosive cumulus development. However, in mesoscale modelling, this enormous responsibility is placed upon the shoulders of mathematical relationships, which must predict the occurrence of deep convection using simple approximations of the subgrid-scale forcing. Thus, in an effort to better parameterize mesoscale forcing, Stensrud and Fritsch introduced a convective trigger function that is sensitive to boundary layer instabilities. This trigger function is activated only when the model boundary layer is convective and the parcel LCL is below the boundary layer lid. Above the top of the boundary layer and in regions where this trigger is not satisfied, the Fritsch-Chappell trigger is employed.

Essentially, the boundary layer trigger function works as follows. In calculating the temperature perturbation, an air parcel at the LCL is assigned upward momentum that is related to the estimated vertical velocity of a parcel in a convective boundary layer. This free convection scaling velocity, w^* (Stull 1988), is proportional to the height of the boundary layer inversion top, z_i, and the surface buoyancy flux, $\left(\overline{w'\theta_v'}\right)_s$, by the equation

$$w^* = \left[\frac{g z_i \left(\overline{w'\theta_v'}\right)_s}{\overline{\theta}_v}\right]^{1/3}, \tag{4.3}$$

where g is the acceleration due to gravity and θ_v is the virtual potential temperature. Thus, the buoyancy of the air parcel at its LCL still determines whether or not it will reach its LFC.

To gauge the vulnerability of the environment in the Garden City storm simulation to this new trigger function, the boundary layer instability was quantified by the dimensionless expression

$$Z/L, \tag{4.4}$$

where Z is the boundary layer depth and L is the Monin-Obukhov length. The latter variable is a measure of the surface sensible heat flux, and is negative for a flux from the surface into the lower troposphere. The areas where Z/L is large and negative represent free convective boundary layers, which are commonly responsible for the initiation of penetrative convection (Rogers and Fritsch 1996).

In the Garden City storm case study, the representation of boundary layer forcing in the Kain-Fritsch scheme proved to be extremely important for the initiation of the Garden City supercell. A plot of Z/L for 2200 UTC 16 May 1995 shows that the area to the west and the northwest of Garden City was highly vulnerable to the conditions of this new trigger (Figure 4.1). Additionally, this local minimum was situated very close to the area where a dryline and upper-level jet streak were positioned near the time of inception of the observed thunderstorm. As will be presented in Chapter 5, the boundary layer trigger function initiated deep convection in this region at 2159 UTC, which is approximately the same time that the observed Garden City storm emerged. It is important to note that with the second trigger function, MC2 was able to initiate convection over southwestern Kansas without compromising the accuracy of the simulation over the remainder of the model domain. However, the modelled storm still did not develop as that observed by VORTEX due to interference from nearby spurious convective cells. The next subsection describes the technique employed to eliminate these unreal cells and further improve our simulation.

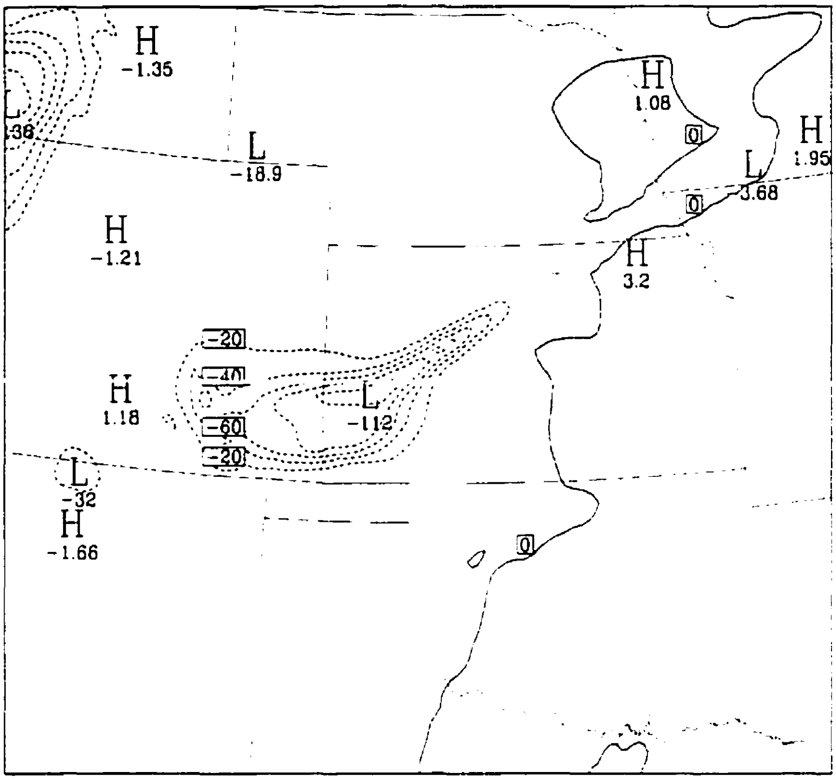

Figure 4.1. Plot of *Z/L* over the central plains for 2200 UTC 16 May 1995. A large negative value indicates a free convective boundary layer.

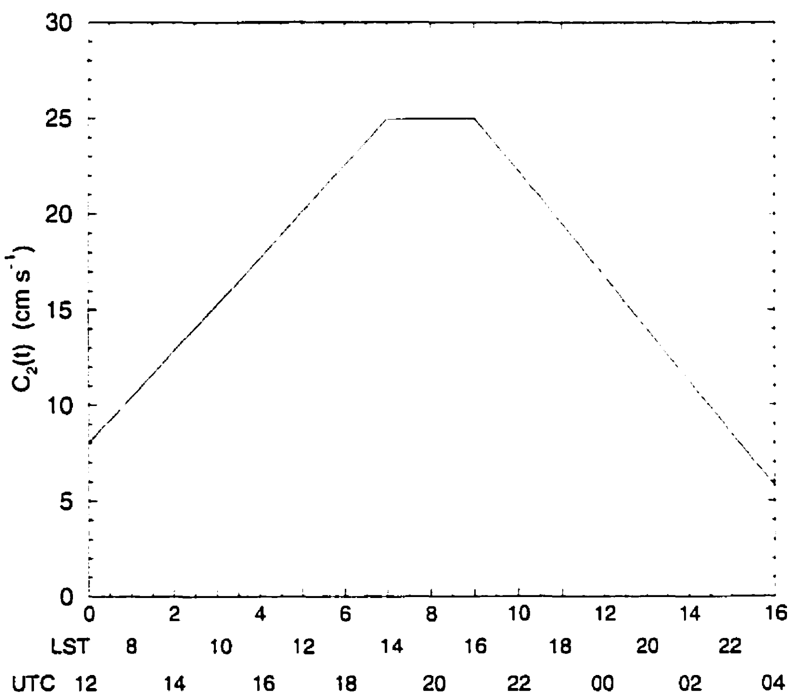

Figure 4.2. Diurnal distribution of the suppression parameter, $C_2(t)$, from Equation (4.5). Filter is shown as a function of model hour, local standard time (LST), and Universal Time Coordinate (UTC).

The successful implementation of the boundary layer trigger function follows that of Stensrud and Fritsch (1994b), who noted that the proper timing of convective initiation in environments where large-scale forcing is weak relies heavily on the inclusion of boundary layer forcing in a CPS. However, another modelling study of the 16 May 1995 case by Hong et al. (1998) reiterates the complexity involved in simulating an environment in which mesoscale forcing dominates over that of the large-scale. In their investigation, Hong et al. also employed a convective trigger function that was sensitive to boundary layer processes. However, at 25 km resolution their model was unable to capture the Garden City storm. A more thorough comparison of our results with those of Hong et al. (1998) will be presented in Chapter 5.

4.2.2 Suppression of spurious convection

An integral part of cumulus parameterization schemes concerns the employment of free parameters, which are necessary to link the model resolved variables to the unresolved process of deep convection. The actual value of these parameters in nature is unknown, therefore, they must be prescribed in a subjective manner according to theory or sensitivity studies. However, this has led to criticism of CPSs since simulations are remarkably sensitive to the values that are assigned to each parameter (Molinari and Dudek 1992; Kain and Fritsch 1992).

One such parameter was introduced to the Fritsch-Chappell scheme in the seminal study by Zhang and Fritsch (1986) to suppress the spurious initiation of convection. The authors noted that in the original Fritsch-Chappell trigger function, the extremely important calculation of the temperature perturbation does not account for diurnal variability (see Equation 4.1). However, it is obvious from observations that daytime heating plays a critical role in the initiation of deep convection, specifically by conditioning a well-mixed PBL so that it is more vulnerable to mesoscale forcing.

The initiation of unreal convection can be extremely detrimental to the accuracy of a simulation since it removes the convective instability of the local atmosphere, and essentially denies the means by which the correct convective cells are to be generated. Hence, a time-dependent parameter, $C_2(t)$, was implemented to limit spurious convection, which is often triggered by model gravity waves in the afternoon hours when the PBL is well-mixed, but environmental forcing is weak. With the addition of this filter function, the temperature perturbation equation becomes

$$\Delta T = C_1 \left[w_{LCL} - C_2(t) \right]^{1/3}. \tag{4.5}$$

The primary effect of this parameter is to reduce the vertical momentum of an air parcel at its LCL, thereby decreasing its ability to overcome negative buoyancy and reach its LFC. However, if C_2 is too restrictive, deep convection may be suppressed to such a large degree that grid elements become completely saturated. This, in turn, will activate the explicit parameterization scheme and numerical grid-point storms may develop (see Zhang et al. 1988). This phenomena refers to the unstable growth of disturbances on the smallest resolvable scales of the model (Molinari and Dudek 1992), and it occurs when saturation is reached in the presence of convective instability. Hence, the purpose of an implicit cloud scheme is to eliminate potential instability before a saturated state is attained.

With this in mind, a series of sensitivity tests were conducted to determine the optimal distribution of C_2 for the Garden City storm case study. Consequently, it was discovered that the diurnal variation used by Zhang and Fritsch in their simulation of the Johnstown Flood case also worked best in our simulation (see Figure 4.2). The addition of this parameter and the boundary layer trigger function to the Kain-Fritsch scheme were crucial for the proper initiation of the Garden City storm in the weakly-forced environment of 16 May 1995.

4.3 The Effect of Shallow Convection

In the real atmosphere, small-scale non-precipitating cumuli transport a considerable amount of moisture from the boundary layer into the lower troposphere. To minimize the tendency of models to excessively moisten the PBL, below a capping inversion which underlies a dry atmosphere, shallow convective parameterization schemes have been formulated (Mailhot 1994). One such scheme that is optional in MC2 is that of Geleyn (1987), which modifies the gradient Richardson number, used in the PBL scheme, according to the severity of the moisture gradient in the inversion layer to enhance vertical diffusion (Mailhot et al. 1998).

To determine the importance of shallow convection in the simulation of convective activity on 16 May 1995, a number of experiments were conducted at 35 km resolution. After running MC2 for several hours with the Kain-Fritsch CPS and the Geleyn scheme activated (SHALON experiment), deep convection was not initiated as extensively as that shown by the observational data. Moreover, there was substantially less convective activity over the central plains at ten hours of integration in this simulation than in an experiment with no shallow convection (SHALOFF experiment). Essentially, the Geleyn scheme acts to warm and moisten the atmosphere immediately above the PBL. In doing so, the Kain-Fritsch convective trigger function (Equation 4.2) was altered in a manner unfavorable for the initiation of deep convection.

Additionally, the inclusion of shallow convection in this case had a profound effect on the evolution of the surface temperature. In the SHALON experiment, the surface temperature increased at a slower rate during the daylight hours, and this was subsequently translated to the lowest layers of the atmosphere. This may be attributed to a number of factors including the change in Richardson number and relative humidity, which in turn modifies the vertical diffusion coefficient and diagnostic clouds, respectively. Consequently, the radiative forcing at the surface is influenced by shallow convection. Figure 4.3 shows a comparison of the analysed surface potential temperature field[1] to the simulated fields when shallow convection was both included and excluded after ten hours of integration. Since orography can produce a misleading analysis of surface temperature, potential temperature was used for this comparison. From these plots, it is clear that the SHALOFF experiment produced a much better simulation of the

[1] MAPS (Mesoscale Analysis and Prediction System) surface analysis available every hour at a standard resolution of 60 km from NOAA/FSL (Forecast Systems Laboratory).

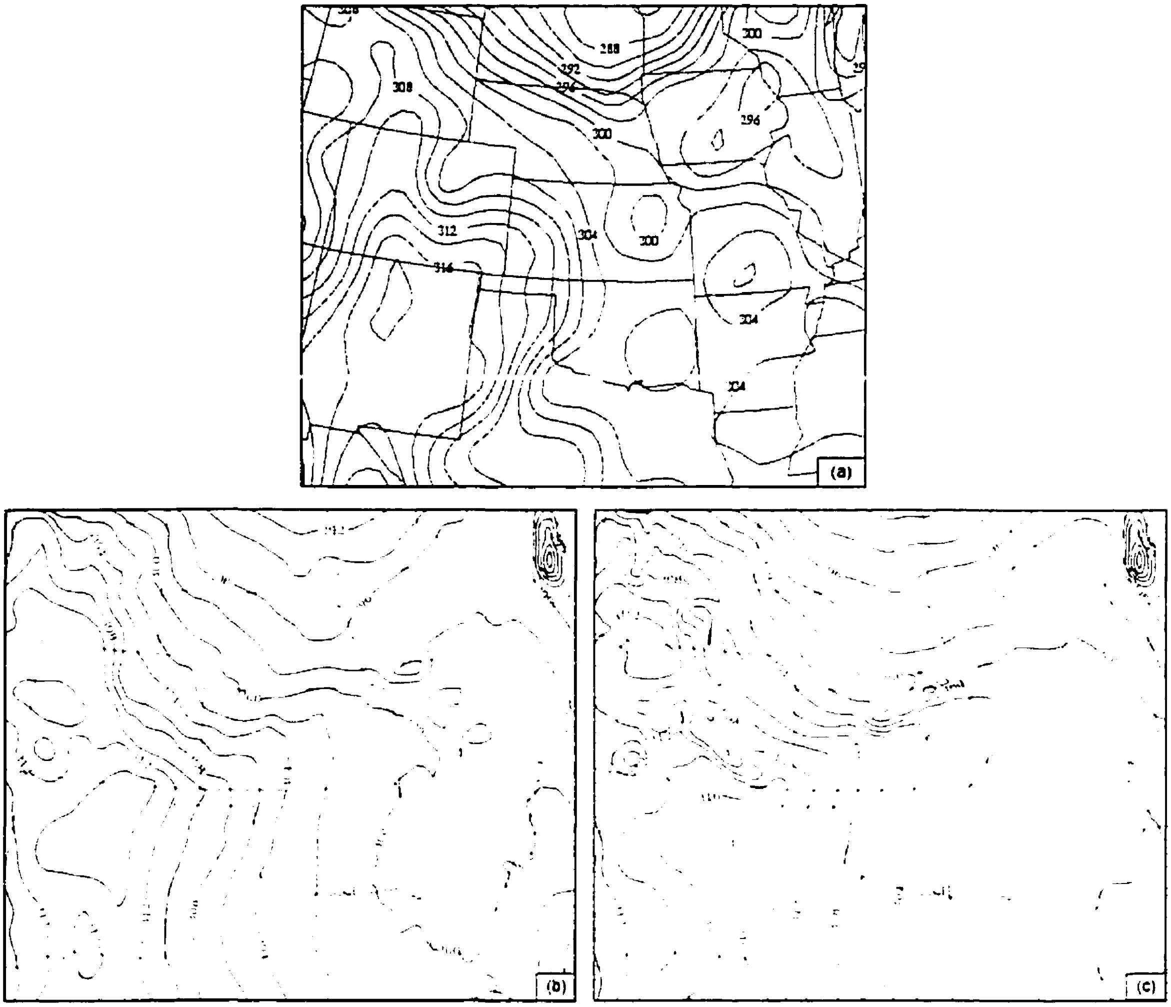

Figure 4.3. Surface potential temperature (K) (solid contours) for 2200 UTC 16 May 1995 from MAPS surface analysis (a), SHALON experiment (b), and SHALOFF experiment (c). Contour interval is 2 K.

surface temperature over the central plains. Of particular significance to our study, surface temperatures over southwestern Kansas were more than 4 °C warmer in the SHALOFF experiment than in the SHALON experiment at the approximate time of initiation of the Garden City storm.

Referring to Figure 4.3 (c), narrow streaks of relatively cold potential temperatures are depicted over the Colorado Rocky Mountains and northern Kansas. These cold-pool pockets are generated by evaporative downdrafts of Kain-Fritsch triggered deep convective cells. These streaks are not evident in the run with shallow convection activated (Figure 4.3 (b)) since deep convection was not nearly as extensive in this simulation, and are absent from the surface analysis due to a coarse resolution. (The cold pocket over Lake Michigan in frames (b) and (c) stems from initial conditions.)

Thus, although the Geleyn scheme is often employed to more properly simulate the atmospheric water cycle, it did not produce a more accurate simulation in this case. Deep convection was suppressed and a poor reproduction of the low-level temperature fields over the VORTEX-95 operating domain was obtained. Consequently, for all other model runs that are discussed in this thesis, the Geleyn scheme was not activated.

Chapter 5

Model Results

5.1 Model Specifications

The basic model features and parameter specifications that were utilized to obtain the numerical output presented and analysed in subsequent sections are now described. An accurate simulation was first obtained with MC2 at a horizontal resolution of 35 km, after which a cascade was performed down to 18 km resolution. For both mesh sizes, the model was initialized at 1200 UTC 16 May 1995. As is normally done, the first simulation was executed with a grid-spacing equivalent to that given by the initial conditions, which for our study were derived from the CMC's regional data assimilation system at 35 km resolution. Boundary conditions were extracted from the same source every six hours.

In achieving a proper simulation at the coarse resolution, several experiments were conducted to determine the optimal configuration of MC2 for the Garden City storm case study. A greater computational efficiency was attained while conducting these sensitivity tests since the employment of a larger mesh size allowed the use of a longer time step. The most important conclusions regarding the setup of MC2 from these experiments concerned the choice of cumulus parameterization scheme and the application of shallow convection.

For these preliminary simulations, a time step of 300 s was applied over an eighteen hour integration period. The domain covered most of North America and the eastern Pacific Ocean with dimensions of 195 x 190 grid points, and an orographic resolution of 35 km (Figure 5.1). A model depth of 25000 m was discretized by twenty-five Gal-Chen levels, and a 6000 m absorption layer extended below the rigid lid. Other specifications consist of a gravity wave drag parameterization (McFarlane 1987), a fully interactive solar radiation scheme (Fouquart and Bonnel, 1980), which was applied every six timesteps, and the explicit microphysical scheme of Kong and Yau (1997).

After it was determined that the best setup for MC2 included the Kain-Fritsch CPS and no representation of shallow convection, a 35 km simulation was conducted over the period 1200 UTC 16 May to 0600 UTC 17 May 1995, with output specified every three hours. An analysis of the resulting solution revealed a subjectively accurate reproduction of the synoptic-scale flows that were observed over the continental U.S.. In addition, the important mesoscale features discussed in Chapter 2 were captured by the model. Consequently, this output was used to derive the lateral boundary conditions that were required to perform a higher resolution simulation at 18 km grid spacing.

A 210 x 180 grid point domain, centred over the state of Kansas, was employed for this cascade (Figure 5.1). The model was run from 1200 UTC 16 May 1995 for sixteen hours with a time step of 60 s. Orographic detail remained at 35 km resolution, and a 25000 m model depth with twenty-five vertical levels was again applied. The 18 km run was supplied with boundary conditions every three hours, as opposed to every six hours for the 35 km simulation. Output was specified every hour to adequately resolve the evolution of the Garden City storm, which had a lifetime of approximately four and a half hours. The model setup for the 18 km simulation was very similar to the final 35 km run, however, to generate the Garden City storm, it was necessary to introduce the boundary layer trigger function of Stensrud and Fritsch (1994b) and the perturbation filter function of Zhang and Fritsch (1986), as discussed in the previous chapter. The basic model properties that were implemented to obtain the control run (CONTROL) are summarized in Table 5.1.

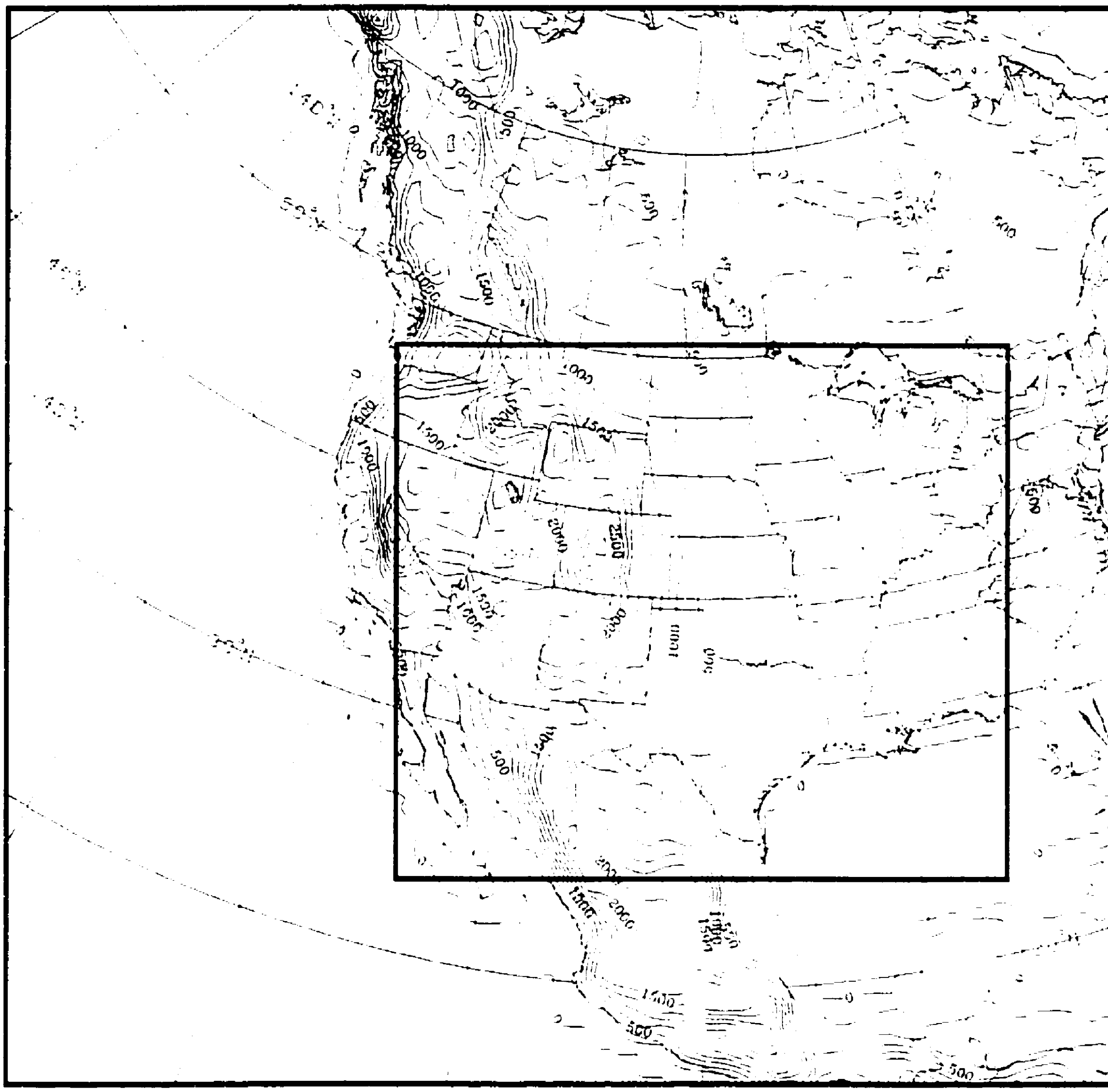

Figure 5.1. 35 km domain (outer box) and 18 km domain (inner box) with orography contoured every 250 m.

Table 5.1. Summary of MC2 properties in control simulation.

Horizontal grid	210 x 180, 18 km resolution
Orographic relief	35 km resolution
Model depth	25000 m
Vertical levels	25 Gal-Chen levels
Time step	60 s
Integration period	1200 UTC 16 May to 0400 UTC 17 May 1995
PBL scheme	based on a prognostic equation for turbulent kinetic energy (Benoit et al. 1989)
infrared radiation scheme	effects of H_2O, CO_2, O_3, and clouds represented (Garand and Mailhot 1990)
solar radiation scheme	accounts for H_2O, CO_2, O_3, and cloud effects, as well as, Rayleigh scattering and multiple scattering (Fouquart and Bonnel 1980); called every 15 time steps
gravity wave drag parameterization	variation in subgrid-scale orography excites gravity waves (McFarlane 1987)
grid-scale condensation	explicit cold microphysics (Kong and Yau 1997)
convective parameterization	Kain-Fritsch (Kain and Fritsch 1993)

5.2 Control Run

5.2.1 Modelled environment over the central plains

Since our primary objective was to simulate a small-scale convective event, the validation of CONTROL was primarily based on comparisons of modelled surface data, vertical atmospheric profiles, and precipitation patterns with station observations and radar imagery. Thus, an intensive quantitative validation of large-scale fields from the 18 km resolution model run was not performed, however, we insisted upon a subjectively accurate simulation of the synoptic environment, which captured the proper conditioning of the atmosphere over the central plains prior to the development of the Garden City storm. As a demonstration of this, the simulated 500-hPa geopotential height, temperature, and wind fields after twelve hours of integration are compared with those from the CMC analysis (Figure 5.2). All three variables match quite closely over the entire model domain, with the exception of the depth of the cut-off low now centred over

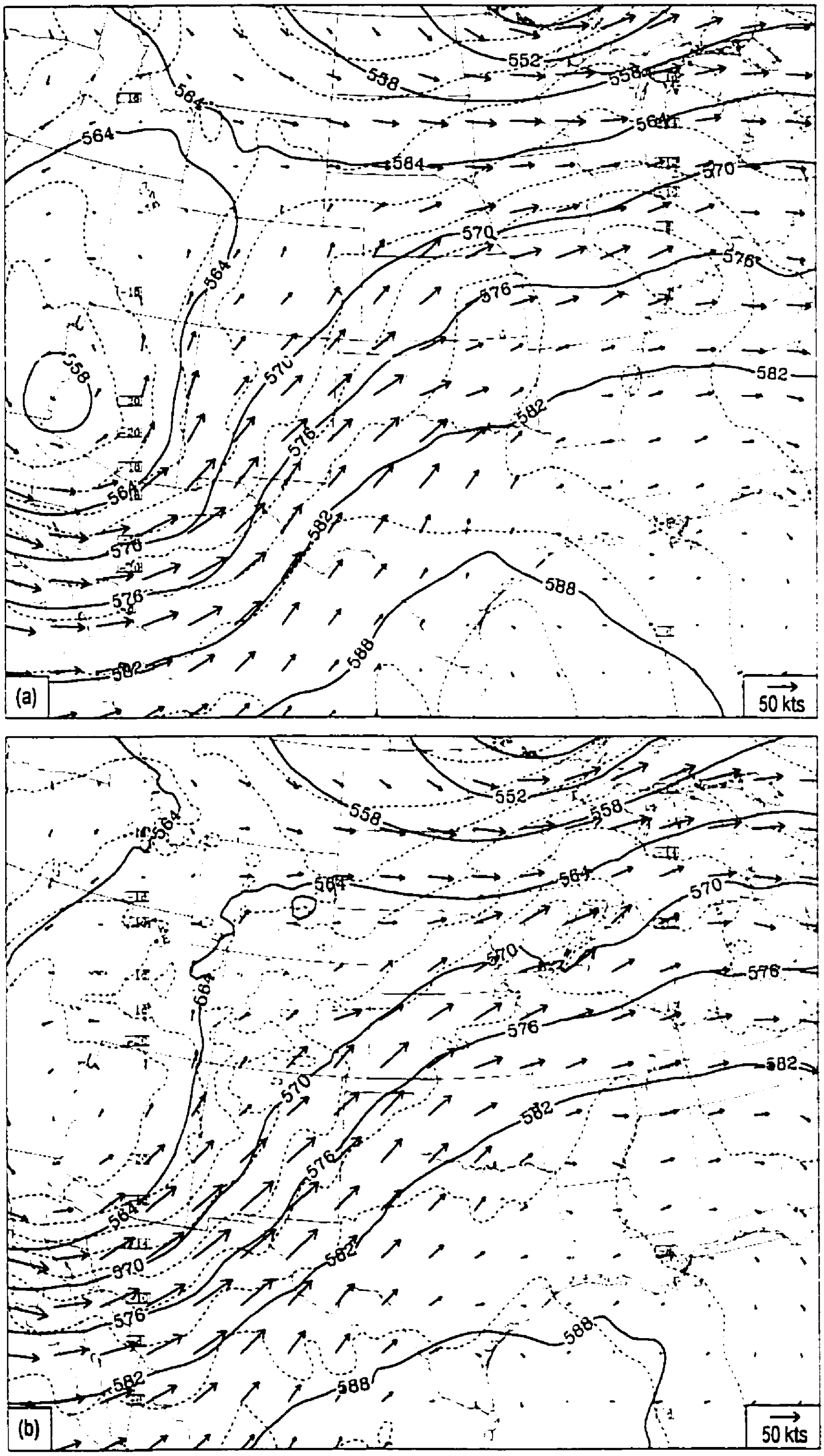

Figure 5.2. 500-hPa geopotential height (dam) (solid lines), temperature (°C) (dashed lines), and wind vector derived from CMC analysis (a) and CONTROL (b) for 0000 UTC 17 May 1995. Contour interval for geopotential height is 6 dam and for temperature is 2 °C.

the California-Arizona state border. In particular, the fields are very similar upwind of southwestern Kansas, which implies that the advection of mid-level dry air over the central plains during the past twelve hours was captured. Equivalently, at 850-hPa, the important low-level moisture transport into the VORTEX-95 operating domain was properly simulated (Figure 5.3). However, both variables have a larger magnitude over the eastern states than that shown by the analysis.

These plots suggest that the model captured the low- and mid-level flows that were instrumental in preparing a convectively unstable atmosphere over southwestern Kansas. To further illustrate this, a vertical profile of the atmosphere from the grid point that corresponds to the location of the Dodge City upper-air station is shown in Figure 5.4. A comparison of this sounding to Figure 2.4 reveals that the high level of convective instability of the observed atmosphere was simulated quite well. More specifically, a deep, dry air pocket aloft characterized by a nearly, dry-adiabatic lapse rate indicates that the model replicated the persistent subsidence of a mid-level air mass down the eastern slopes of the Rocky Mountains. Furthermore, the shallow capping lid which separates this dry shaft from a moist, well-mixed ABL was also reproduced. At this time, the atmosphere over Dodge City is extremely susceptible to deep convection, however, the absence of a sufficiently strong lifting mechanism to overcome negative buoyancy has prevented the occurrence of convection in the model, as was also the case in the real atmosphere.

To fully satisfy our objectives, it was necessary that the model reproduce the very important mesoscale features discussed in Chapter 2. Referring to Figure 5.3, the position of the simulated dryline, which may be approximated by the western boundary of the steep gradient in isohumes, agrees reasonably well with that shown by the analysis. In particular, the important northern section of the eastward bulge is accurately located over southwestern Kansas, although there appears to be a small westward bias in the model. Another mesoscale feature that contributed to the initiation of the Garden City thunderstorm was the upper-level jet streak. Contrasting Figure 5.5 and Figure 2.6, it is evident that although the simulated wind speeds are in many places higher than those

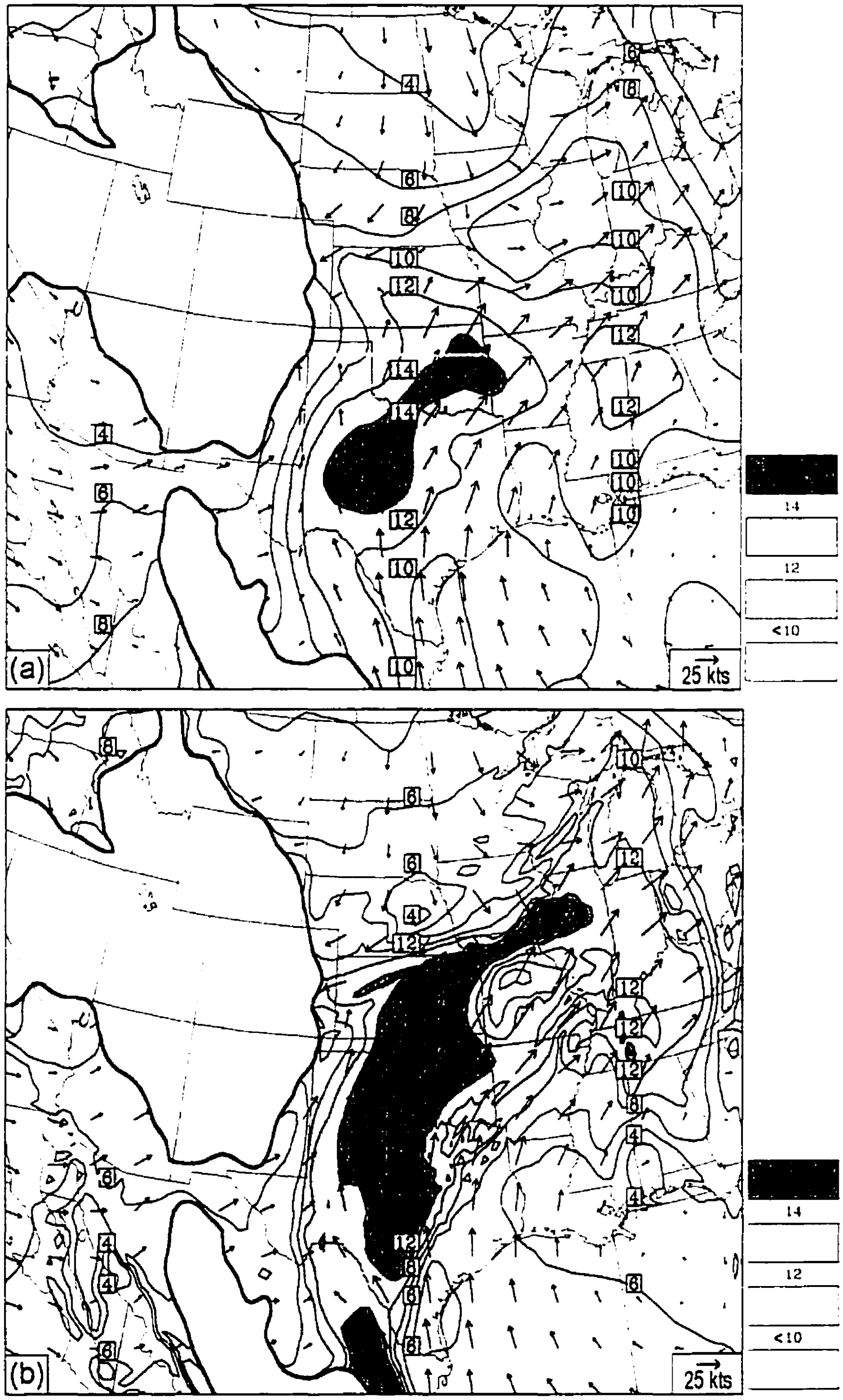

Figure 5.3. 850-hPa specific humidity (g kg^{-1}) (thin solid lines) and wind vector derived from CMC analysis (a) and CONTROL (b) for 0000 UTC 17 May 1995. Contour interval for specific humidity is 2 g kg^{-1}, and values greater than 10 g kg^{-1} are shaded. Heavy solid line denotes the area below surface.

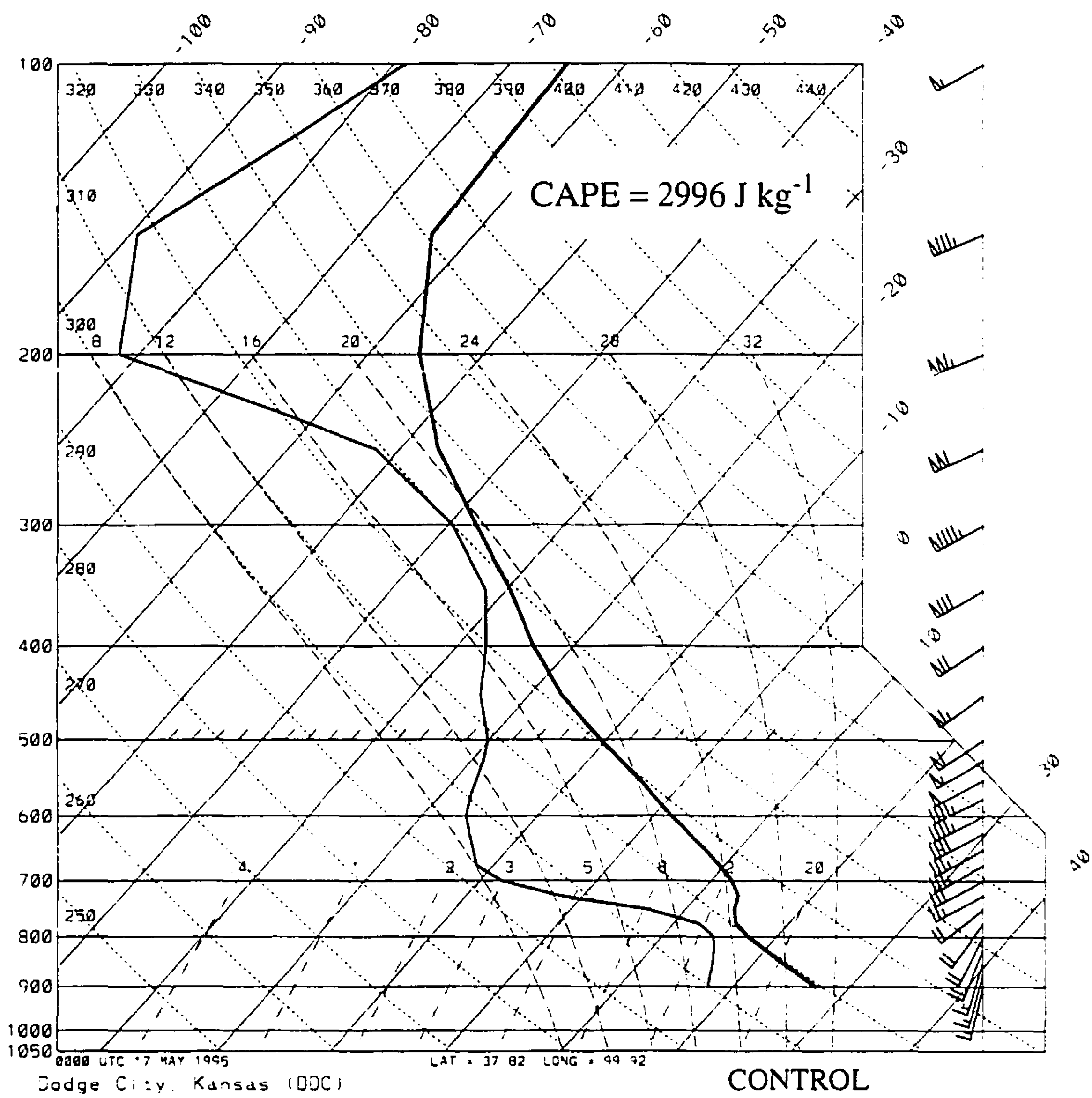

Figure 5.4. Vertical profile of the atmosphere at the grid point corresponding to Dodge City (DDC) from CONTROL after 12-hours of integration (see Figure 2.4 for wind speed notation).

observed, MC2 reproduced approximately the correct orientation of the 250-hPa wind maximum at 0000 UTC 17 May 1995.

To study more closely the numerical reproduction of the mesoscale environment over the central plains prior to the initiation of the Garden City supercell, a surface analysis of MC2 output was constructed at 2100 UTC 16 May 1995 (Figure 5.6). This solution is compared with the analysis by Wakimoto et al. (1998) shown in Figure 2.5. Although the nine hour simulated surface pressures are lower than observed over our region of interest, the position of the surface trough, which we have subjectively drawn in, divides Kansas in much the same way as in the analysis by Wakimoto et al.. Additionally, the simulated dryline, which was located by the 9 g kg^{-1} surface specific humidity contour, lies in a very similar manner to that shown in Figure 2.5. However, as previously indicated, a westward bias of approximately 80 km is present in the numerical solution. The simulated Garden City storm was triggered one hour after this analysis at approximately the location of the surface trough-dryline intersection shown in Figure 5.6.

Thus, with 18 km horizontal resolution, MC2 was able to successfully simulate the environment over southwestern Kansas. This includes the conditioning of a deep-layer, convectively unstable atmosphere by the large-scale flow, and the important mesoscale features of a dryline and upper-level jet streak, which provided forcing for ascent. However, to trigger convection accurately with respect to location and time, it was necessary to implement a second convective trigger function that was sensitive to the presence of a free convective boundary layer. As well, a filter to eliminate spurious convection generated by model gravity waves was also required.

The following subsection provides a description of the simulated Garden City storm. This discussion does not include the effects of the previous convective system, as described in Chapter 2, since it was not captured in our control run. The reasons for this inaccuracy and the adjustments that were implemented to generate the neighbouring storm will be presented later in this chapter as a sensitivity study.

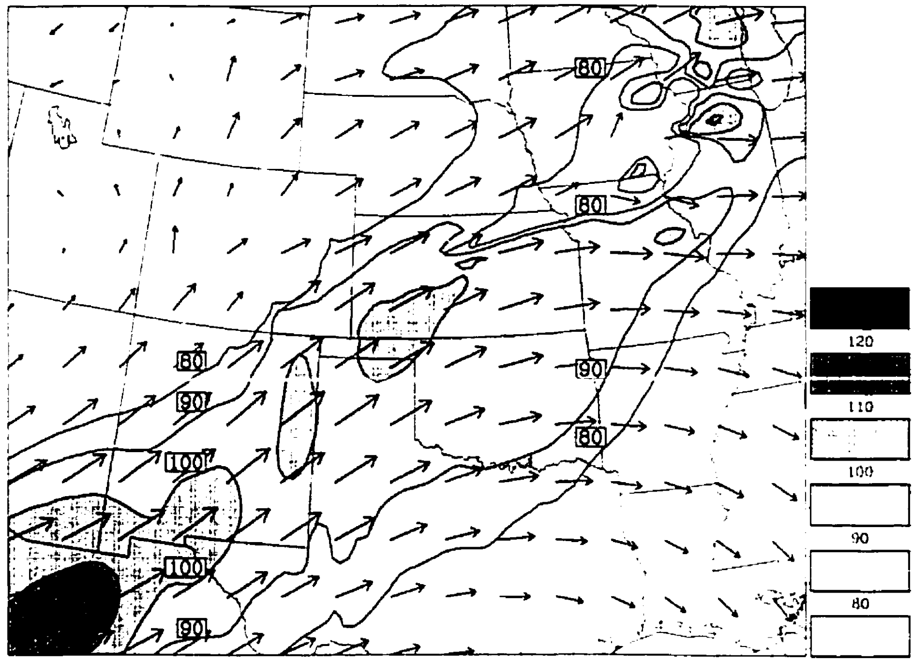

Figure 5.5. Simulated 250-hPa wind vector and wind speed (shaded contours) for 0000 UTC 17 May 1995. Only wind speeds greater than 80 knots are indicated, and with a contour interval of 20 knots.

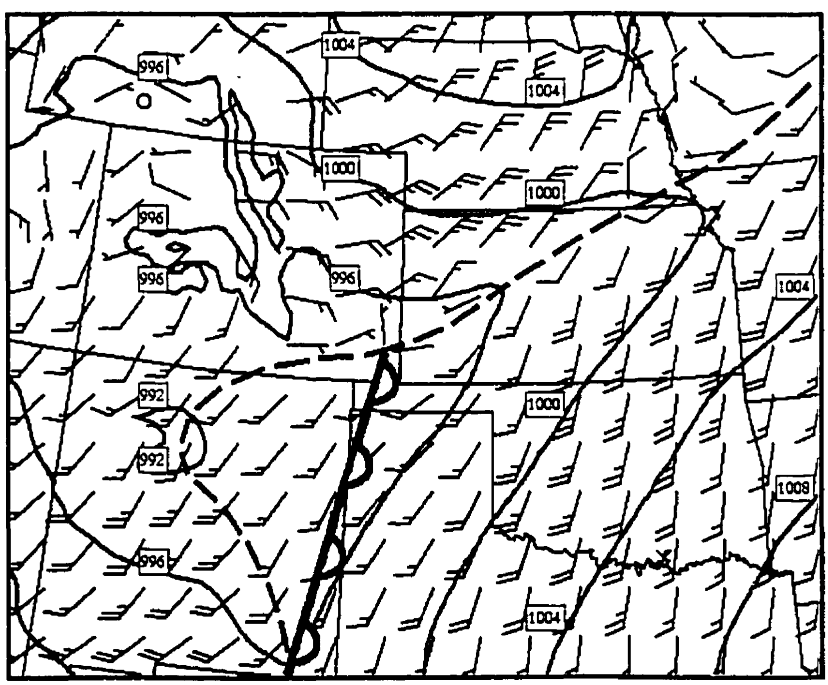

Figure 5.6. Simulated temperature (^oC), dewpoint temperature (^oC), and wind speed and direction for 2100 UTC 16 May 1995 (see Figure 2.4 for wind speed notation). Isobars (solid lines), surface trough (dashed line), and dryline (scalloped line) are also indicated. Isobars have a contour interval of 4 mb.

5.2.2 Modelled Garden City storm

At 2159 UTC, deep convection was initiated immediately west of the southern Colorado-Kansas state border, almost 80 km from the inception point of the observed Garden City storm. Although the model-resolvable vertical velocity at these grid points was downward, air parcels originating from within a free convective boundary layer were able to overcome the negative buoyancy and reach their LFC. The subsequent release of close to 3000 J kg^{-1} of CAPE marked the emergence of the simulated Garden City storm. Over the next hour, convective activity spread westward and eastward from this region to give the storm an areal extent of approximately 100 km x 50 km. A comparison of the hourly evolution of the simulated storm to that of the real Garden City supercell, as observed by the Dodge City radar, is given in Figure 5.7. Since the first hour of the modelled storm's development was slower than that of the observed thunderstorm, the panels showing the numerical output are displaced forward one hour to more closely correspond to the radar imagery. That is, the radar imagery shown is for 2200 UTC, 2300 UTC, 0000 UTC, and 0100 UTC, while the model derived plots are for 2300 UTC, 0000 UTC, 0100 UTC, and 0200 UTC. To construct the dBZ fields depicted in panels (b), (d), (f), and (h) of this figure, the model's precipitation rate at each hour was converted into a radar reflectivity value using a standard Z-R relationship[1]. The smaller magnitudes of peak reflectivity generated by the model are indicative of its inability to capture the high precipitation intensity of the observed supercell at a horizontal resolution of 18 km.

Accompanying this comparison are plots of the horizontal cross-section of vertical velocity at 500-hPa from 2300 UTC 16 May to 0200 UTC 17 May in Figure 5.8. In each frame of this figure, the cellular region of positive vertical velocity indicates roughly those grid points that are producing convective precipitation. Hence, this upward motion extends throughout a large depth of the troposphere, and thus, it may be used to track the approximate position of the Garden City thunderstorm throughout its course.

In Figure 5.7 (b), two insignificant spurious convective cells lie east of the recently initiated modelled storm, which is precipitating over a larger area than the observed storm

[1] $Z = 200R^{1.6}$, where $10 \log Z$ is the reflectivity factor (dBZ) and R is the precipitation rate (mm hr^{-1}). (from Rogers and Yau 1989)

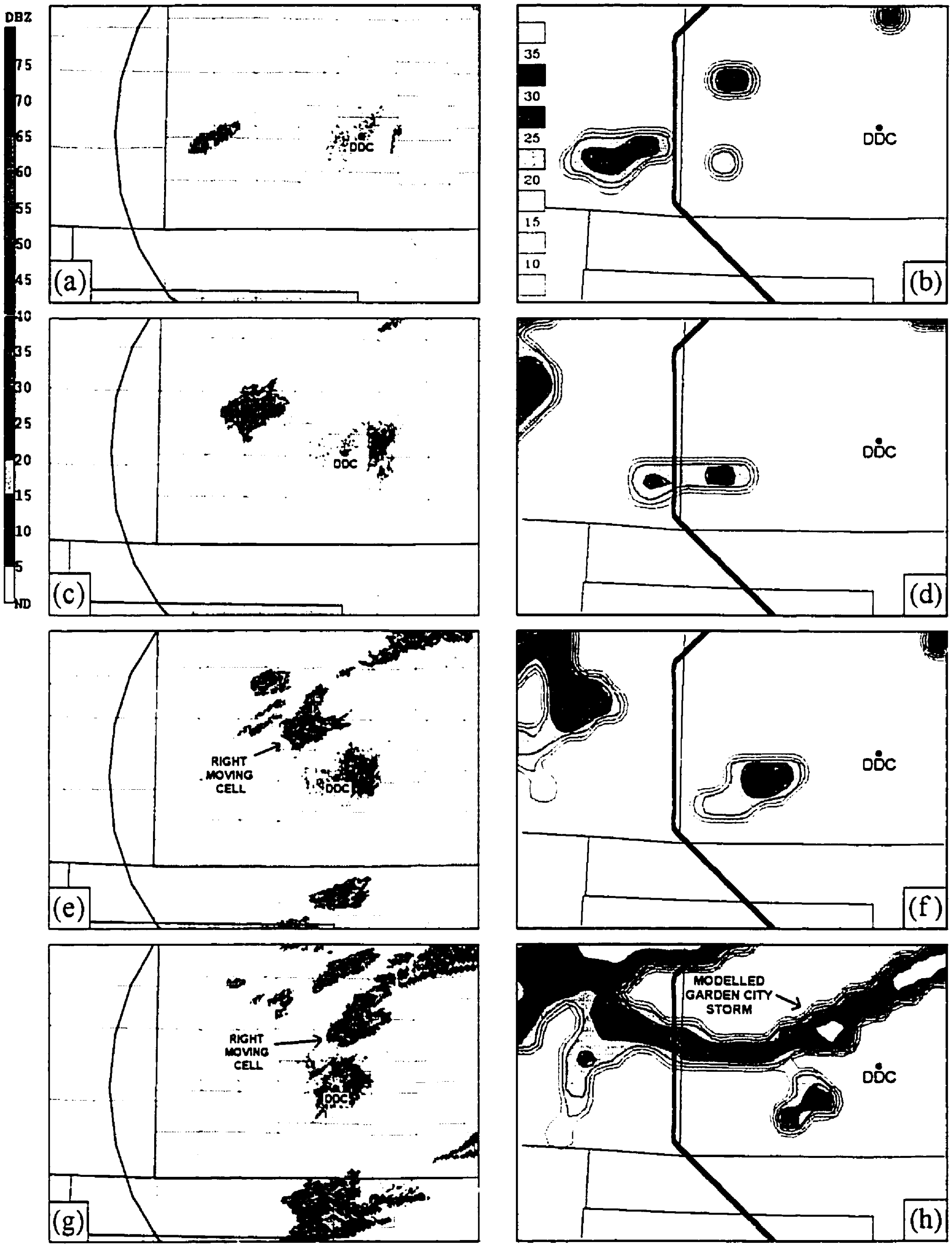

Figure 5.7. 1.5° elevation angle plan position indicator (PPI) scan of radar reflectivity from the Doppler radar located at Dodge City (DDC) for 2200 UTC (a), 2300 UTC (c), 0000 UTC (e), and 0100 UTC (g). In each of (b), (d), (f), and (h) is the corresponding reflectivity factor calculated using the precipitation rate from CONTROL at 2300 UTC, 0000 UTC, 0100 UTC, and 0200 UTC, respectively. The heavy solid line indicates the limiting range of the radar at 230 km. The legend for the model derived plots is shown in (b), with units of dBZ.

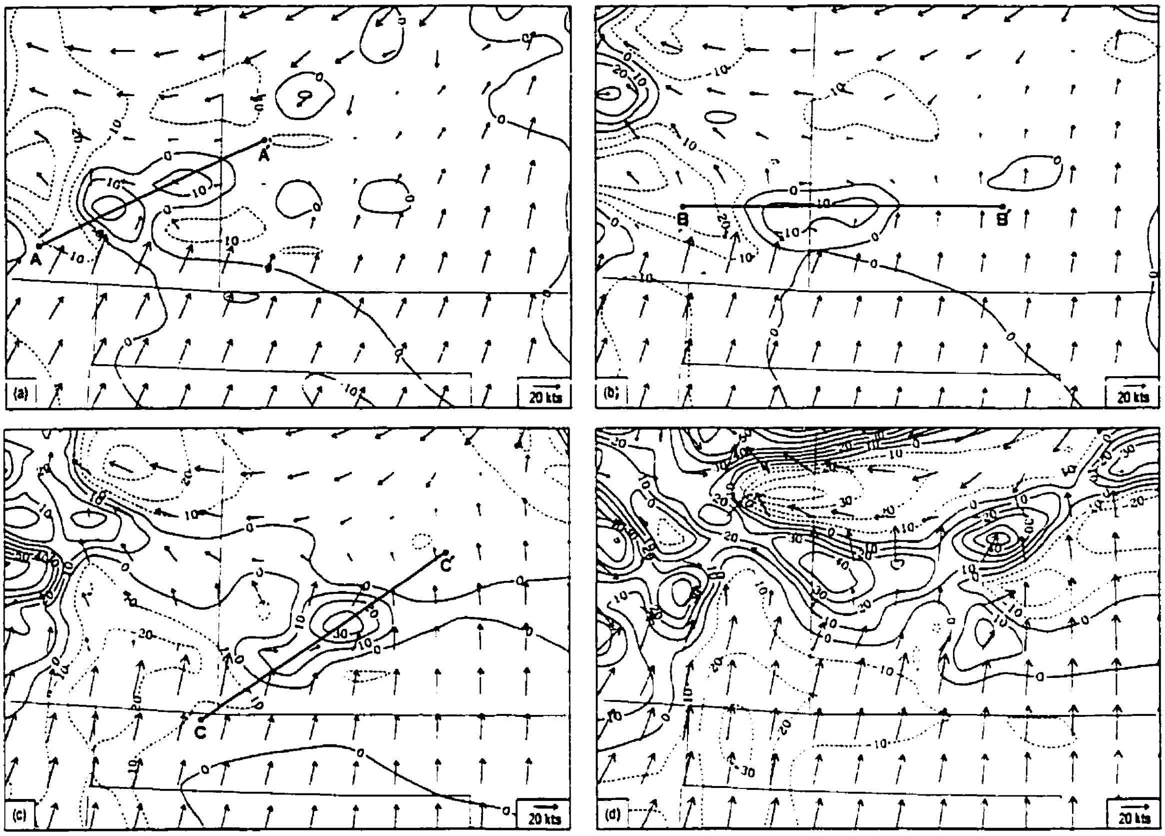

Figure 5.8. 500-hPa vertical velocity (cm s^{-1}) (solid/dashed contours) and surface wind vector for 2300 UTC (a), 0000 UTC (b), 0100 UTC (c), and 0200 UTC (d) from CONTROL. Contour interval for vertical velocity is 10 cm s^{-1}, with negative values indicated by dashed contours. The identifiers A, A', B, B', C, and C' denote the endpoints of the vertical cross-sections shown in Figure 5.9.

depicted in the corresponding reflectivity imagery in Figure 5.7 (a). Between 2300 UTC and 0100 UTC, the modelled storm propagated to the east-northeast, slightly south of the surface trough, which is approximately located by the shift in surface wind vectors shown in Figure 5.8 (a) to (c) (see also Figure 5.7 (b), (d), and (f)). A vertical cross-section through the storm at each of these hours is given in Figure 5.9. Referring to Figure 5.9 (a), a large depth of the troposphere is characterized by convective instability. The storm's updraft, which extends up to the tropopause, is removing this instability by transporting high values of equivalent potential temperature from the lower atmosphere into the mid- and upper-levels. Behind this column of positively buoyant air, the storm's downdraft has produced a 50-hPa pocket of low equivalent potential temperature that is often referred to as the cold-pool. At 0000 UTC, the storm's updraft and downdraft columns have expanded horizontally, while the storm has propagated with the mean winds into the area of greatest convective instability (Figure 5.9 (b)). The cold-pool in this plot appears weak, however, this is only due to the placement of the cross-section. By 0100 UTC, the storm's updraft has increased in magnitude considerably, with two maxima at 750-hPa and 350-hPa (Figure 5.9 (c)). Much of the convective instability in the immediate area of the updraft and to the southwest has been eliminated by this time. Also, the cold-pool appears very strong immediately below the main updraft. From Figure 5.7 (f), it is evident that the precipitation intensity has increased in proportion to the strength of the updraft of the modelled storm.

Over the next hour, the storm continued to propagate to the northeast into the region of the largest convective instability. However, by 0200 UTC, convective activity over western Kansas spread and intensified over an area beyond that observed by the Dodge City radar (Figure 5.7 (g) and (h)). The Garden City cell moved properly to the northeast to meet up with the squall line that was propagating to the southwest along the surface trough over northeastern Kansas. However, rather than dissipating over the previous hour as the observed storm did, the simulated cell continued to strengthen as other spurious convection was initiated to the west and northwest. A new convective cell also emerged to the south, which from Figure 5.7 (g), appears to be misplaced northward from its observational counterpart by approximately 75 km.

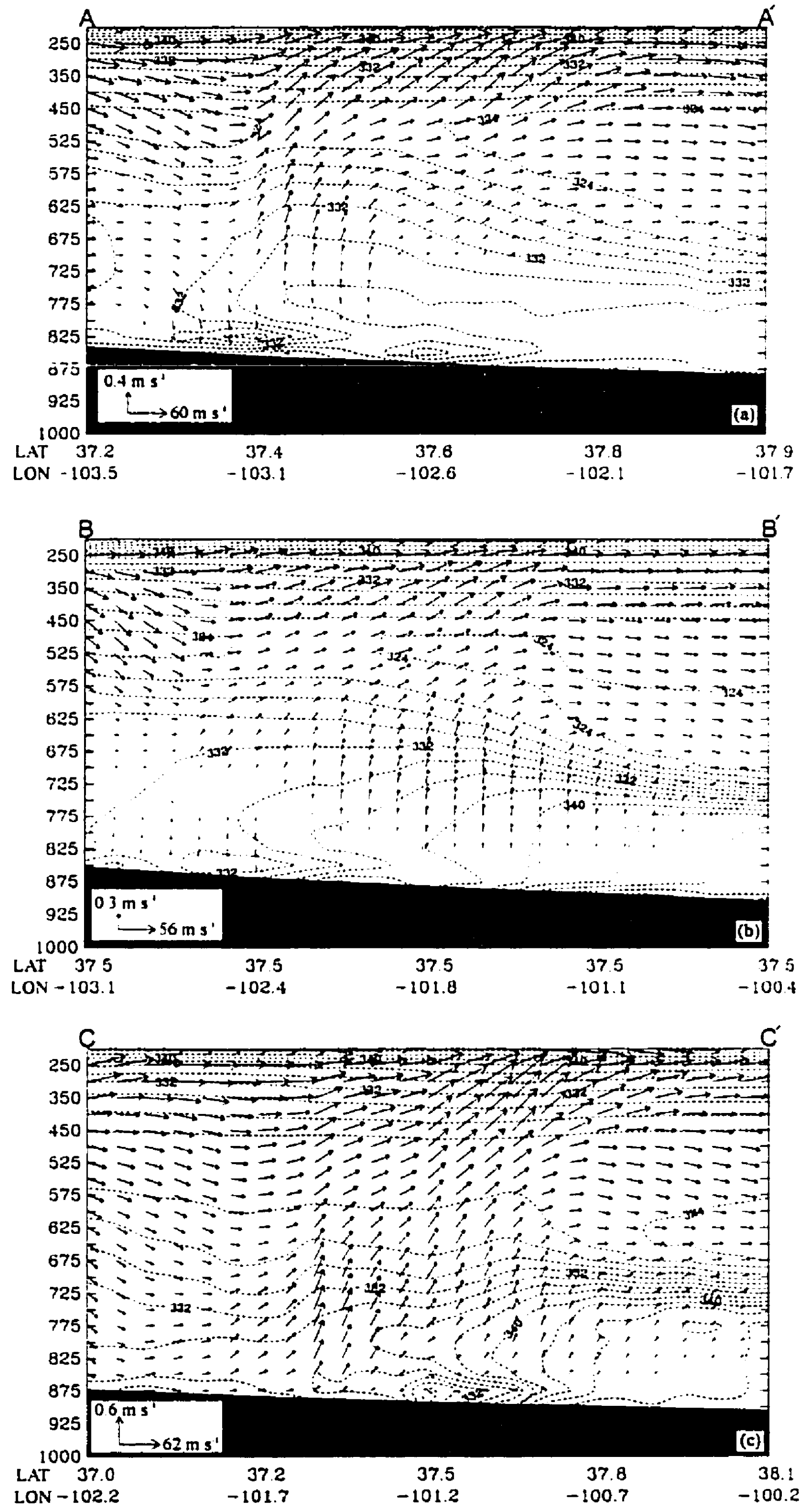

Figure 5.9. Vertical cross-section through the simulated Garden City storm showing wind vector and equivalent potential temperature (K) (dashed contours) at 2300 UTC (a), 0000 UTC (b), and 0100 UTC (c). The orientiation of each cross-section is shown in Figure 5.8. Contour interval for equivalent potential temperature is 2 K.

The decline in the quality of this simulation after thirteen hours of integration may be attributed to a prolonged accumulation of moist static energy in the lower atmosphere. Hence, the large magnitude of the suppression parameter that was required to limit the spurious initiation of convection so that the Garden City storm could be properly triggered, unfortunately also led to the eventual deterioration of the simulation. To successfully model an environment that is characterized by a large degree of convective instability, it is critical that the CAPE be consumed properly. If this energy accumulates to a very high level, the simulated environment becomes extremely volatile, and convection may breakout in an inaccurate manner to release this energy. It is again stressed that it is very difficult to trigger convection properly in an atmosphere where grid-resolvable forcing is neither strong, nor well-defined. Although the behavior of the simulated convective activity over the central plains is not accurate after thirteen hours of integration, the Garden City storm was correctly initiated with respect to time and location, and three hours of its evolution were properly reproduced. Thus, a majority of the remainder of this chapter will focus on these results.

5.2.3 Analysis of environmental parameters over southwestern Kansas

There are numerous advantages to studying a particular atmospheric event using a numerical model rather than observational data alone. For instance, a mesoscale model generates a uniform, high-resolution, dynamically consistent data set that cannot be produced by current observational networks (Molinari and Dudek 1992). This allows for a more comprehensive analysis, as well as, tremendous flexibility regarding the location, time period, or atmospheric process with which to focus on. In the study of small-scale severe weather events, several diagnostic parameters have been derived to exploit the high consistency of model output. Four such parameters, which characterize an atmosphere's susceptibility to tornadic supercell development, are analysed in this section to better understand the local environment of the modelled Garden City storm. The severe weather parameters to be discussed are the bulk Richardson number (BRN), the bulk Richardson number shear (BRNSHR), the storm-relative environmental helicity

(SREH), and the energy-helicity index (EHI). Outlined below is the basic theory that governs each of the parameters.

Bulk Richardson number

The bulk Richardson number quantifies the relationship between the magnitude of the available potential energy to the vertical wind shear (Moncrieff and Green 1972), and is calculated using the formula

$$BRN = \frac{CAPE}{0.5\left(\bar{u}^2 + \bar{v}^2\right)}, \tag{5.1}$$

where $\bar{u}$ and $\bar{v}$ are the wind components of the difference between the density-weighted mean winds over the lowest 6000 m and the lowest 500 m above ground level (Stensrud et al. 1997). The CAPE is defined as the positive buoyant energy available to a parcel that has reached its LFC, and it may be computed with the equation

$$CAPE = g\int_{LFC}^{EL} \frac{\theta(z) - \bar{\theta}(z)}{\bar{\theta}(z)}\,dz, \tag{5.2}$$

where g is the acceleration due to gravity, $\theta(z)$ is the potential temperature of the rising air parcel, $\bar{\theta}(z)$ is the potential temperature of the environment, and EL is the equilibrium level of the air parcel.

Using a numerical cloud-model, Weisman and Klemp (1984) have shown that modelled supercells are likely when BRN has a value between 10 and 50. For higher values of BRN, the storm's downdraft is overly intense such that it propagates away from the convective cell, thereby inhibiting the development of a supercell. For very low values of BRN, an extremely strong vertical shear separates the updraft and downdraft columns to a distance that limits the storm's intensity. For intermediate values, there is a balance between buoyant energy and vertical wind shear.

Bulk Richardson number shear

The BRNSHR is defined by the denominator of Equation (5.1). Droegemeier et al. (1993) have shown this parameter to be highly correlated with the maximum vertical vorticity of modelled thunderstorms. In another numerical analysis, Stensrud et al. (1997) found that the magnitude of BRNSHR is closely related to the likelihood of low-level mesocyclogenesis. Essentially, they used the BRNSHR as a proxy for the mid-level storm-relative winds, which are important to the development of low-level rotation in thunderstorms (see Brooks et al. 1994). According to Stensrud et al. (1997), for low values of BRNSHR, there are weak mid-level storm-relative winds, such that low-level mesocyclones are short-lived, occur early in the storm's lifetime, and the storm is dominated by low-level outflow. For high values of BRNSHR, storm-relative winds are very strong, so that low-level mesocyclones develop slowly, if at all, and outflow is weak since precipitation is carried away from the storm. In the middle of these two extremes, a balance exists between the storm-relative winds and the low-level rotation, and therefore, mesocyclones are normally long-lived. In their study of nine severe weather events, Stensrud et al. (1997) found that low-level mesocyclogenesis is likely when BRNSHR has a value between 40 $m^2 s^{-2}$ and 100 $m^2 s^{-2}$.

Storm-Relative Environmental Helicity

The SREH (Davies-Jones et al. 1990) is a measure of the likelihood that an environment will support thunderstorm rotation at mid-levels (Brooks et al. 1994). It is calculated with the formula

$$SREH = \int_0^H \left(\underline{v} - \underline{c}\right) \cdot \underline{\omega}\, dz, \tag{5.3}$$

where H is an assumed inflow depth (normally chosen to be 3000 m), $\underline{v}$ is the wind vector, $\underline{c}$ is the storm motion vector, and $\underline{\omega}$ is the vorticity vector. A storm that encounters a region with high values of SREH may develop a mid-level mesocyclone, and thus, be classified as a supercell thunderstorm (Davies-Jones et al. 1990). A minimum value typically considered in tornadic storm forecasting is 100 $m^2 s^{-2}$.

However, since areas may exhibit values that exceed this threshold without the development of a supercell thunderstorm, it can only be said that supercells are *possible* in regions where SREH is greater than 100 $m^2 s^{-2}$ (Stensrud et al. 1997). Furthermore, Markowski et al. (1998b) have shown that SREH can be extremely variable in both space and time, and that this variability cannot be resolved by current mesoscale models.

Nevertheless, an analysis of SREH fields relative to a modelled convective cell still yields valuable information, especially if used in combination with other parameters. In the calculation of SREH for our case study, the storm motion was assumed to be equal to the translation speed of the Garden City mesocyclone. Using VORTEX observational data, this was determined to be 15.4 m s^{-1} from 254° (Wakimoto et al 1998).

Energy-Helicity Index

The EHI (Davies 1993), which is calculated by the following equation, is used operationally for forecasting the development of supercells and tornadoes.

$$EHI = \frac{CAPE * SREH}{1.6 \times 10^5} \tag{5.4}$$

Values greater than 1.0 indicate a potential for supercells, and those greater than 2.0 indicate a high probability of supercells (Rasmussen and Blanchard 1998).

Evolution of parameter fields relative to the modelled Garden City storm

According to *Storm Data* reports four tornadoes were spawned by the Garden City supercell over a three hour period beginning at approximately 2320 UTC (NCDC 1995). The following study of the simulated storm with respect to the four parameters described above covers much of this period with analyses at 2300 UTC, 0000 UTC, and 0100 UTC (Figure 5.10 to Figure 5.15). The storm's position is approximated using the 500-hPa vertical velocity field.

At 2300 UTC, the environment of the simulated storm does not yet exhibit all of the qualities of a supercell. The BRN is extremely low over the mid-level updraft area, which indicates a dominance of vertical shear over the CAPE (Figure 5.10 (a)). Values of the BRNSHR are greater than 100 $m^2 s^{-2}$ over most of the storm's area, which implies strong storm-relative winds such that a low-level mesocyclone will develop slowly, if at all (Figure 5.10 (b)). The generation of a mesocyclone in this environment is dependent upon the presence of a very high magnitude of low-level rotation (Stensrud et al. 1997), which is not demonstrated by the SREH field in Figure 5.11 (a). The plot of the parameter EHI at this time indicates that a supercell is possible in this environment (Figure 5.11 (b)).

After twelve hours of integration, at 0000 UTC, the parameters portray a more mature stage of the Garden City storm. From Figure 5.12, almost half of the storm lies in a region of BRN that is within the range for modelled supercells, which indicates a balance between available potential energy and vertical wind shear. The southern section of the storm is characterized by an equilibrium of storm-relative winds and low-level rotation according to BRNSHR. Therefore, low-level mesocyclogenesis is likely, however, the northern part of the storm is still dominated by large storm-relative winds. According to Figure 5.13 (a), the entire storm possesses enough low-level rotation to be classified as a supercell. However, a plot of the operational forecast parameter EHI depicts that only the northeastern half of the storm resides in an environment with the potential for supercells (Figure 5.13 (b)). The low magnitude of EHI over the western side of the storm is due to a small value of CAPE since moist downdrafts have produced a low-level cold-pool in this region (see Figure 5.9 (b)).

Over the next hour, the modelled storm continued to intensify, exhibiting an updraft of greater than 30 cm s^{-1} at the 500-hPa level at 0100 UTC (Figure 5.14). At this stage, the BRN and EHI fields both reflect the efficient removal of CAPE by convective overturning induced by the Kain-Fritsch scheme over the main updraft shaft (Figure 5.14 (a), Figure 5.15 (b), see Figure 5.9 (c)). In Figure 5.14 (b), the ambient BRNSHR indicates that the entire storm is characterized by a balance of low-level rotation and mid-level winds. As well, values of SREH greater than 100 $m^2 s^{-2}$ over most of the storm's area suggest that it may be a supercell (Figure 5.15 (a)). Together, these fields indicate that supercell mesocyclogenesis would be most likely to occur in the eastern sector of the convective cell.

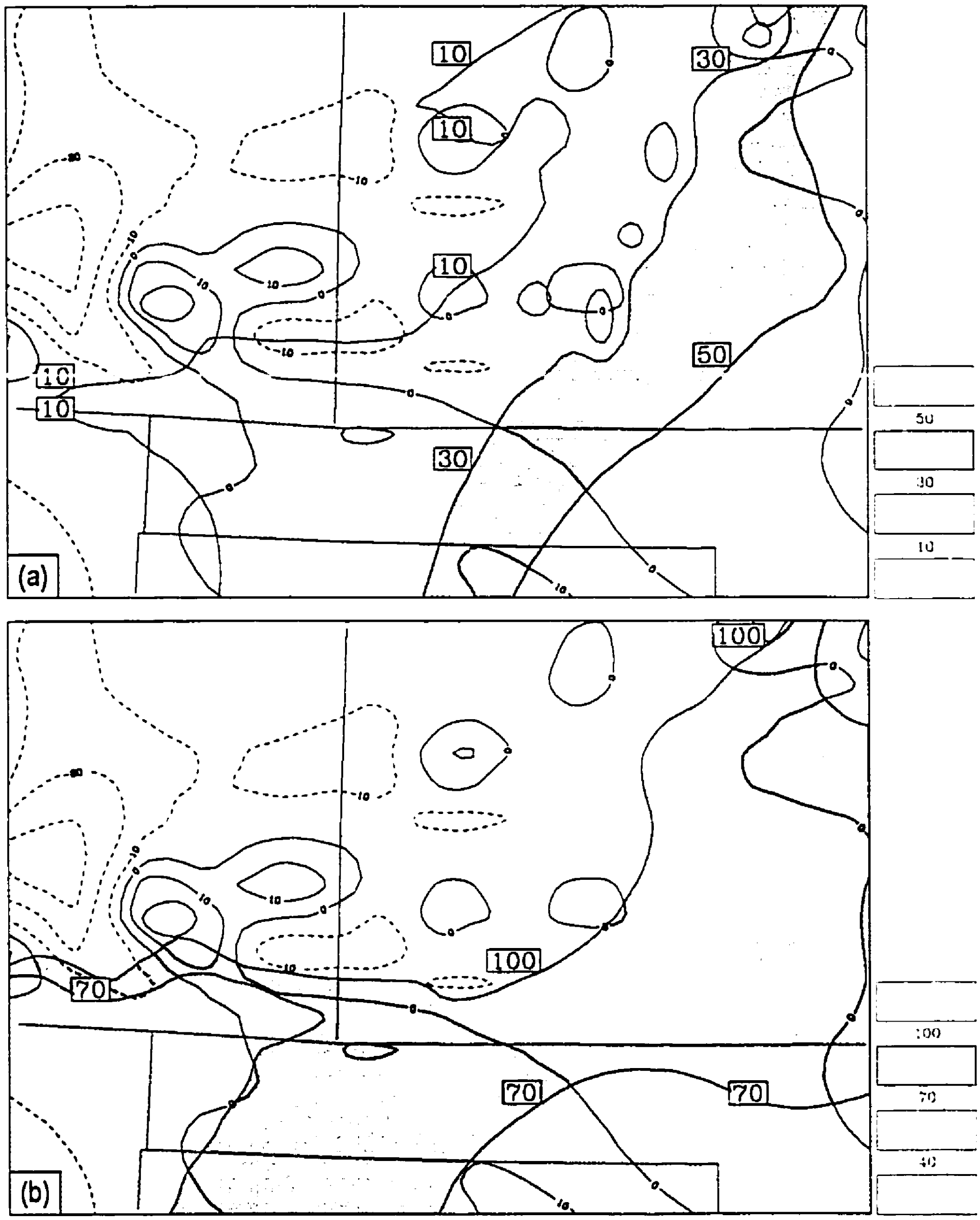

Figure 5.10. 500-hPa vertical velocity (cm s^{-1}) (solid/dashed contours) superimposed on BRN (no units) (a) and BRNSHR (m^2 s^{-2}) (b) fields (shaded contours) for 2300 UTC 16 May 1995. Contour interval for vertical velocity is 10 cm s^{-1}, with negative values indicated by dahsed contours.

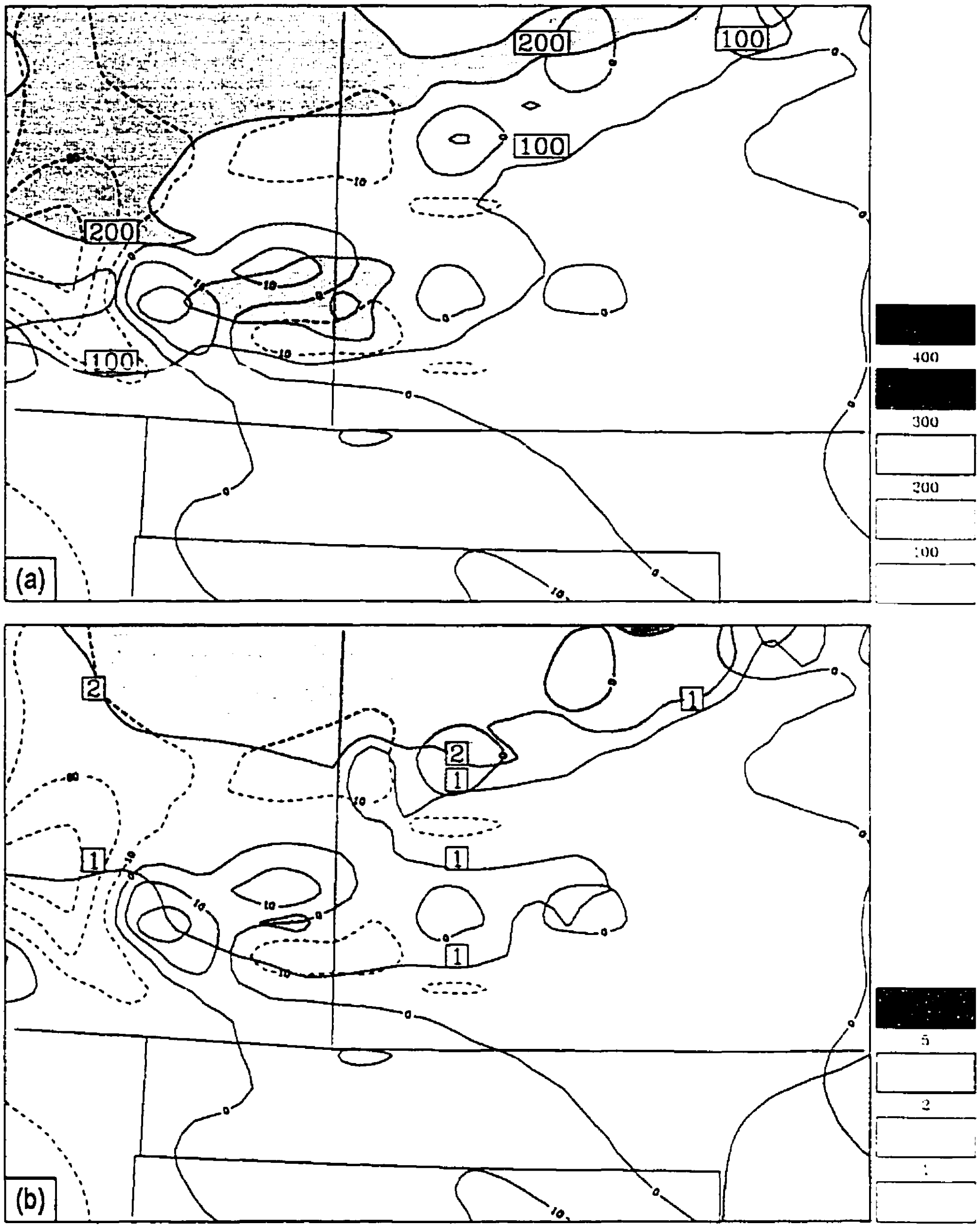

Figure 5.11. As in Figure 5.10, except for SREH (m^2 s^{-2}) (a) and EHI (no units) (b) fields (shaded contours).

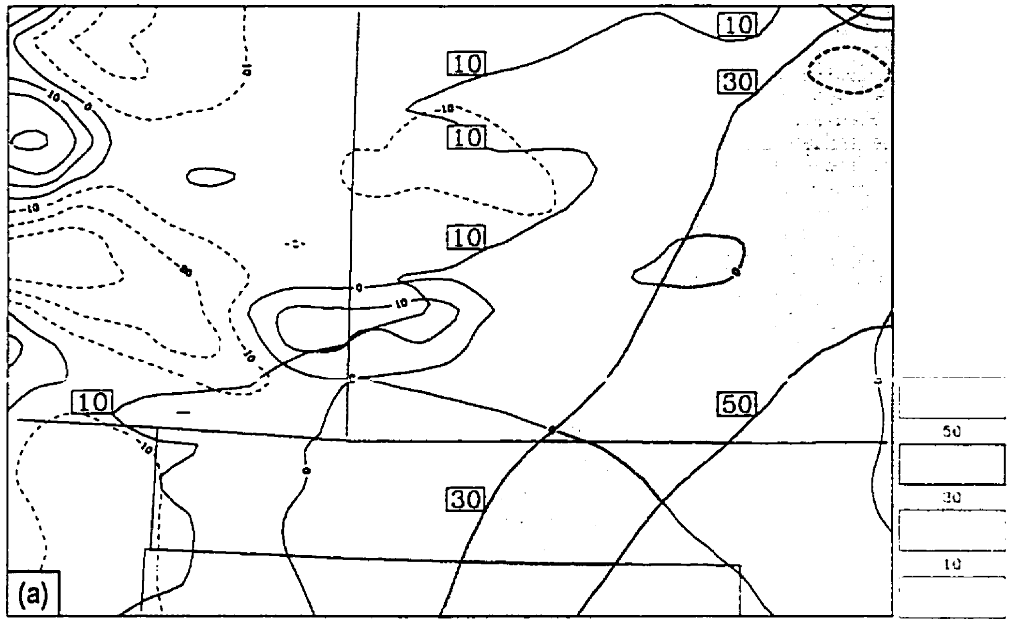

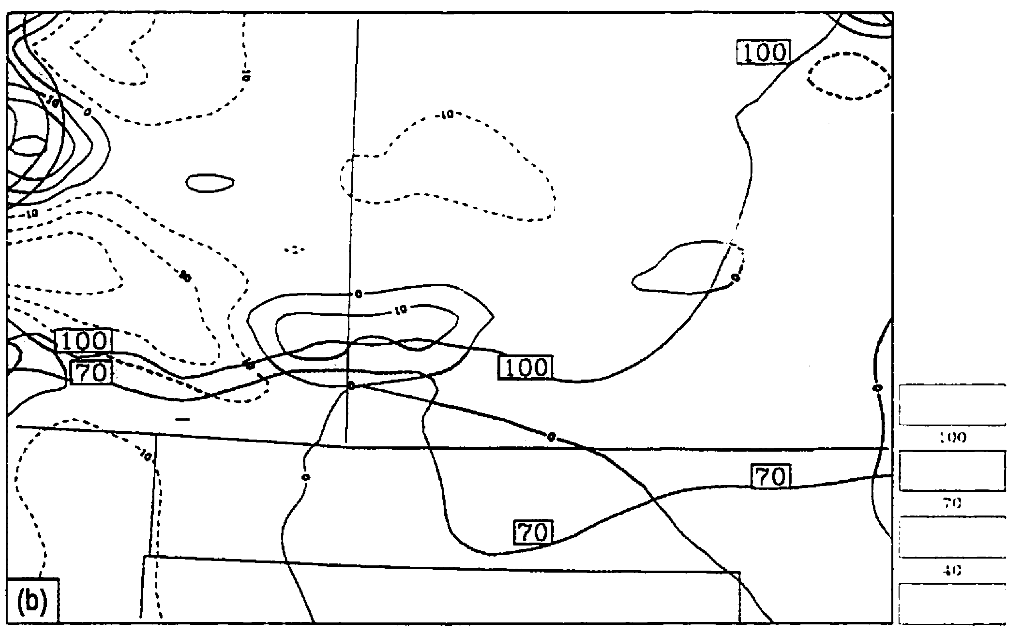

Figure 5.12. As in Figure 5.10, except for 0000 UTC 17 May 1995.

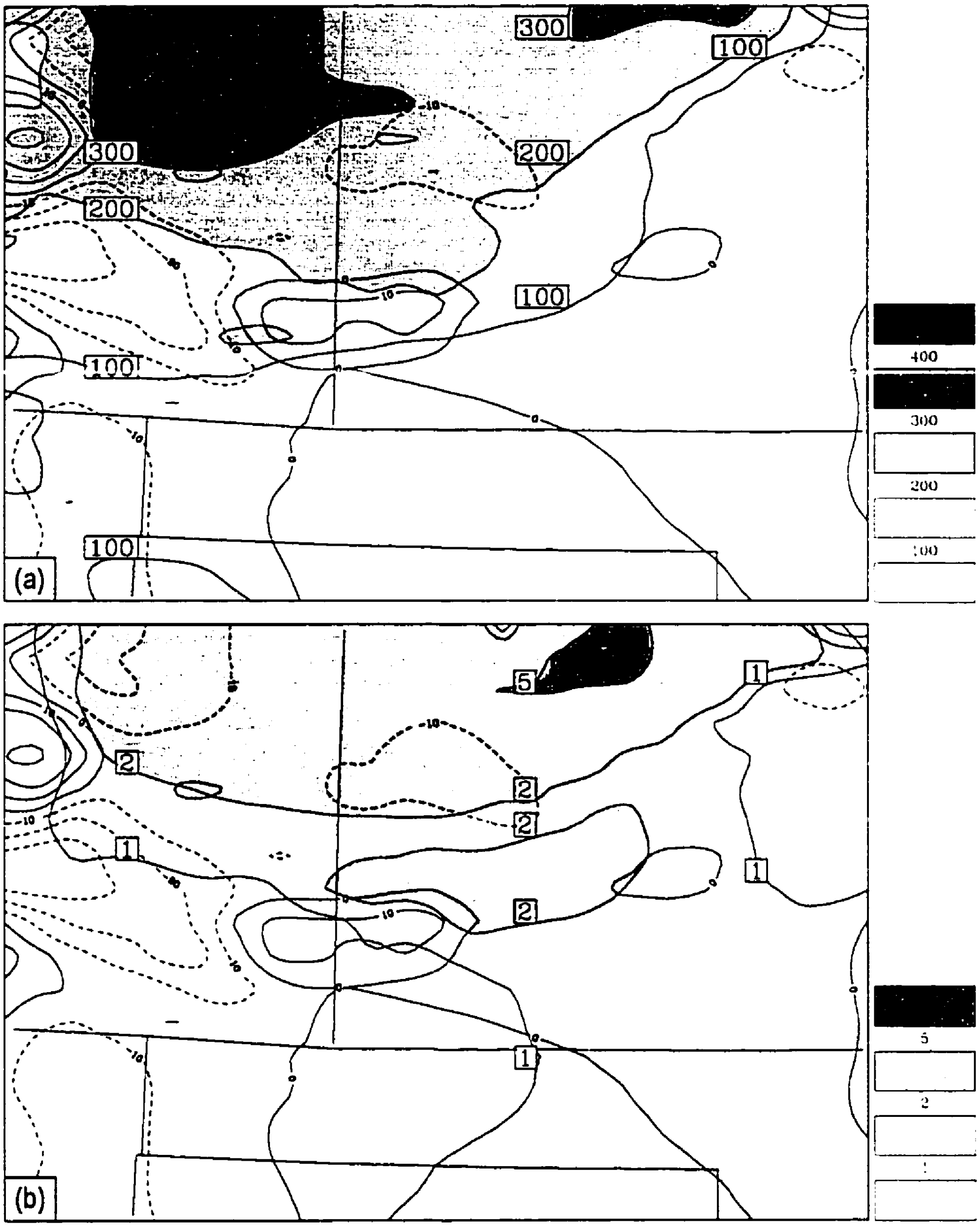

Figure 5.13. As in Figure 5.11, except for 0000 UTC 17 May 1995.

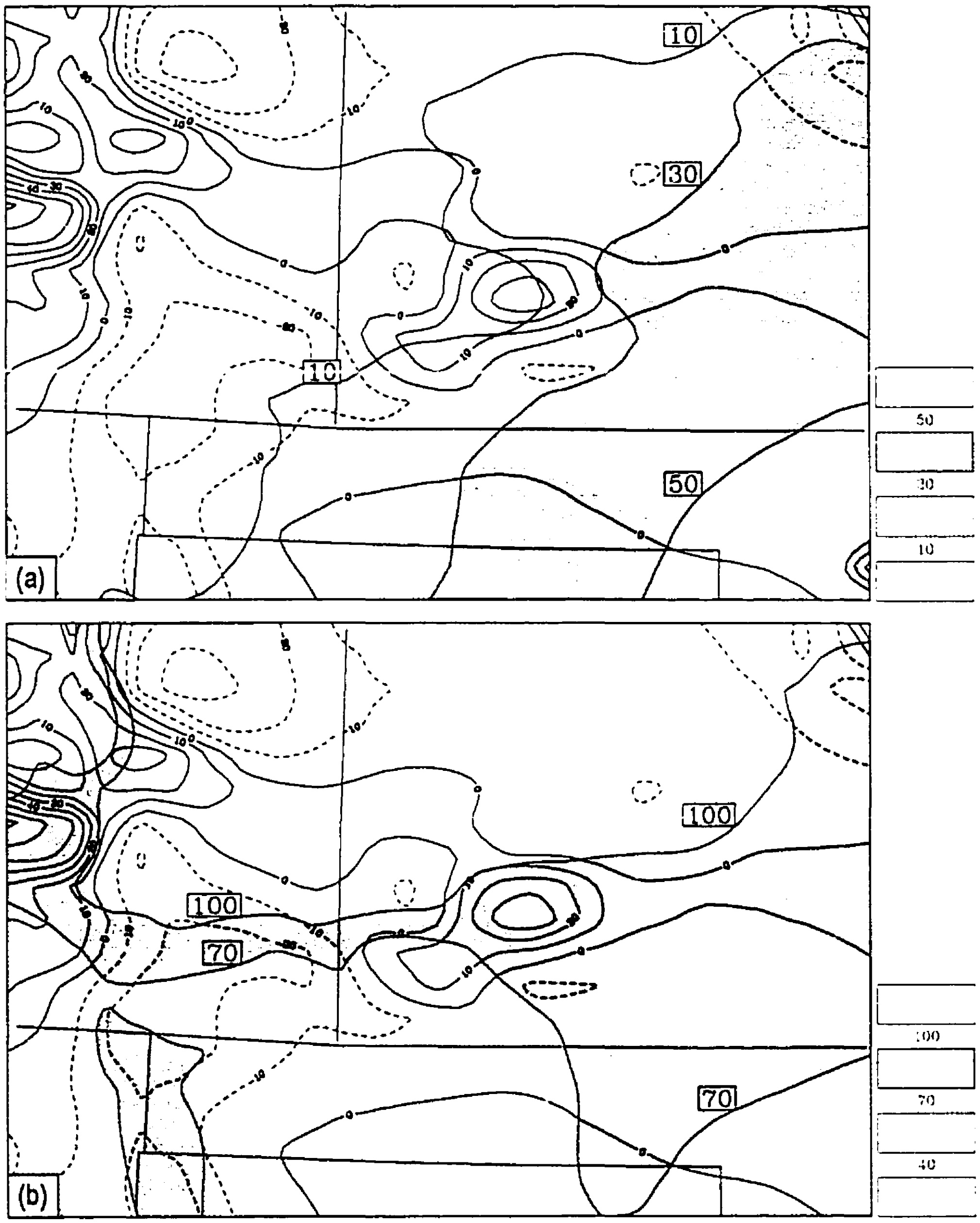

Figure 5.14. As in Figure 5.10, except for 0100 UTC 17 May 1995.

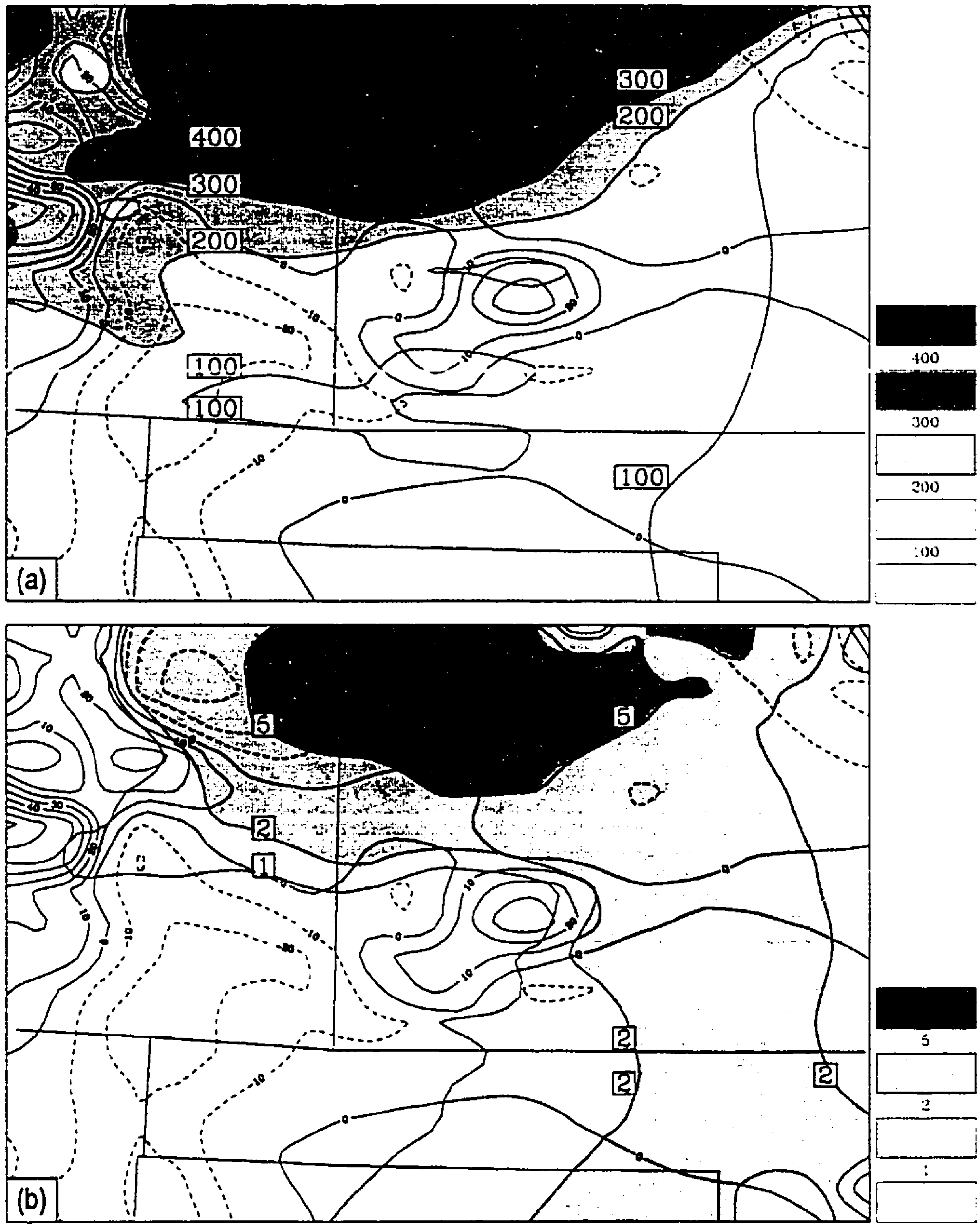

Figure 5.15. As in Figure 5.11, except for 0100 UTC 17 May 1995.

After thirteen hours integration, convective activity over western Kansas was not well-simulated, and therefore, further analysis on the modelled Garden City storm could not be performed. Nevertheless, the study of these parameters relative to the simulated convective cell suggests that the local mesoscale environment was conducive to the generation of a tornadic thunderstorm. Thus, MC2 did very well to reproduce the proper severe weather conditions within which the Garden City storm developed on 16 May 1995.

5.3 Generation of the Previous Convective System: A Sensitivity Study

In the previous chapter, modifications based on sensitivity experiments were applied to MC2 to improve the simulation of the convective events of 16 May 1995. Although the primary objective of reproducing the initiation and developing stages of the Garden City storm was attained by these adjustments, our second intention to study an interaction between multiple storms could not be satisfied since the previous convective system, described in Chapter 2, was not captured by this version of the model. Recall, that precipitation associated with this storm first appeared 110 km to the south of Dodge City at approximately 1730 UTC, after which point it intensified while proceeding to the northeast over the following three and a half hours. It has been hypothesized that a low-level outflow boundary emanating from this system influenced tornadogenesis in the Garden City supercell, over three hours after it was first produced.

A comprehensive analysis of the observational data obtained by VORTEX provided some explanation as to why MC2 was unable to generate this system. A plot of the air temperature at numerous surface observing stations surrounding the initiation point of this storm at 1800 UTC revealed a local maximum over the eastern sector of the Oklahoma panhandle (Figure 5.16). At the two Oklahoma mesonet stations identified by the codes SLAP and BUFF, the surface temperature was 2 °C to 3 °C greater than at

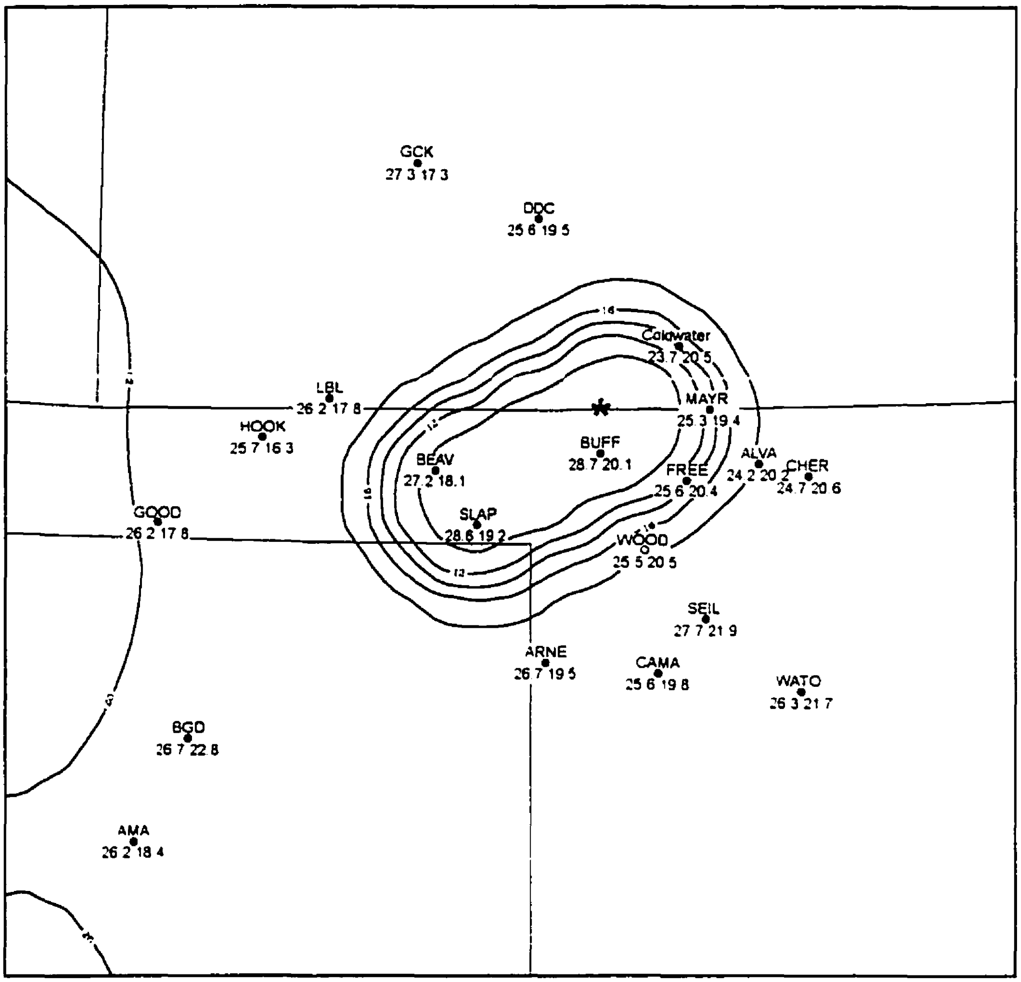

Figure 5.16. Observed temperature (°C) and dewpoint temperature (°C) for all surface stations surrounding the inception region of the previous convective system at 1800 UTC 16 May 1995. Surface albedo (percent) (contours) is superimposed, with values less than 10 percent shaded. Surface station WOOD (open circle) marks the launch site of the (NCA) sounding shown in Figure 5.17 (a). The star indicates the initiation grid point of the simulated previous convective system in ALBEDO.

surrounding sites only 75 km away, although the dewpoint temperature did not show any indication of a similar trend. This feature suggests that the local surface characteristics in the immediate area of these stations may be unique. Hong and Pan (1998) noted that surface inhomogeneities can be integral to triggering convection, particularly during the warm-season daytime hours.

Further evidence of the distinctive character of this region is provided by a sounding that was launched by a mobile unit at 1734 UTC (Figure 5.17 (a)). A comparison of this sounding with the routine six-hourly NWS soundings launched at Amarillo, Texas, Norman, Oklahoma, and Dodge City at 1800 UTC (Figure 5.17 (c), Figure 5.18 (a) and (c)) shows that a substantial amount of mixing in the lower atmosphere has occurred over a select area of an environment that is otherwise dominated by a formidable low-level inversion. An analysis of the corresponding vertical profiles that were extracted from CONTROL indicates that the model reproduced the environment over the VORTEX-95 operating domain very well, with the exception of the very distinct profile that developed over the eastern region of the panhandle ((b) and (d) of Figure 5.17 and Figure 5.18).

The enhanced heating of the surface would contribute to a lowering of the LCL and a subsequent reduction in the negative buoyancy of the lower atmosphere. Additionally, it might produce a free convective boundary layer, which would also favour the outbreak of deep convection. Tripoli and Cotton (1989) theorized that an MCS may develop on the lee-side of mountains when convective activity encounters forcing for ascent provided by both orographically excited gravity waves and thermally produced upslope flow. However, it is likely that neither process would have been resolved by our control simulation, just as the localized peak in surface heating and the resulting vigorous vertical mixing was not captured. Additionally, the initial conditions provided by CMC did not display any peculiar low-level anomalies, nor did the climatological surface fields demonstrate any properties that might be responsible for this feature.

Therefore, to investigate the effect of the previous convective system on the Garden City storm, it was necessary to conduct a sensitivity study, which is hereby referred to as the ALBEDO run. To reproduce the localized maximum in the low-level temperature field over the Oklahoma panhandle, we applied a simplistic solution of lowering the

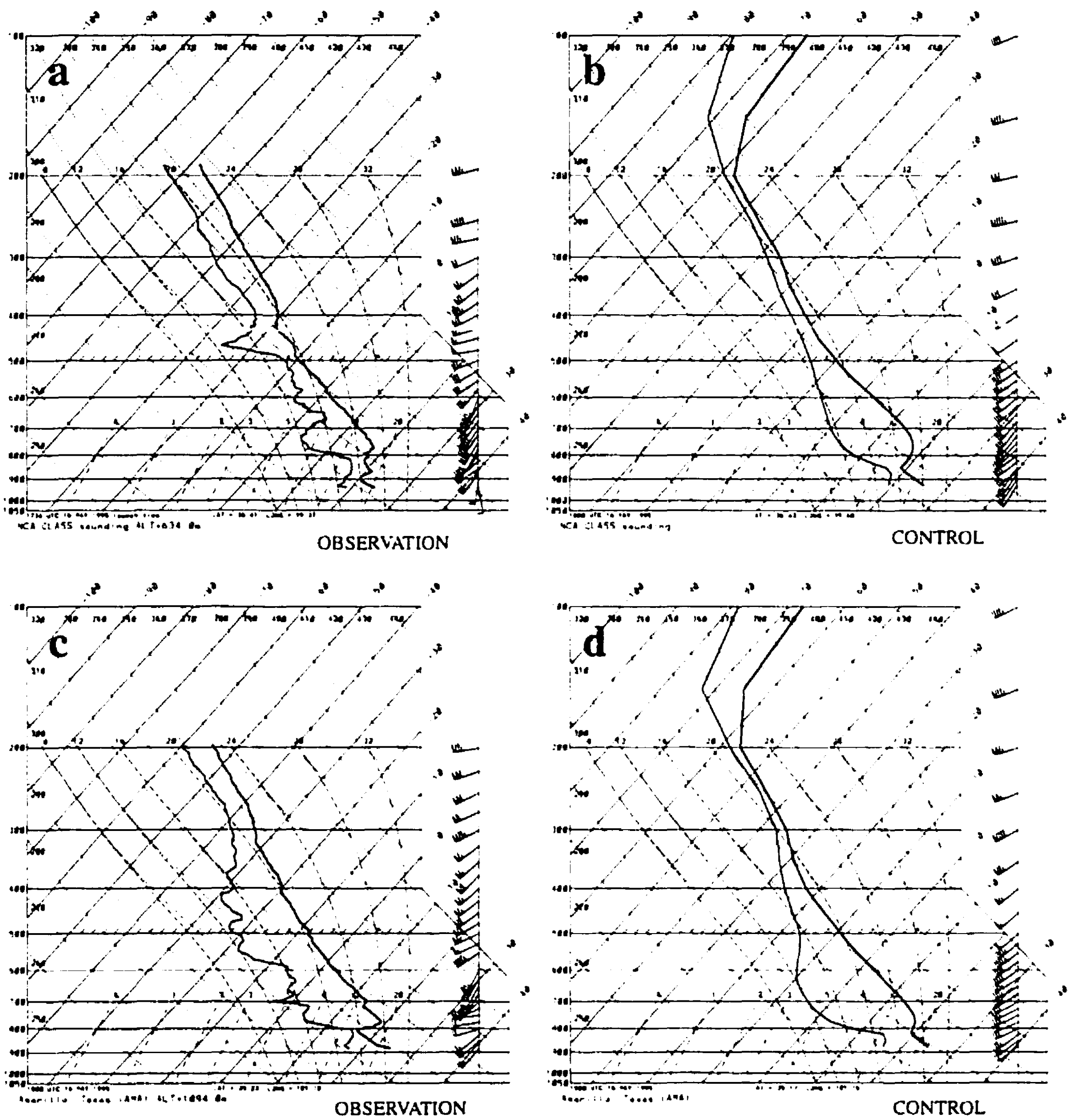

Figure 5.17. Observed and modelled vertical profiles of the atmosphere at a mobile launch site in (a) and (b), respectively, and at Amarillo, Texas, in (c) and (d), respectively (see Figure 2.4 for wind speed notation). The observed sounding in (a) was launched at 1734 UTC from the site marked by the identifier WOOD (open circle) in Figure 5.16. All other soundings are for 1800 UTC 16 May 1995.

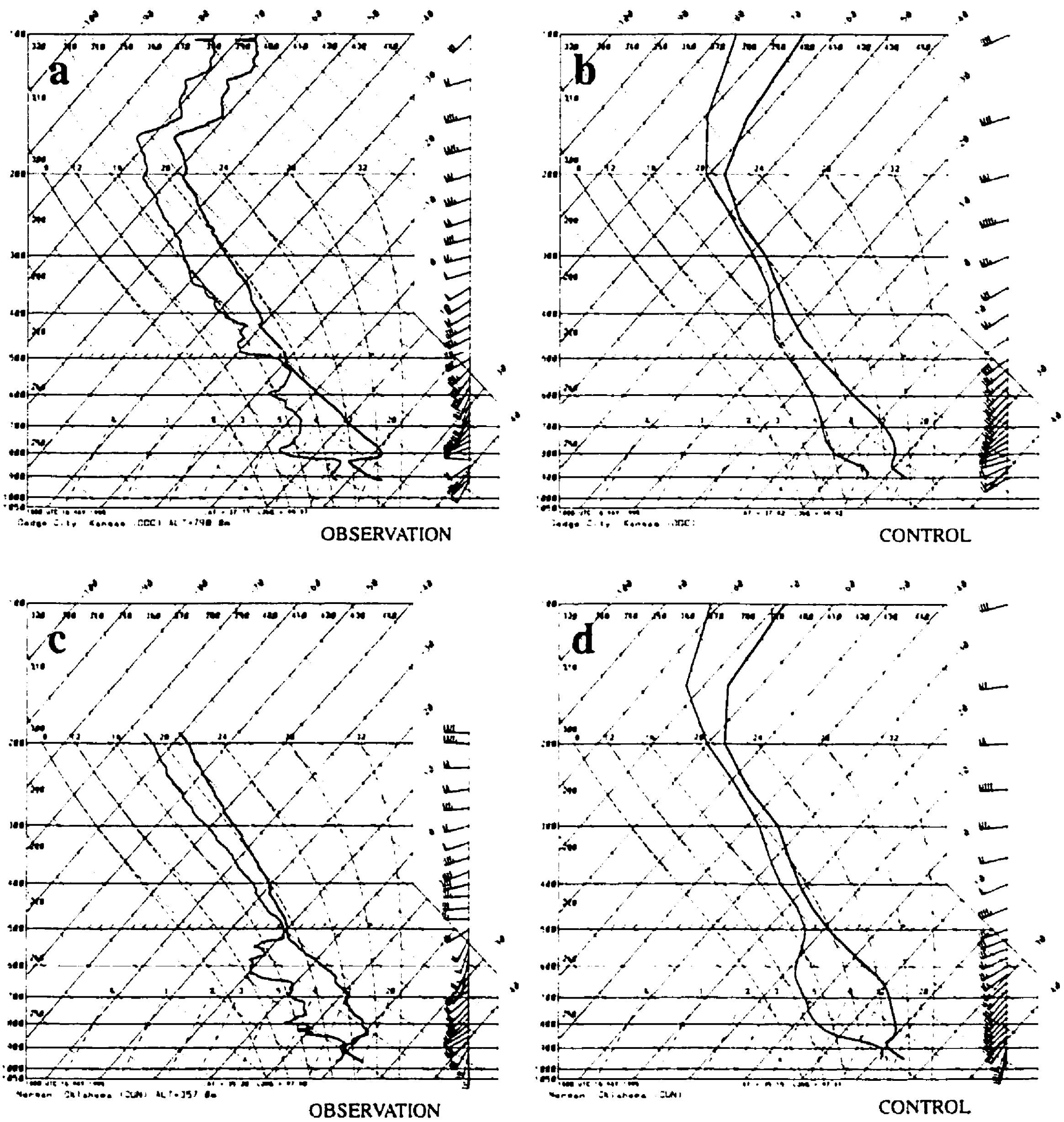

Figure 5.18. Observed and modelled vertical profiles of the atmosphere at Dodge City, Kansas, in (a) and (b), respectively, and at Norman, Oklahoma, in (c) and (d), respectively, for 1800 UTC 16 May 1995 (see Figure 2.4 for wind speed notation).

albedo over a patch corresponding roughly to the areal extent of the warm anomaly identified by a few surface stations. The resulting amplification in solar forcing over this region was further enhanced by our removal of the cooling effect of surface latent heat fluxes from the prognostic equation for surface temperature within the region where the albedo was prescribed a value of 0.10 or less (see Figure 5.16). As justification for this modification, it was assumed that a canopy extended over this area which would allow insolation to heat the earth, but would communicate any evaporative cooling through the top of the canopy. Since the canopy top is not represented by the model, the ground would be subject to maximum heating.

With these adjustments implemented into the initial conditions and MC2 code, the surface temperature within the modified patch increased throughout the early morning hours to more closely match that observed by the local meteorological stations. This heat was subsequently translated into the lowest layers of the atmosphere, thereby producing an environmental state that was much more conducive to deep cumulus development in the early afternoon. Shutting off the latent heat fluxes over most of the patch had the additional effect of moistening the lowest layers, which also increased the likelihood that an air parcel would freely convect. In Figure 5.19, a comparison is provided of the vertical profiles of the atmosphere from CONTROL and ALBEDO at the grid point where the conventional Kain-Fritsch trigger was successful in initiating convection in the sensitivity study. Implicit rainfall was generated over the modified area, approximately 100 km to the south-southeast of Dodge City, at 1921 UTC.

Although the artificial adjustments described above forced the development of the previous convective system at the correct location, this storm did not evolve as that observed in radar imagery. Firstly, the modelled storm was late by about two hours. More importantly, however, the convective cell did not propagate to the northeast as it developed, which observations showed the real storm to do. The propagation of the observed system followed that of a multicell storm, where new updrafts form along the cold-outflow boundary and grow as separate entities. This is different from supercell propagation, whereby new updrafts feed the main updraft of the storm (Wilhelmson and Chen 1982). In the model, deep convection persisted in the area that was the most willing

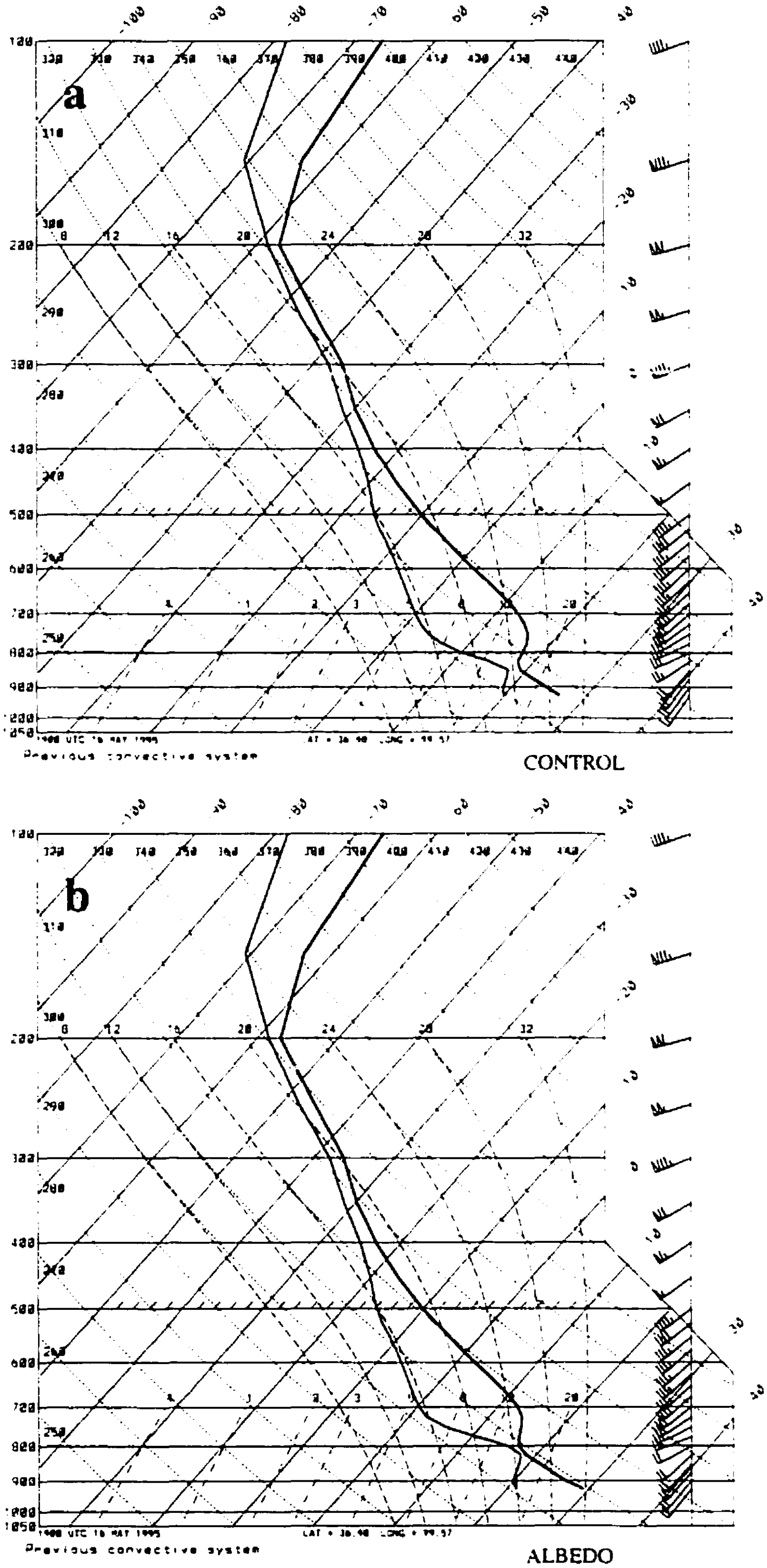

Figure 5.19. Vertical profile of the atmosphere at the initiation point of the previous convective system in CONTROL (a) and ALBEDO (b) model runs (see Figure 2.4 for wind speed notation). The location of the grid point is indicated by a star in Figure 5.16.

to accommodate buoyant parcels of air. Hence, the modelled storm did not propagate to the northeast, but rather maintained its position over the artificially created warm sector for over three hours. Note, that at this time the surrounding environment was still characterized by a strong low-level inversion, and it was not until the late afternoon hours, after the capping lid had been weakened considerably elsewhere, that the modelled storm traveled beyond the Oklahoma panhandle. During this time, the storm maintained its strength for a much longer period than the observed system, and actually moved into the path of the oncoming modelled Garden City storm at 0100 UTC. This improper behavior would suggest that the method we employed to initiate the storm was not accurate. Nevertheless, an analysis was performed to test whether it was possible that the non-interfering first few hours of this convective system may have influenced the modelled Garden City storm.

To do this, low-level fields of the horizontal vorticity vector were computed at 2100 UTC, 2200 UTC, 2300 UTC, and 0000 UTC. Horizontal vorticity, which is a measure of rotation in the atmosphere about a horizontal axis, is generated by either vertical shear of the horizontal winds or horizontal shear of the vertical winds. Typically, the former source is two orders of magnitude larger than the latter, so that horizontal vorticity, $\underline{\omega}_h$, may be approximated by the formula

$$\underline{\omega}_h = \left(-\frac{\partial v}{\partial z}, \frac{\partial u}{\partial z} \right) \tag{5.5}$$

A plot of the streamlines of the layer-averaged horizontal vorticity between the ground and cloud-base, which in this case was estimated to be 750-hPa, showed that the dominant component of this vector in the environment surrounding the previous convective system was oriented along the y-axis (Figure 5.20). Consequently, fields of the y-component were constructed for each of the model layers between the surface and 600-hPa to analyse the vertical structure of horizontal vorticity in the lower troposphere. An examination of the plots in Figure 5.21 to Figure 5.24 indicates that a low-level maximum propagated northward from the system between 2100 UTC and 0000 UTC. A

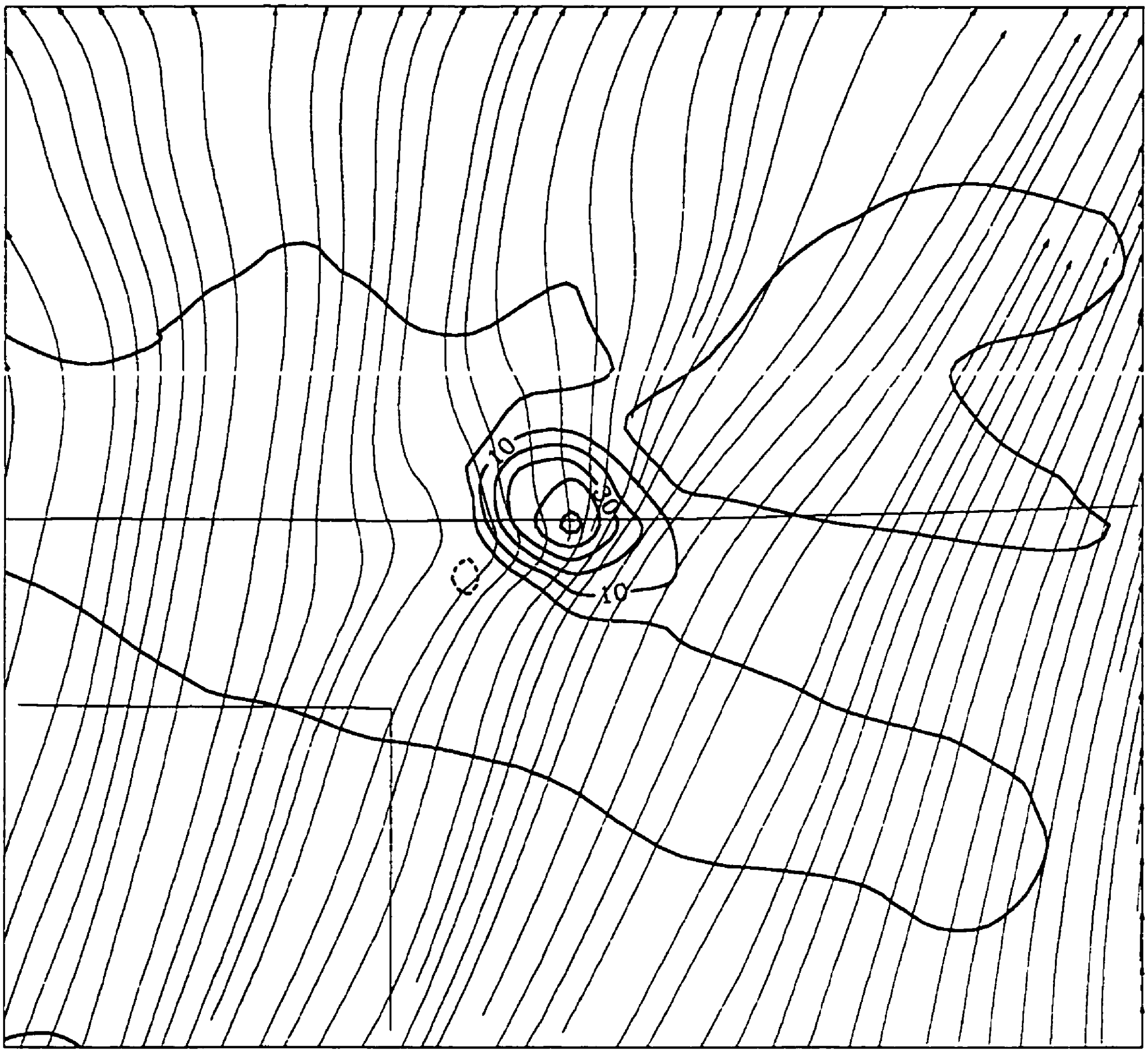

Figure 5.20. Streamlines of layer-averaged horizontal vorticity between cloud-base and ground-level for the previous convective system at 2100 UTC. Vertical velocity at 500-hPa (cm s^{-1}) (bold contours) is superimposed with a contour interval of 10 cm s^{-1}, and negative values are indicated by dashed contours.

vertical cross section through this vortex tube accompanies each figure to show its intensity relative to the surrounding environment.

It is evident from these plots that the magnitude of horizontal vorticity when the vortex tube was first shed from the previous storm was greater than 0.01 s^{-1} (Figure 5.21). Over the following three hours, the amplitude decreased by approximately half as the anomaly propagated to the north (Figure 5.22 to Figure 5.24). Note, that the movement of this anomaly was different from that of the observed outflow-boundary, which propagated westward from the previous convective system. An analysis of the cold-pool generated by the modelled storm did not show any indication of a propagating outflow-boundary at 18 km horizontal resolution. Nevertheless, Markowski et al. (1998a) have suggested that the intensity of the horizontal vorticity anomaly that was identified is significant since it is one to two orders of magnitude larger than the normal amplitude of vertical vorticity at a boundary. Thus, the presence of a vortex tube of this strength could lead to low-level mesocyclones upon tilting without requiring as much stretching as pre-existing low-level vertical vorticity would require (Markowski et al. 1998a).

Therefore, although the source storm was not recreated with great accuracy, a vortex tube was identified to propagate away from the previous convective system and into the path of the developing Garden City storm. Interference from the previous convective system during the speculated updraft-boundary interaction stage in the sensitivity run prevented a direct analysis to determine if there was any modification to the Garden City storm's rotational properties. However, it appears from this experiment that a region of enhanced low-level horizontal vorticity, generated by the previous storm, could have propagated a sufficiently large distance, while maintaining an intensity for a sufficiently long period that would influence the rotational character of the Garden City storm. It would be highly desirable to determine how the previous convective system could be reproduced more properly so that a more rigorous test of this hypothesis could be performed.

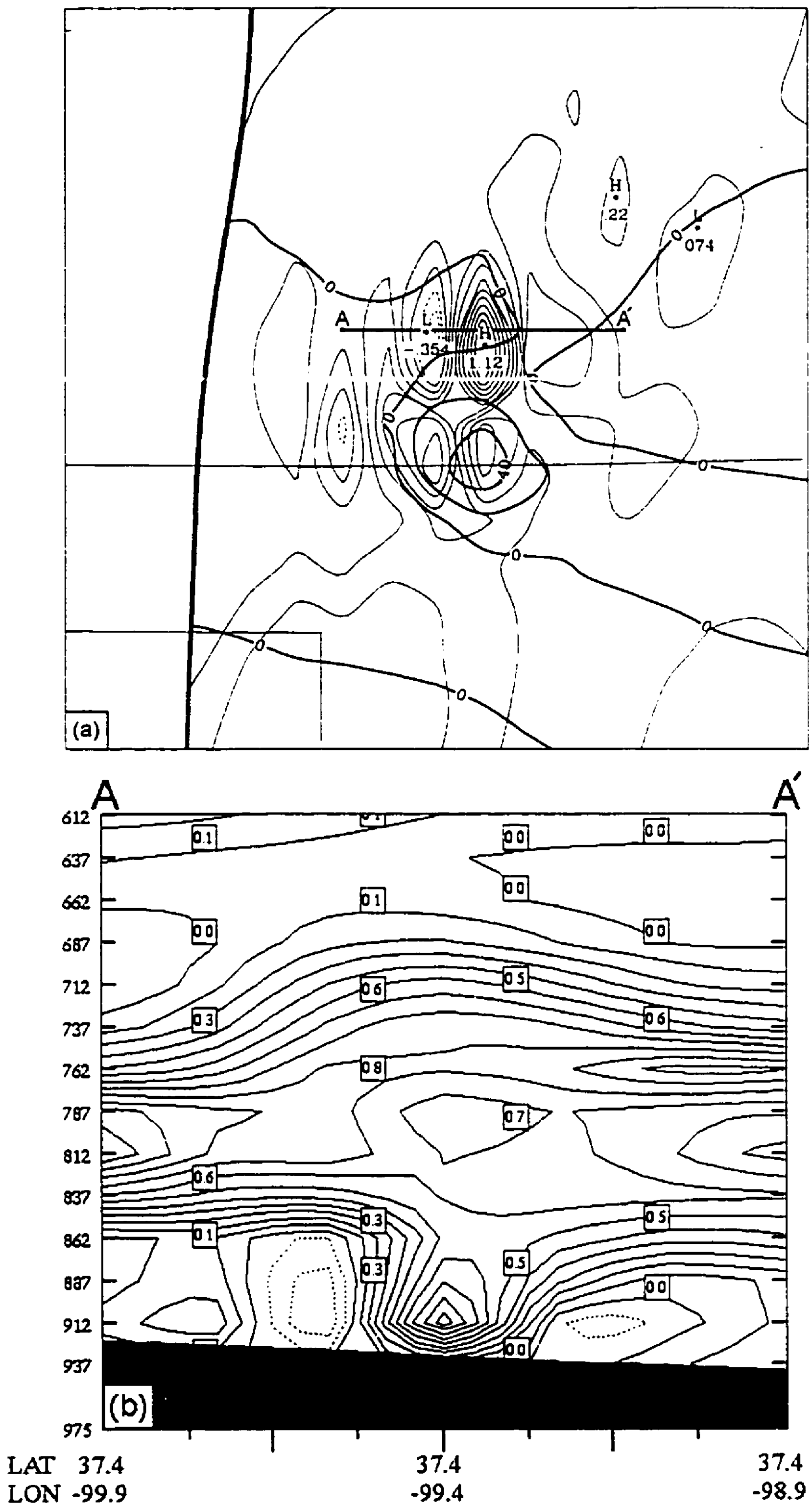

Figure 5.21. Horizontal cross-section through the previous convective system showing vertical velocity at 500-hPa (cm s^{-1}) (bold contours) and the y-component of horizontal vorticity at 912-hPa (1 x 10^{-2} s^{-1}) (thin contours) at 2100 UTC in (a). Heavy solid line denotes the area below surface. In (b), a vertical cross-section of the y-component of the horizontal vorticity vector between the endpoints A and A' is shown. Contour interval for vertical velocity is 20 cm s^{-1}, and for horizontal vorticity is 0.1 x 10^{-2} s^{-1}.

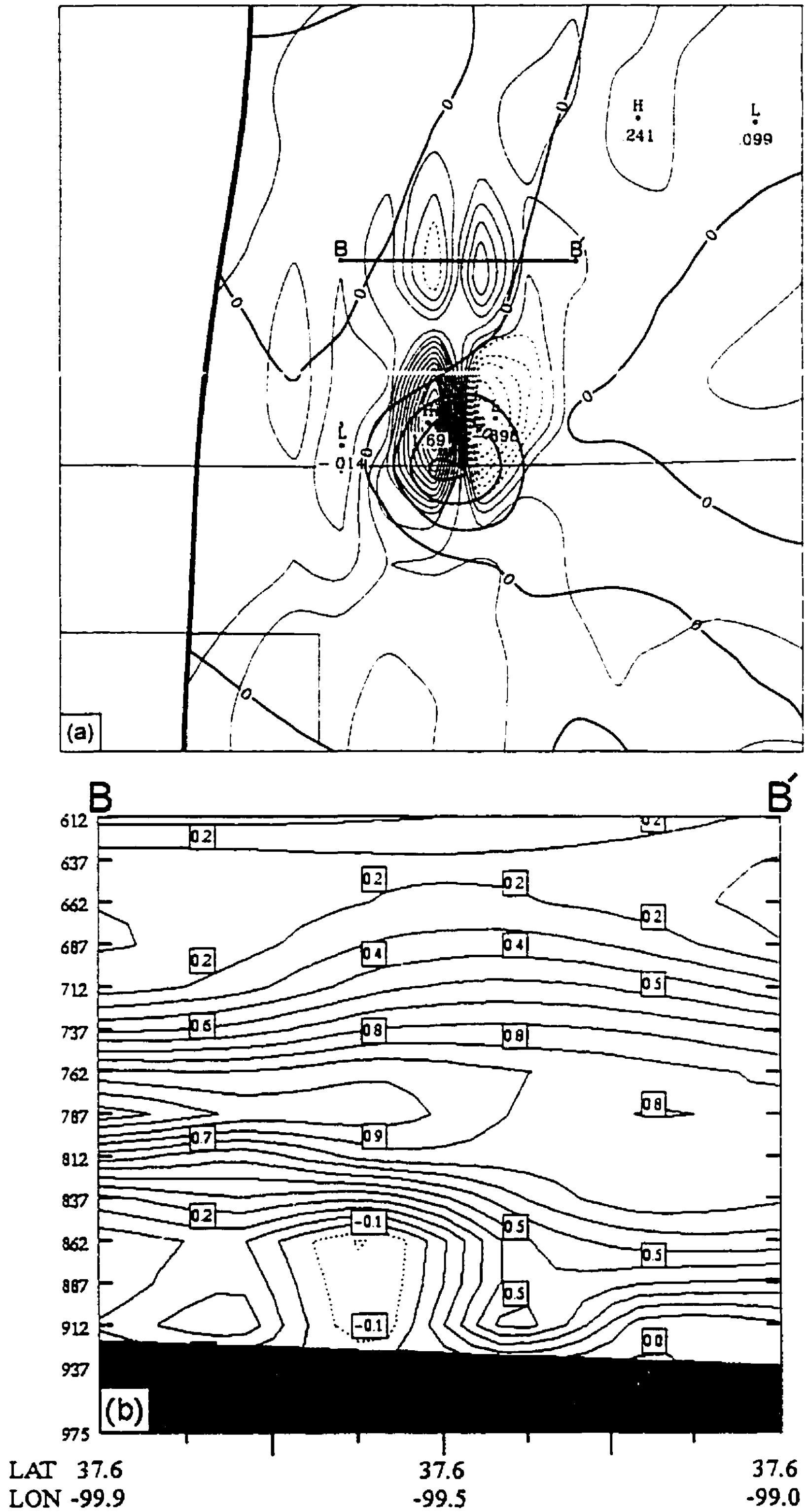

Figure 5.22. As in Figure 5.21, except for 2200 UTC, and vertical cross-section is now between the endpoints B and B'.

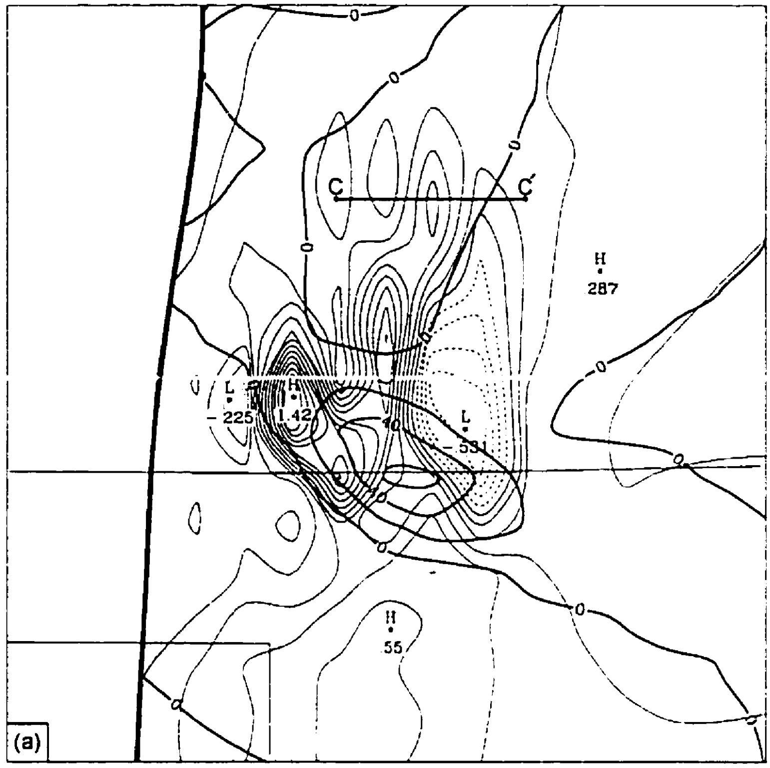

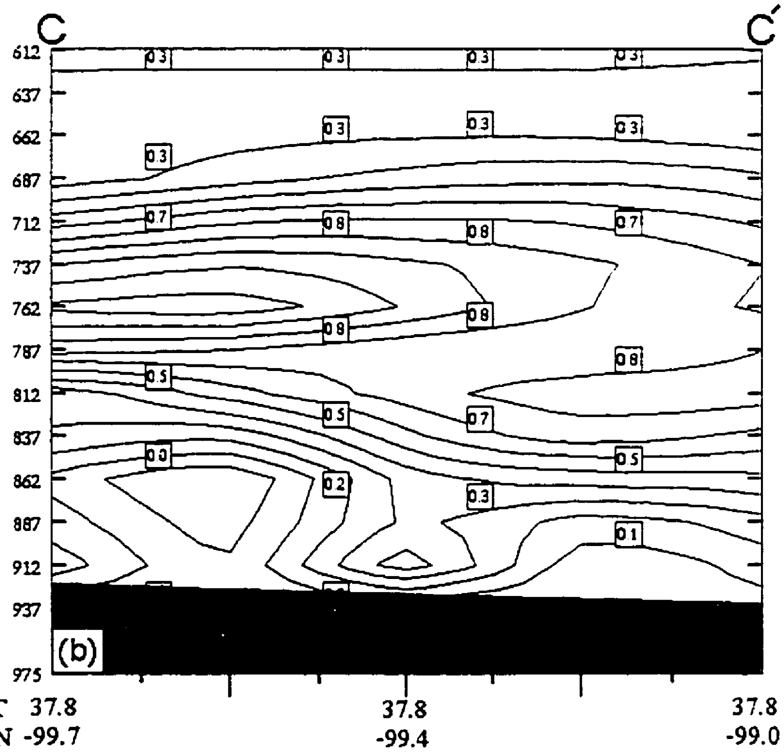

Figure 5.23. As in Figure 5.21, except for 2300 UTC, and vertical cross-section is now between the endpoints C and C'.

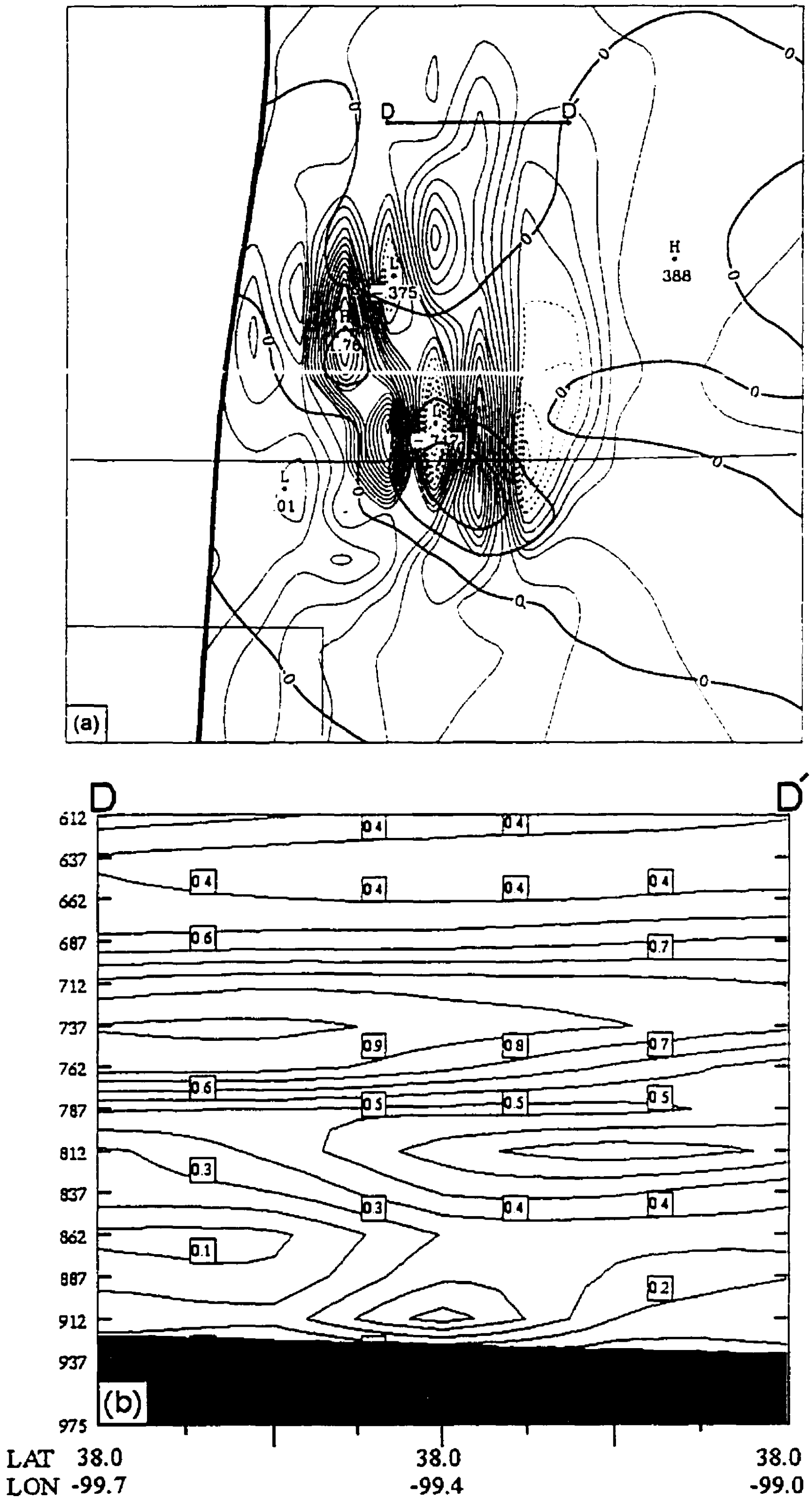

Figure 5.24. As in Figure 5.21, except for 0000 UTC, and vertical cross-section is now between the endpoints D and D'.

5.4 Comparison with the Results of Hong and Pan (1998) and Hong et al. (1998)

To further illustrate the extreme difficulty involved in simulating warm-season convective events, particularly in a convectively unstable environment with weak large-scale forcing, the study presented in the companion papers by Hong and Pan (1998) and Hong et al. (1998) is now considered. In the preliminary paper by Hong and Pan (1998), a convective trigger function that explicitly couples boundary layer and convective precipitation processes was applied to the heavy rain episode of 15-17 May 1995. The trigger, which is a modified version of that developed by Rogers and Fritsch (1996), is sensitive to subgrid-scale perturbations that are produced by surface inhomogeneities and turbulence-induced buoyancy. Hong and Pan (1998) implemented this trigger function into the Regional Spectral Model (RSM) of the National Centers for Environmental Prediction (NCEP), and conducted several sensitivity experiments with a grid-spacing of approximately 25 km to compare its performance to the standard operational trigger. For all of their simulations, the model was initialized at 1200 UTC 15 May 1995 and ran for 48 hours. After concluding that the new convective trigger function enhanced precipitation predictability, the authors implemented it and an explicit precipitation scheme, which was selected after other sensitivity runs, into the RSM to obtain a control run (Hong et al. 1998).

The main goal of their study was to improve the predictability of precipitation in environments where grid-resolvable forcing is weak and CAPE is high by applying a new convective trigger function to the simulation of a heavy rain case. Although this differs greatly from our primary objective, there are similarities to our study in that the authors aimed to overcome the difficulties presented by the environment of 16 May 1995 by employing a convective trigger function that is sensitive to subgrid-scale boundary layer forcing. Therefore, it is interesting to compare the results of our study to those obtained by Hong et al. (1998), keeping in mind that the mesoscale models, their physics packages, and the horizontal resolutions applied in these simulations are different.

A plot of the observed 24-hour accumulated precipitation beginning at 1200 UTC 16 May 1995, adapted from Hong et al. (1998), is shown in Figure 5.25 (a), while Figure 5.25 (b) shows the precipitation pattern in Hong et al's control run. For comparison, the 16-hour accumulated precipitation fields in our control and sensitivity simulations are plotted respectively in Figure 5.26 (a) and (b). Although the period of integration of our model runs was not sufficiently long to enable a direct quantitative comparison between these plots and those of Figure 5.25, differences that are relevant to the focus of our study over southwestern Kansas are easily identified. In particular, the modelled Garden City storm in our control simulation generated a proper amount of accumulated rainfall over this region, as verified against the observational data. In contrast, there is a notable absence of precipitation over the area occupied by the Garden City storm in Figure 5.25 (b).

Therefore, despite the representation of boundary layer forcing in their convective parameterization scheme, Hong et al. (1998) were unable to generate the Garden City storm. This shortcoming may be due to a different formula to parameterize boundary layer forcing, or alternatively, to the use of initial conditions that were derived at an earlier time (1200 UTC 15 May 1995) and from a different source. Regardless, Hong et al.'s failure to initiate the Garden City storm further demonstrates the high degree of complexity involved in numerically modelling MCSs using a mesoscale model that is initialized with real data.

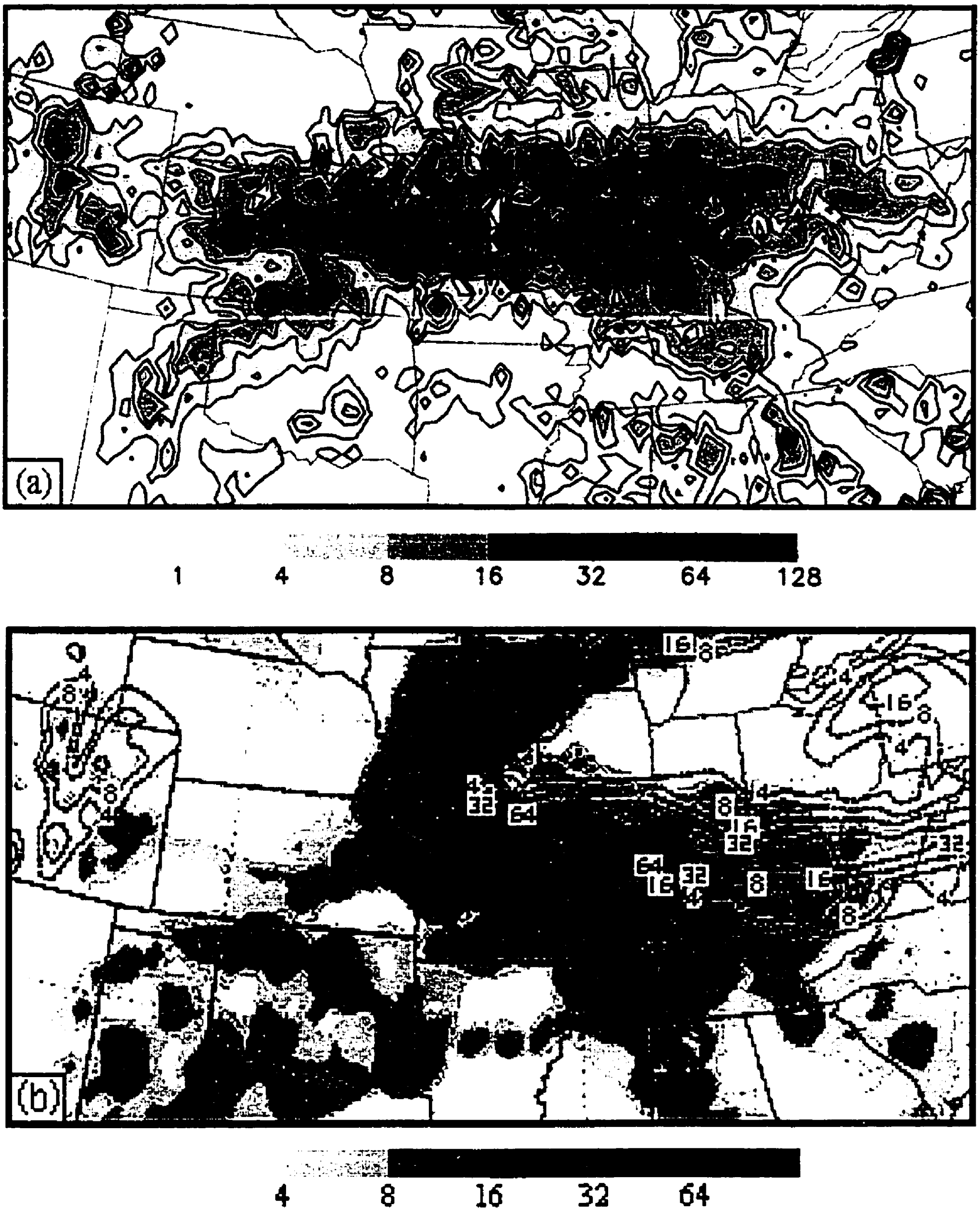

Figure 5.25. In (a), analysed 24-hour accumulated rainfall (mm) ending at 1200 UTC 17 May 1995. Values are box averages on a 25 km grid from station data. (from Hong et al. 1998) In (b), predicted 24-hour accumulated rainfall (mm) valid at 1200 UTC 17 May 1995 (48-hour forecast time) from Hong et al's (1998) control run. Shaded areas and contours denote the subgrid-scale (implicit) and grid-resolvable (explicit) rain, respectively.

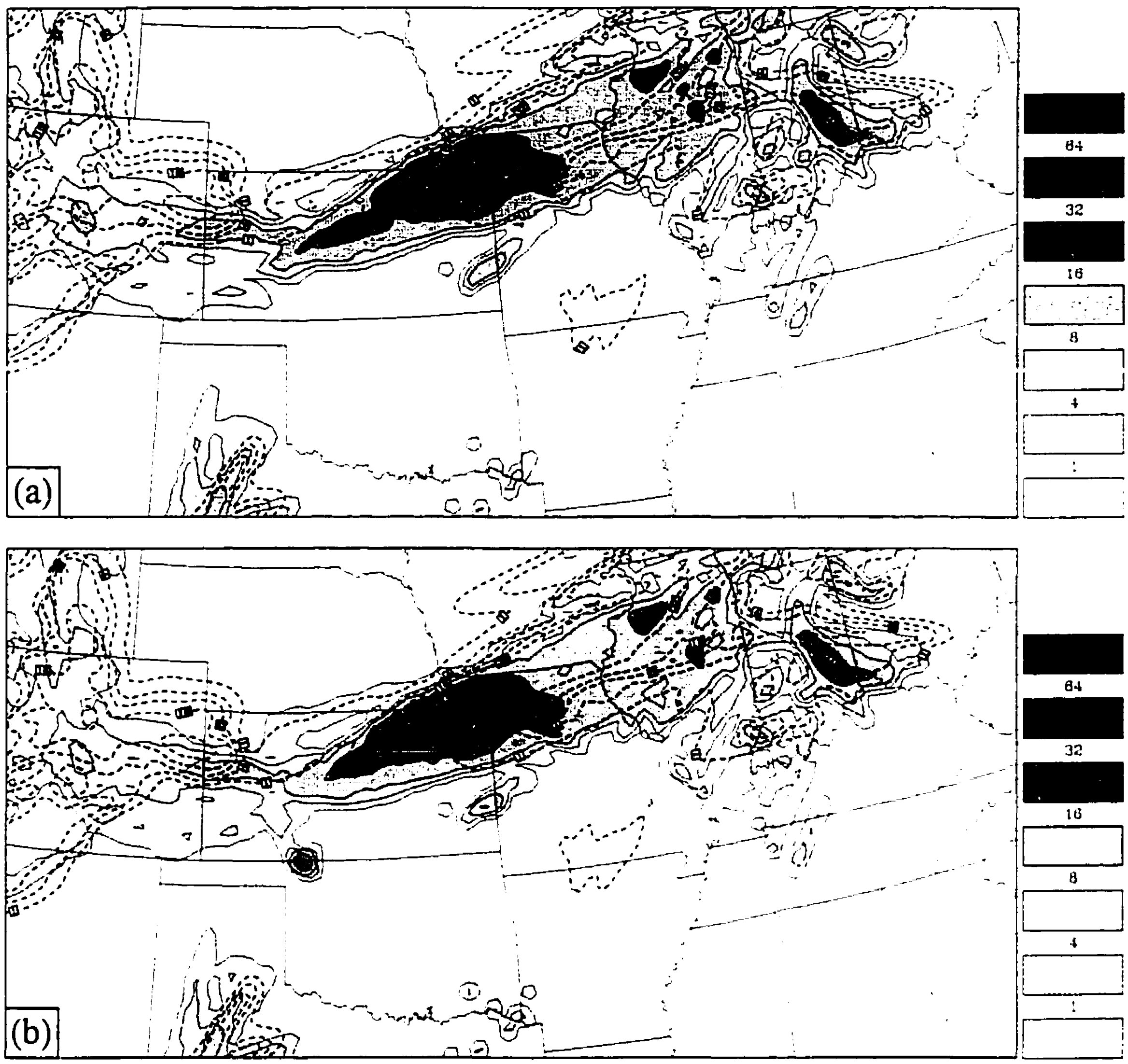

Figure 5.26. Simulated 16-hour accumulated precipitation (mm) valid at 0400 UTC 17 May 1995 from CONTROL (a) and ALBEDO (b). Shaded areas and dashed contours denote the convective (implicit) and stratiform (explicit) rainfall, respectively.

Chapter 6

Summary and Future Work

In this thesis, an accurate real-data simulation of an isolated thunderstorm, obtained using a sophisticated three-dimensional mesoscale model, was presented and analysed. The subject of this experiment was a well-documented tornadic supercell, which formed in an environment characterized by weak large-scale forcing and a high level of convective instability (Wakimoto et al. 1998; Wakimoto and Liu 1998; Hong and Pan 1998; Hong et al. 1998). This type of environment is known to be extremely difficult to model and, indeed, this conclusion was reinforced by our study.

This work was greatly motivated by the fact that, thus far, most numerical simulations of supercells have been conducted using cloud-models initialized from horizontally homogeneous initial conditions. Hence, the primary objective of this study was to demonstrate the process by which an accurate reproduction of an observed supercell thunderstorm and its environment could be achieved when a mesoscale model is initialized with real-data. To accomplish this ambitious goal, numerous difficulties were overcome, the greatest of which was resolved by modifying the model's convective parameterization scheme. These modifications were the incorporation of a second convective trigger function that is sensitive to boundary layer instabilities (Stensrud and Fritsch 1994b), and the introduction of a time-dependent perturbation filter into the conventional Kain-Fritsch trigger function to suppress the spurious initiation of convection (Zhang and Fritsch 1986). Sensitivity tests at 35 km resolution indicated that the inclusion of shallow convection degraded the quality of the simulation. As a result, shallow convection was turned off in our control run.

With these modifications in our mesoscale model and a horizontal resolution of 18 km, we were able to reproduce the proper atmospheric conditions for deep cumulus development observed over the central plains on 16 May 1995. This included the assembly of a deep-layer, convectively unstable atmosphere over southwestern Kansas by a combination of low-level moisture transport from the Gulf of Mexico and the mid-level advection of a dry air mass from the Mexican Plateau down the eastern slopes of the Rocky Mountains. A capping lid separated a deep shaft of dry-adiabatically warmed air from a moist, well-mixed ABL to produce a Miller Type I vertical sounding. The absence of well-defined forcing for ascent on the synoptic-scale hindered the initiation of convection in this extremely volatile atmosphere. Instead, vertical lifting was provided by mesoscale features in the form of an upper-level jet streak and a surface dryline, both of which were simulated reasonably well. However, the presence of a free convective boundary layer west of Garden City, Kansas, and the additional trigger function were necessary to generate the simulated Garden City storm at the correct time and location. The filter function was also critical in limiting the erroneous outbreak of convection during this period. The modelled Garden City storm was initiated at 2200 UTC, immediately west of the location where the observed storm emerged. This small westward bias matched the slight misplacement of the influential northern section of the dryline bulge also present in the numerical solution.

Although the modifications that were applied to MC2 met with success in our simulation, Hong et al.'s (1998) study of the heavy rainfall episode that occurred between 15 May and 17 May 1995 also employed a convective trigger function sensitive to boundary layer processes, but was unable to generate the Garden City convective cell. This outcome further demonstrates the complexity of MCS modelling and underscores our fundamental lack of understanding of the fine-scale processes which lead to the initiation of small-scale convective events in numerical models.

A comparison of our control simulation with radar imagery showed that our model properly reproduced the Garden City storm during its initial few hours of evolution, although the simulated storm's development was approximately one hour slower than that of the observed storm. To further evaluate the model's performance, several severe weather parameters in the environment of the modelled storm were examined. It was shown from the BRN, BRNSHR, SREH, and EHI fields that the model successfully produced an environment susceptible to the formation of tornadic thunderstorms over southwestern Kansas.

Despite our success in simulating the initiation and developing stages of the Garden City storm, we were unable to properly reproduce all of the convective activity occurring on 16 and 17 May 1995. In particular, after thirteen hours of integration, the suppression of spurious convection was no longer effective, and the quality of the simulation of the Garden City storm degraded considerably. Another shortcoming of our control run concerned the inability to trigger the convective system located about 110 km south of Dodge City, and which formed five hours prior to the appearance of the Garden City supercell. This multicell storm was observed to develop under extremely unfavorable conditions for deep convection, but it may have played an important role in promoting tornadogenesis in the Garden City storm. An examination of VORTEX-95 observational data revealed a prominent positive anomaly in the surface temperature field in the vicinity of this multicell storm. There was also evidence of low-level vertical mixing, which may have locally degraded the strength of the capping lid. The failure of MC2 to capture these features was most likely the result of either an insufficiently fine horizontal resolution, incomplete initial conditions, or inadequately detailed data to define the local surface characteristics.

Consequently, a sensitivity study was performed in which the surface albedo, as well as the ground's response to solar heating, were altered over a small area of the Oklahoma panhandle. This produced a localized atmospheric instability, and hence, enabled the initiation of the previous convective system. A subsequent analysis of low-level horizontal vorticity fields showed that the presence of a severe storm in this location may have enhanced the rotational character of the Garden City supercell, which developed hours later. Specifically, a vortex tube extending through the lowest 50-hPa was identified in model output to propagate from this system a distance of approximately 90 km in three hours, while maintaining an intensity that would significantly augment the ambient vertical vorticity if it were to encounter a strong updraft. However, the timing and behavior of this earlier storm was not well simulated, suggesting that the artificial method we employed to trigger it may not be accurate.

Thus, for future work, it would be highly desirable to correctly determine the exact mechanism responsible for the formation of the previous convective system. If we can properly simulate its evolution, we would be in a better position to conclude more confidently on the influence of the pre-existing outflow boundary on tornadogenesis in the Garden City supercell. Despite our effort in this thesis, we were unable to provide a clear answer to the important question posed by Wakimoto et al. (1998) as to whether the low-level mesocyclogenesis observed in the Garden City thunderstorm would have occurred in the absence of the pre-existing outflow boundary.

Future work for this case study should include a higher resolution simulation with the aim of reproducing the mesocyclogenesis within the Garden City supercell. If successful, the analysis of a real-data numerical simulation of this extremely complex process would improve significantly our understanding of mesocyclones and supercell tornadogenesis.

References

Arakawa, A., and M.-D. Cheng, 1993: The Arakawa-Schubert cumulus parameterization. *The Representation of Cumulus Convection in Numerical Models, Meteor. Monogr.*, No. 46, Amer. Meteor. Soc., 123-136.

Benoit, R., J. Côté, and J. Mailhot, 1989: Inclusion of a TKE boundary layer parameterization in the Canadian regional finite-element model. *Mon. Wea. Rev.*, **117**, 1726-1750.

________, M. Desgagné, P. Pellerin, S. Pellerin, Y. Chartier, and S. Desjardins, 1997: The Canadian MC2: A semi-Lagrangian, semi-implicit wideband atmospheric model suited for finescale process studies and simulation. *Mon. Wea. Rev.*, **125**, 2382-2415.

Betts, A. K., and M. J. Miller, 1993: The Betts-Miller scheme. *The Representation of Cumulus Convection in Numerical Models, Meteor. Monogr.*, No. 46, Amer. Meteor. Soc., 107-121.

Bluestein, H. B., 1993: *Synoptic-Dynamic Meteorology in Midlatitudes.* Vol. II, *Observations and Theory of Weather Systems*, Oxford University Press, 594 pp.

________, and S. S. Parker, 1993: Modes of isolated, severe convective storm formation along the dryline. *Mon. Wea. Rev.*, **121**, 1354-1372.

Brandes, E. A., 1993: Tornadic thunderstorm characteristics determined with Doppler radar. *The Tornado: Its Structure, Dynamics, Prediction, and Hazards, Geophys. Monogr.*, No. 79, Amer. Geophys. Union, 143-159.

________, ________, and R. B. Wilhelmson, 1994: The role of midtropospheric winds in the evolution and maintenance of low-level mesocyclones. *Mon. Wea. Rev.*, **122**, 126-136.

Brown, R, A., 1998: Nomogram for aiding the interpretation of Tornadic Vortex Signatures measured by Doppler radar. *Wea. Forecasting*, **13**, 505-512.

Burgess, D. W., R. J. Donaldson Jr., and P. R. Desrochers, 1993: Tornado detection and warning by radar. *The Tornado: Its Structure, Dynamics, Prediction and Hazards, Geophys. Monogr.*, No. 79, Amer. Geophys. Union, 203-221.

Chouinard, C., J. Mailhot, H. L. Mitchell, A. Staniforth, and R. Hogue, 1994: The Canadian regional data assimilation system: Operational and research applications. *Mon. Wea. Rev.*, **122**, 1306-1325.

Davies, J. M., 1993: Hourly helicity, instability, and EHI in forecasting supercell tornadoes. Preprints, *17th Conf. on Severe Local Storms*, St. Louis, MO, Amer. Meteor. Soc., 107-111.

Davies-Jones, R. P., 1993: Helicity trends in tornado outbreaks. Preprints, *17th Conf. on Severe Local Storms*, St. Louis, MO, Amer. Meteor. Soc., 56-60.

________, D. Burgess, and M. Foster, 1990: Test of helicity as a tornado forecast parameter. Preprints, *16th Conf. on Severe Local Storms*, Kananaskis Park, AB, Canada, Amer. Meteor. Soc., 588-592.

Droegemeier, K. K., S. M. Lazarus, and R. Davies-Jones, 1993: The influence of helicity on numerically simulated convective storms. *Mon Wea. Rev.*, **121**, 2005-2029.

Emanuel, K. A., and D. J. Raymond, Eds., 1993: *The Representation of Cumulus Convection in Numerical Models. Meteor. Monogr.*, No. 46, Amer. Meteor. Soc., 246 pp.

Fawbush, E. J., and R. C. Miller, 1954: The types of air masses in which North American tornadoes form. *Bull. Amer. Meteor. Soc.*, **35**, 154-165.

Fouquart, Y., and B. Bonnel, 1980: Computations of solar heating of the earth's atmosphere: A new parameterization. *Contrib. Atmos. Phys.*, **53**, 35-62.

Fritsch, J. M., and C. F. Chappell, 1980: Numerical prediction of convectively driven mesoscale pressure systems. Part I: Convective parameterization. *J. Atmos. Sci.*, **37**, 1722-1733.

________, and J. S. Kain, 1993: Convective parameterization for mesoscale models: The Fritsch-Chappell scheme. *The Representation of Cumulus Convection in Numerical Models, Meteor. Monogr.*, No. 46, Amer. Meteor. Soc., 159-164.

Fujita, T. T., 1981: Tornadoes and downbursts in the context of generalized planetary scales. *J. Atmos. Sci.*, **38**, 1511-1534.

Garand, L., and J. Mailhot, 1990: The influences of infrared radiation in numerical weather forecasts. *Proceedings of the Seventh Conference on Atmospheric Radiation*, July 23-27 1990, San Francisco, U.S.A., Amer. Meteor. Soc., J146-J151.

Geleyn, J.-F., 1987: Use of a modified Richardson number for parameterizing the effect of shallow convection. *Short- and Medium-range Numerical Weather Prediction, Collection of Papers Presented at the WMO/IUGG NWP Symposium*, Tokyo, 4-8 August 1986, 141-149.

Gilmore, M. S., and L. J. Wicker, 1998: The influence of midtropospheric dryness on supercell morphology and evolution. *Mon. Wea. Rev.*, **126**, 943-958.

Grasso, L. D., and W. R. Cotton, 1995: Numerical simulation of a tornado vortex. *J. Atmos. Sci.*, **52**, 1192-1203.

Hong, S.-Y., H.-M. H. Juang, and Q. Zhao, 1998: Implementation of prognostic cloud scheme for a regional spectral model. *Mon. Wea. Rev.*, **126**, 2621-2639.

________, and H.-L. Pan, 1998: Convective trigger function for a mass-flux parameterization scheme. *Mon. Wea. Rev.*, **126**, 2599-2620.

Kain, J. S., and J. M. Fritsch, 1990: A one-dimensional entraining/detraining plume model and its application in convective parameterization. *J. Atmos. Sci.*, **47**, 2784-2802.

________, and ________, 1992: The role of the convective "trigger function" in numerical forecasts of mesoscale convective systems. *Meteor. Atmos. Phys.*, **49**, 93-106.

________, and ________, 1993: Convective parameterization for mesoscale models: The Kain-Fritsch scheme. *The Representation of Cumulus Convection in Numerical Models, Meteor. Monogr.*, No. 46, Amer. Meteor. Soc., 165-170.

________, and ________, 1998: Multiscale convective overturning in mesoscale convective systems: Reconciling observations, simulations, and theory. *Mon. Wea. Rev.*, **126**, 2254-2273.

Kong, F., and M. K. Yau, 1997: An explicit approach to microphysics in MC2. *Atmos.-Ocean.*, **35**, 257-291.

Kulie, M. S., and Y.-L. Lin, 1998: The structure and evolution of a numerically simulated high-precipitation supercell thunderstorm. *Mon. Wea. Rev.*, **126**, 2090-2116.

Kuo, H. L., 1974: Further studies of the parameterization of the influence of cumulus convection on large-scale flow. *J. Atmos. Sci.*, **31**, 1232-1240.

Kuo, Y., R. J. Reed, and Y. Liu, 1996: The ERICA IOP 5 storm. Part III: Mesoscale cyclogenesis and precipitation parameterization. *Mon. Wea. Rev.*, **124**, 1409-1434.

Maddox, R. A., K. W. Howard, D. L. Bartels, and D. M. Rodgers, 1986: Mesoscale Convective Complexes in the middle latitudes. *Mesoscale Meteorology and Forecasting*, P. S. Ray, Ed., Amer. Meteor. Soc., 390-413.

________, L. R., Hoxit, and C. F. Chappell, 1980: A study of tornadic thunderstorm interactions with thermal boundaries. *Mon. Wea. Rev.*, **108**, 322-336.

Mailhot, J., 1994: The regional finite-element (RFE) model scientific description. Part 2: Physics. [Available from RPN, 2121 Trans-Canada, Dorval, QC H9P 1J3, Canada]

________, S. Bélair, R. Benoit, B. Bilodeau, Y. Delage, L. Fillion, L. Garand, C. Girard, and A. Tremblay, 1998: Scientific description of RPN physics library. Version 3.6. [Available from RPN, 2121 Trans-Canada, Dorval, QC H9P 1J3, Canada]

Markowski, P. M., E. N. Rasmussen, and J. M. Straka, 1998a: The occurrence of tornadoes in supercells interacting with boundaries during VORTEX-95. *Wea. Forecasting*, **13**, 852-859.

________, J. M. Straka, E. N. Rasmussen, and D. O. Blanchard, 1998b: Variability of storm-relative helicity during VORTEX. *Mon. Wea. Rev.*, **126**, 2959-2971.

McFarlane, N. A., 1987: The effect of orographically excited gravity wave drag on the general circulation of the lower stratosphere and troposphere. *J. Atmos. Sci.*, **44**, 1775-1800.

Molinari, J., and M. Dudek, 1992: Parameterization of convective precipitation in mesoscale numerical models: A critical review. *Mon. Wea. Rev.*, **120**, 326-344.

Moncrieff, M. W., and J. S. A. Green, 1972: The propagation and transfer properties of steady convective overturning in shear. *Quart. J. Roy. Meteor. Soc.*, **98**, 336-352.

NCDC, 1995: *Storm Data*. Vol. 37, No. 5, 268pp. [Available from National Climatic Data Center, Asheville, NC 28801.]

Rasmussen, E. N., and D. O. Blanchard, 1998: A baseline climatology of sounding-derived supercell and forecast parameters. *Wea. Forecasting*, **13**, 1148-1164.

________, J. M. Straka, R. Davies-Jones, C. A. Doswell III, F. H. Carr, M. D. Eilts, and D. R. MacGorman, 1994: Verification of the Origins of Rotation in Tornadoes Experiment: VORTEX. *Bull. Amer. Meteor. Soc.*, **75**, 995-1006.

Raymond, and Emanuel, 1993: The Kuo cumulus parameterization. *The Representation of Cumulus Convection in Numerical Models, Meteor. Monogr.*, No. 46, Amer. Meteor. Soc., 145-147.

Rhea, J. O., 1966: A study of thunderstorm formation along drylines. *J. Appl. Meteor.*, **5**, 58-63.

Rogers, R. F., and J. M. Fritsch, 1996: A general framework for convective trigger functions. *Mon. Wea. Rev.*, **124**, 2438-2452.

Rogers, R. R., and M. K. Yau, 1989: *A Short Course in Cloud Physics. Third Edition*, Pergamon Press, 290 pp.

Schaefer, J. T., 1986: The dryline. *Mesoscale Meteorology and Forecasting*, P. S. Ray, Ed., Amer. Meteor. Soc., 549-572.

Smith, S. B., and M. K. Yau, 1993: The causes of severe convective outbreaks in Alberta. Part I: A comparison of a severe outbreak with two nonsevere events. *Mon. Wea. Rev.*, **121**, 1099-1125.

Stensrud, D. J., J. V. Cortinas Jr., and H. E. Brooks, 1997: Discriminating between tornadic and nontornadic thunderstorms using mesoscale model output. *Wea. Forecasting*, **12**, 613-632.

________, and J. M. Fritsch, 1993a: Mesoscale convective systems in weakly forced large-scale environments. Part I: Observations. *Mon. Wea. Rev.*, **121**, 3326-3344.

________, and ________, 1994a: Mesoscale convective systems in weakly forced large-scale environments. Part II: Generation of a mesoscale initial condition. *Mon. Wea. Rev.*, **122**, 2068-2083.

________, and ________, 1994b: Mesoscale convective systems in weakly forced large-scale environments. Part III: Numerical simulations and implications for operational forecasting. *Mon. Wea. Rev.*, **122**, 2084-2104.

Stull, R. B., 1988: *An Introduction to Boundary Layer Meteorology*. Kluwer Academic Publishers, 666 pp.

Thomas, S. J., C. Girard, R. Benoit, M. Desgagné, and P. Pellerin, 1998: A new adiabatic kernel for the MC2 model. *Atmos.-Ocean*, **36**, 241-270.

Tripoli, G. J., and W. R. Cotton, 1989: Numerical study of an observed orogenic mesoscale convective system. Part I: Simulated genesis and comparison with observations. *Mon. Wea. Rev.*, **117**, 273-304.

Wakimoto, R. M., and C. Liu, 1998: The Garden City, Kansas, storm during VORTEX 95. Part II: The wall cloud and tornado. *Mon. Wea. Rev.*, **126**, 393-408.

________, ________, and H. Cai, 1998: The Garden City, Kansas, storm during VORTEX 95. Part I: Overview of the storm's life cycle and mesocyclogenesis. *Mon. Wea. Rev.*, **126**, 372-392.

Wang, W., and N. L. Seaman, 1997: A comparison study of convective parameterization schemes in a mesoscale model. *Mon. Wea. Rev.*, **125**, 252-278.

Weaver, J. F., and S. P. Nelson, 1982: Multiscale aspects of thunderstorm gust fronts and their effects on subsequent storm development. *Mon. Wea. Rev.*, **110**, 707-718.

Weisman, M. L., and J. B. Klemp, 1984: The structure and classification of numerically simulated convective storms in directionally varying wind shear. *Mon. Wea, Rev.*, **112**, 2479-2498.

Wicker, L. J., and R. B. Wilhelmson, 1995: Simulation and analysis of tornado development and decay within a three-dimensional supercell thunderstorm. *J. Atmos. Sci.*, **52**, 2675-2703.

Wilhelmson, R. B., and C.-S. Chen, 1982: A simulation of the development of successive cells along a cold outflow boundary. *J. Atmos. Sci.*, **39**, 1466-1483.

Wilson, J. W., T. M. Weckwerth, J. Vivekanandan, R. M. Wakimoto, and R. W. Russell, 1994: Boundary layer clear-air radar echoes: Origin of echoes and accuracy of derived winds. *J. Atmos. Oceanic Technol.*, **11**, 1184-1206.

Zhang, D.-L., and J. M. Fritsch, 1986: Simulation of the meso-β scale structure and evolution of the 1977 Johnstown flood. Part I: Model description and verification. *J. Atmos. Sci.*, **43**, 1913-1943.

________, E.-Y. Hsie, and M .W. Moncrieff, 1988: A comparison of explicit and implicit prediction of convective and stratiform precipitating weather systems with a meso-β-scale numerical model. *Quart. J. Roy. Meteor. Soc.*, **114**, 31-60.

Ziegler, C. L., and E. N. Rasmussen, 1998: The initiation of moist convection at the dryline: Forecasting issues from a case study perspective. *Wea. Forecasting*, **13**, 1106-1131.

Zipser, E. J., 1982: Use of a conceptual model of the life-cycle of mesoscale convective systems to improve very-short-range forecasts. *Nowcasting*, K. A. Browning, Ed., Academic Press, New York, 191-204.